ዘዴ

SêN?ƒ ›`Ÿ=‚¡„‹ SN” Ç=ƒ‹“ ¾›=ƒÄ"Á

ISSN: 0514-6216

Indexed on AJOL

zede

Journal of Ethiopian Engineers and Architects

41 ሐምሌ 0፲፭ July 2023

Annual Publication of the Addis Ababa Institute of Technology
Addis Ababa University

²È

¾›=fÄ“Á SN”Ç=f‹ ›`Ÿ=‚i„‹ SêN?f

Zede

Journal of Ethiopian Engineers and Architects

¾}ssS¨<	ሐምሌ	41	þ.X.l ›Ç=e ›uv
Established 1963	July 2023		P.O. Box 385 Addis Ababa

Editor-in- Chief
Zebene Kiflie

Asso. *Editor*
Birhanu Beshah

Editorial Board Members
Adil Zekaria
Agizew Nigussie
Gyeong Man
Mengesha Mamo
Heyaw Terefe

Publisher
Addis Ababa University
Addis Ababa Institute of Technology
P.O. Box 385
Addis Ababa
Ethiopia

Postal Address
Addis Ababa University, AAiT
P.O. Box 385
Addis Ababa
Ethiopia

Website: **www.aait.edu.et/zede**
Email: zede@aait.edu.et

CONTENTS **Pages**

THE EDITORIAL BOARD IS NOT RESPONSIBLE FOR VIEWS EXPRESSED BY INDIVIDUAL AUTHORS.

Guide to Authors

ZEDE is a scientific journal on engineering science and application, produced under the auspices of the Addis Ababa Institute of Technology, Addis Ababa University. The main objective of the journal is to publish research articles, findings and discussions on engineering sciences, technology and architecture thereby assisting in the dissemination of engineering knowledge and methodologies in solving engineering problems. Technical Notes of significant contribution may be considered for publication.

Original papers for publication in the journal should be submitted in triplicate to the Editor-in-Chief, P.O. Box 385, Addis Ababa, Ethiopia. All articles submitted for publication in the journal should comply with the following requirements:

1. Title of Paper: The title of the paper should be phrased to include only key words and must have a length of not exceeding *80* characters including spaces.

2. Format of Manuscript: The manuscript should be (double-spaced single column draft and single spaced double column final) in *A-4* sized paper with MS word 2007or later version. Margins of *25 mm* should be used on all sides of the paper.

3.Length of Article: The length of the article should not exceed word equivalent of 6000 words, or *20* pages, double spaced using font size *12* typed in Times New Roman.

4. Author's Affiliation: The author's full name, institutional affiliation and rank, if applicable, must appear on the paper.

5. Abstract: All articles submitted must include an abstract of length not exceeding *200* words in *italics*.

6. Keywords: All articles submitted must include Keywords not exceeding 6 in number.

7. Style of Writing: It is recommended that third person pronoun/s be used when referring to author/s.

8. Illustrations: Figures should be drawn in black, at a size with a *50%* reduction to fit in *160 mm* width of journal. Photographs should be submitted as glossy prints. Explanations and descriptions must be placed in the text and not within figures. All figures must include numbered captions. See example:

Figure 1 Typical creep strain versus time curve

9. Tables: Tables must be numbered in the same order as cited in the text. Explanations of tables must appear in the text.

10. Equations: Equations numbers should be right-justified. See example:

$$u(x, y) = -y\theta(x) \qquad (1)$$

11. References: References in the body of the Article should be cited at the end of the paper by placing a reference number in square brackets and should be arranged sequentially as they appear in the text. Ethiopian names may be given in direct order, i.e. given name followed by father's name. All main words in titles (papers, books, reports) should be initialized by capital letters. Items in citations should be separated by commas. Page numbers should be included whenever applicable

.

Examples:

1. ***References to Journal Articles and Proceedings***

   Spillers,W.R. and Lefeochilos, E., "*Geometric Optimization Using Simple Code Representation*", Journal of the Structural Division, ASCE, vol. 106, no. ST5, 1980, pp. 959-971.

2. ***References to Books and Reports***

   Korsch, H.L. and Jodl, H. –J., "*Chaos: A Program Collection for the PC*", Springer-Verlag, 1994.

12. Units: *SI* units must be used.

13. Conclusions: A set of conclusions must be included at the end of the paper.

14. Submission of Paper:

Any paper submitted for publication in ZEDE must not have been published previously, or submitted for publication elsewhere; and if accepted for publication by ZEDE, the author/s shall transfer the copy right to ZEDE.

NATIONAL AND INTERNATIONAL ADVISORY BOARD

Prof. Abrham Engida, Michigan State University, USA

Ato Asrat Bulbula, Consultant, Ethiopia

Dr. Anuradha Jabasingh, Addis Ababa University

Dr. Beshawired Ayalew, Clenson University, USA

Prof. Carlo Rafele, Politechinico, Italy

Prof. Ja Choon Koo, Sungkyunkwan University, Korea

Prof. Amde M. Amde, University of Maryland, USA

Prof. Beyong Soo Lim National University of Korea

Dr. Fekadu Shewarega, Universitaet-Duisburg, Essen, Germany

Prof. Gunter Busch, TU-Cottbus, Cottbus, Germany

Dr. Kibret Mequanint, University of Western Ontario, Canada

Dr. Mekonnen Gebremichael, University of Connecticut, USA

Dr. Mulugeta Metaferia, Consultant, Ethiopia

Dr. Solomon Assefa, IBM, USA

Dr. Tesfaye Bayou, Consultant, Ethiopia

Dr. Woubshet Berhanu, Self Help Africa, Ethiopia

ACKNOWLEDGEMENTS

The Editorial Board of Zede Journal of Ethiopian Engineers and Architects would like to express its sincere gratitude to the following individuals for reviewing the manuscripts that were originally submitted for publication in Zede Volume: 41

Dr. Abrham Gebre
Dr. Anuradha Jabasingh
Prof. Byong Soo Lim
Dr. Bedilu Habte
Dr. Beteley Tekola
Dr. Celestin Nkundineza
Dr. Dereje Shiferaw
Dr. Edessa Diribssa
Dr. Getachew Biru
Dr. Eshetie Berhan

Dr. Getu Segni
Dr. Haileleoul Shhle
Prof. Joo Wun Kang
Dr. Mengesha Mamo
Dr. Matiyas Bezabeh
Prof. Ngendra P. Singh
Dr. Solomon Melaku
Dr. Solomon Tesfamaria
Dr. Tesfaye Alemu
Dr. Yohannes Legesse

Berhanu Bekeko (Managing Editor)

INVESTIGATING THE EFFECT OF SLUDGE/CLAY RATIO AND FIRING TEMPERATURE ON THE COMPRESSION STRENGTH AND WATER ABSORPTION CAPACITY OF BRICK USING RESPONSE SURFACE METHODOLOGY

Tsegay Gebremedhin[1], Shimelis Kebede [2*], Zebene Kiflie[2]

[1] Department of Chemical Engineering, College of Engineering, Debrebirhan University, Debrebirhan, Ethiopia.

[2, *] School of Chemical and Bio Engineering, Addis Ababa Institute of Technology, Addis Ababa University, Addis Ababa, Ethiopia

Corresponding author's Email : shimelis.kebede@aait.edu.et

ABSTRACT

Presently, the sludge generated from the Zero Liquid Discharge (ZLD) facility in Hawassa Industrial Park is collected inside a nearby big constructed shed without any treatment. This study investigated the utilization of this textile sludge as input for the production of brick construction material as the sludge management tool. The study focused on finding optimum parameters for the production of bricks using response surface methodology. The proportion of sludge mix and the firing temperature were selected as the study independent parameters with the compressive strength and water absorption as the experimental responses. Based on the analysis of variance (ANOVA), linear and quadratic model equations were selected for compressive strength and water absorption capacity, respectively. The regression analyses have shown that the model equations ware satisfactory enough to predict the selected responses within the experimental range with 94.98 % and 99.71 % variability in the same order. Based on numerical optimization, a sludge mix of 18.66 % and a temperature of 1000^{o}C were selected as optimum synthesis parameters predicting bricks with 3.5 MPa comprehensive strength and 16 % water absorption.

Keywords: Statistical Optimization, textile sludge, bricks, zero liquid discharge.

1. INTRODUCTION

The world's ever-increasing population and the progressive adoption of industrial-based lifestyle have inevitably led to an increased anthropogenic impact on the biosphere [1]. Generally speaking, environmental pollution is a serious global environmental issue due to an unavoidable consequence of economic development and people's desire to improve their standard of living [2]. Among the worldwide environmental problems, sludge generated from industrial wastewater treatment plants and dumped as worthless material is one of the major issues.

Industries have a decisive role in the economic development of a country. This can be seen from two main perspectives. Primarily, they employ a significant number of people and create a good opportunity for knowledge as well as technology transfer.

Secondly, they generate a high amount of foreign exchange. More specifically, the textile industry is one of the prominent industries that plays a crucial role in the development of a country as far as it produces one of the basic needs of human beings - clothe materials.

The textile industry is both water and chemicals intensive in its manufacturing and treatment processes [3]. As a result, it discharges wastewater effluents containing various pollutants. For purifying such waste water to an allowable discharge limit, various treatment processes that use conventional or zero liquid discharge technologies are employed depending on the wastewater characteristics. In both ways, a large quantity of semisolid by-product known as sludge is generated from the treatment plant. The quality and quantity of the sludge produced depend upon the amount of wastewater and the type of treatment adopted for treating the wastewater [4].

Recently, several industrial parks which use common zero liquid discharge (ZLD) facility for the treatment of the wastewater are built in Ethiopia. However, the management or recycling of the sludge discharged from the treatment plants is not considered so far. Presently, Ethiopia has inaugurated the largest industrial park in Africa named Hawassa Industrial Park aiming to produce textile and garment products. The Industrial Park uses an advanced wastewater treatment plant, the so-called ZLD facility, aiming to recycle 90 % of disposed water fulfilling international standards. However, the main problem encountered in the industrial park is the sludge disposal. The sludge generated from the ZLD facility is collected inside a nearby big constructed shed without any treatment. Since the sludge contains the chemicals removed by the purification processes, it is considered to be a non-biodegradable waste material [5].

The disposal of sludge is an inescapable by-product of textile wastewater treatment processes due to the use of various chemicals like dyes, pigments, and other complex compounds used in the manufacturing and treatment processes [3]. For this reason, it includes a cluster of organic and inorganic compounds with high concentrations of heavy metals such as Fe, Cu, Cd, Zn, Pb, Cr, etc. It also contains obnoxious odor leading to potential health and environmental threats. Compositions of sludge vary considerably depending on the wastewater composition and the treatment processes used [6].As the magnitude of the sludge produced increases, the sludge disposal problem will be escalated exorbitantly [7].

There are different sludge management methods that are in use to date. These include use of the sludge as fertilizer for agriculture, incineration, land filling, mixing with cement, as a substrate for biogas generation, as an additive in construction materials such as concrete, bricks, tiles, etc. [8]. The conventional management methods like land filling and incineration may not be suitable. Landfill disposal of the sludge has drawbacks like high cost of transportation, difficulty in getting suitable sites for land filling, heavy metal contamination of the land, emission of foul gases, etc., [9]. The residues from the sludge incinerators can also induce secondary pollution [10]. The use of textile sludge in construction materials could serve as an alternative solution to disposal and reduce pollution provided that it satisfies the engineering properties of building materials and leaches toxic metals to a permissible limit [11]. Thus, this mechanism is a win-win strategy for the reason that it not only converts the wastes into useful construction materials but also improves the environmental quality [12]. This is owing to the destruction of the toxic elements and oxidation of organic matter in the sludge while at the same time eliminating pathogens during firing [13]. Some studies have revealed that during the firing process, heavy metals' transformation may take place significantly reducing their concentration [14]. However, the amount of textile sludge used as a partial substitute in the production of construction materials such as bricks directly affects the quality of the final product. Furthermore, the production of textile sludge-based bricks mainly depends on the percentage of sludge mix and firing temperature. Therefore, in order to get a good quality of product in terms of mechanical strength and water absorption, the two parameters need to be optimized.

In different preceding studies, these operational parameters have been investigated using the "one-factor-at-a-time approach". Although such kind of approach is a common and acceptable approach, it lacks in estimating the interaction effects between the factors and predictive capability [15].

This study has attempted to statistically optimize the sludge mixing proportion and firing temperature to the responses: suitability of mechanical strength and water absorption, using the central composite design (CCD) response surface methodology (RSM), Flowingly, brick samples were synthesized at the optimum statistically optimized condition and leaching tests were carried out to check the possibility of leaching of heavy metals to the environment.

2. MATERIALS AND METHODS

2.1 Raw materials

The textile sludge employed in the present study was collected from Hawassa industrial park Zero liquid discharge facility, Hawassa, Southern part of Ethiopia. The sludge was collected in the form of a semi-liquid by-product.

The clays (Red + White) and sand were collected from Ethio bricks factory, Addis Ababa, Ethiopia and nearby construction site, respectively. Red clay has relatively high amount of iron oxide, and a small amount of magnesia, but the white clay has small amount of iron oxide.

2.2 Design of experiment

The statistical optimization of synthesis parameters is used to determine the best condition of the selected operational factors that can be suitable to produce the best quality of final product bricks in terms of mechanical strength and water absorption. The experiments were designed based on the central composite design (CCD) of the response surface methodology (RSM). To examine the effects of synthesis parameters on the mechanical strength and water absorption, two important factors were selected and designated as A (percentage of sludge mix) and B (firing temperature). The selected factors and their levels are given in Table 1.

Table 1: Selected Experimental factors and levels

Designation	Factors	Unit	Levels		
			Low (-1)	Medium (0)	High (+)
A	Sludge Mix	%	10	15	20
B	Firing temperature	ºC	800	900	1000

Based on RSM-CCD a total number of 13 experiments (8 factor and 5 center points) were determined using the following formula.

$$N = 2^k + 2k + C \quad (1)$$

Where N is the number of the experimental run, k is number of factors, 2^k points are in the corners, 2k axial points and C is a central replication point [16]. Table 2 shows all experimental points which are arranged according to RSM-CCD.

A second-order polynomial equation was used to find the interaction effects between the study factor and pinpoint the optimum synthesis parameter on the given response. For the selected two factors, the general equation can be expressed as:

$$Y = \beta o + \beta_1 A + \beta_2 B + \beta_{12} AB + \beta_{11} A^2 + \beta_{22} B^2 + \varepsilon \quad (2)$$

Where Y is the response factor which maybe mechanical strength or water absorption, βo is a constant term, A is sludge mix, B is the firing temperature, β_{is} are the coefficients for linear factor, β_{ij}s are the coefficients for cross-product interaction factors, β_{ii}s are the coefficients for quadratic factors and ε is the random error [17]. The regression analysis and estimation of these coefficients on experimental data were performed using statistical software package Design-Expert® version 10.0.1.0 (Stat-Ease, Inc. 2016). Analysis of variance (ANOVA) was employed to evaluate the adequacy of the model equations. The goodness of fit of the model equations was expressed using a coefficient of determination (R^2), prediction coefficients of determination (Pred R^2), and adjusted coefficients of determination (adj-R^2). Furthermore, their statistical significance was evaluated based on the F-test, P-value, and coefficients of variation (CV).

Table 2: Central composite design experimental points with actual and predicted responses

Factors		Responses			
A: Firing Temperature (oC)	B: Sludge Mix (%)	Compressive strength (N/mm^2)		Water absorption (%)	
		Actual value	Predicted value	Actual value	Predicted value
900	15	3.71	3.63	14.9	14.77
900	15	3.57	3.63	14.56	14.77
1000	20	3.4	3.37	17.1	17.26
900	15	3.66	3.63	14.81	14.77
1000	10	4.2	4.32	12.4	12.36
900	10	4.17	4.10	13.22	13.38
900	20	3.03	3.15	18.98	18.74
900	15	3.67	3.63	14.72	14.77
800	20	2.93	2.94	21.33	21.41
1000	15	3.97	3.85	13.64	13.52
900	15	3.52	3.63	14.78	14.77
800	10	3.83	3.88	15.7	15.58
800	15	3.5	3.41	17.17	17.21

2.3 Brick preparation

The textile sludge sample was kept in a refrigerator at 4℃ before use. It was then dried in an oven at 105 ℃ for 24h, was crushed to powder and sieved to less than 1 mm. Then, the sample was packed in airtight sealed polyethylene bags until further analysis and preparation of bricks. For the preparation of sludge-based bricks, the proportion of sludge mixing was varied from 10 to 20 % by dry weight and firing temperature from 800 to 1000°C as indicated in Table 2. The textile sludge was used to replace both clays' proportions which are practiced in commercial brick factories i.e., the ratio of three white soil to one red soil.

Primarily, dry mixing of the aforementioned raw materials was done for proper homogenization. Thereafter, the mixture was mixed properly by adding a sufficient amount of water. Finally, it was transferred into an oil-lubricated mold to obtain the desired shape. Mold size of 10 x 10 x 5 cm^3 was used to shape the mixed materials into bricks. The molded brick specimens were then kept inside the laboratory (20°C and % 51.1relative humidity) for a week and 2 days for uniform drying.

Before the firing process began, most of the water was evaporated in this process aiming to prevent cracking. After nine days of the air-drying period, the bricks were ready for firing. The dried bricks were fired in a muffle furnace (Nabertherm, LH 60/40, Germany) at temperatures of 800, 900 and 1000°C, respectively. The sintering process was performed for 3 h with different heating rates corresponding with the temperature. Consequently, the bricks were allowed to cool naturally and transferred for physical and mechanical property analysis test.

2.4 Characterization of textile sludge

The textile sludge used in this study was characterized by various parameters. The organic content, proximate components, heavy metals and chemical constituents were determined as per by standard APHA method (APHA, 1998), ASTM and AOAC (2000), respectively. The pH and calorific value were determined using digital pH meter and adiabatic oxygen bomb calorimeter.

The proximate analysis includes the determination of moisture content, volatile organic matter, fixed carbon and ash content present in the sludge sample. The moisture content was determined by drying a weighed quantity of the sludge sample in an oven at 105℃ for 24 hours and taking the difference. It was determined according to the APHA method (APHA 2540 G). The amount of VOC was determined by igniting the oven-dried textile sludge sample in a muffle furnace according to ASTM (ASTM D 3175). The ash content was determined by burning the sample in a muffle furnace according to AOAC (2000) using the official method 923.03. The percentage of fixed carbon was determined directly by deducting the sum of total volatile matter and ash percentage from 100. Furthermore, the extent of organic compounds was evaluated by chemical oxygen demand (COD), biological oxygen demand (BOD), and total organic carbon (TOC) test. More specifically, the BOD was determined by the BOD apparatus and using analytical reagents. The formula used to compute the BOD_5 was taken from the difference of initial and final dissolved oxygen according to standard methods for the examination of wastewater (APHA 5210 B).COD determination was used to measure the organic and inorganic matter content by digesting it in a COD reactor followed by spectrophotometer measurement. The total organic carbon (TOC) measurement was also performed using TOC analyzer (Shimadzu TOX-5000). In the same manner, the heavy metal analysis for Cr, Cd, Mg, Ca, Mn, Pb, Fe, Cu, Ni, and Zn were conducted using flame Atomic Absorption Spectrophotometer (PG 990, FAAS Hydride and cold Hg technique, Germany) by applying digestion of the textile sludge before investigation. Lastly, to determine the chemical constituents in the textile sludge X-ray fluorescence (Thermo Fisher ARL 9900, United States) and chemical analysis (ASTM C 114/00) methods were used.

The produced sample bricks were then tested for compressive strength and water absorption as per standards. Since the prime objective of this research was to use textile sludge waste as a resource material for making bricks, it was necessary to check the conformity of the product properties to standard values. In this regard, the compressive strength and water absorption are the most important properties that are used to determine the quality of building materials [10,18]. Accordingly, the compressive strength test was conducted using a compression testing machine (CONTROLS, USA) according to ASTM. The water absorption was measured from the ratio of the weight difference between the amount of water embedded by the brick after a 24h submersion of the test brick in water and dry weight of the unit over its dry weight.

2.5 Leachate test of the bricks

Leachate analysis test is highly important to know the concentration of the toxic heavy metals leached from the textile sludge-based bricks. The test was performed based on the procedure described by Xu et al. (2014) with minor modifications [19]. Accordingly, 10 g of brick powder (100 mesh, dry weight, precision 1 mg) and deionized water, with a powder-to-water ratio of 1:30, were mixed and stirred for 10 min, and, then, allowed to sit statically for 24 h in a conical flask with continuous stirring for 10 min every 8 h. Then, the leachate was separated from the residue by filtering through a filter paper and transferred into a 500-ml volumetric flask and diluted to the mark with deionized water. Finally, the heavy metals were measured by Inductively Coupled Plasma (ICP-OES) examination method.

3. RESULTS AND DISCUSSION

3.1 Characteristics of the textile sludge

Table 3 shows the overall physic-chemical characteristics of textile sludge. The textile sludge was alkaline with pH range of 8.1 – 8.4 with a mean value of 8.2. Previous studies have also reported pH values in the range of 7.8 to 9 similar to the present findings [12,20]. Such pH values may be due to the addition of coagulating chemicals during the pre-treatment stage of textile wastewater.

The heating value of the textile sludge was found to be 7867.26 kJ/kg. The calorific value of the present study doesn’t show a significant variation as compared to the result reported in different literatures. This might be due to the existence of a high level of organic chemical compounds in the sludge. Such calorific value can be related high carbon content which may reduce the strengths of concrete and increase the shrinkage upon drying.

The results obtained for BOD, COD, and TOC were 535 mg/l, 9820 mg/l, and 51.3 %, respectively. These indicate that the textile sludge has a high amount of organic and inorganic pollutants which may be attributed to the addition of various chemicals in the production process as well as in the wastewater treatment stage. Patel & Pandey (2017) have reported the value of total organic carbon (TOC) in the range from 1.23 % to 17.82% [12]. However, this shows that the TOC found in our study is much higher than that reported above and this difference may be due to the difference in chemical doses and treatment processes practiced from industry to industry. The COD and BOD values were also found a bit higher as compared to the allowable discharge limits indicated in the Ethiopian provisional standards for industrial pollution control.

The proximate analysis results are given in Table 3. The results show that the moisture, ash, organic matter, and fixed carbon contents of the textile sludge were 82.5%, 44%, 48.4%, and 7.6%, respectively. This result shows that the sludge released from the ZLD facility has a high amount of moisture, ash and organic content (volatile matter) but with low amount of fixed carbon.

Table 3: Physico-chemical characteristics of textile sludge sample

physic-chemical analysis	Results
pH	8.2
Calorific value (cal/g)	1880.32
BOD (mg/l)	535
COD (mg/l)	9820
TOC (%)	51.3
Proximate analysis (%)	
Moisture content	82.5
Ash	44
Volatile organic matter	48.4
Fixed carbon	7.6
Heavy Metals (mg/kg)	
Cu	5.23
Zn	30.45
Fe	323.63
Pb	2.25
SiO_2	279.60
Ca	0.28
Mg	3.58
Cd	ND
Cr	8.08
Mn	6.75
Ni	ND

ND: not detected

The investigation of the inorganic elements content of the textile sludge sample, particularly the heavy metals is also reported in the same table. The results show that iron is found as the leading constituent and the most harmful metals Cd and Ni are below discharging permissible limits by USEPA. The high concentration of iron could be owed to the addition of chemical coagulants such as iron chloride in the treatment process. The concentration of lead is also below the regulatory limits of the provisional standards for industrial pollution control in Ethiopia. On the contrary, among the toxic heavy metals that commonly exist in textile sludge, only Cu, Zn and Cr were found to be a little bit above the permissible limit values.

The heavy metal concentrations reported in the literature differ from researcher to researcher. This is because the presence of heavy metals in the sludge is highly dependent on the dosage of the dyes, water and other chemicals utilized in the manufacturing process [5,8,10–12,18,21–23]. The literature results show the concentration of the heavy metals is quite high while the findings of this study are not as significant. Nevertheless, the disposal of this sludge to the environment can cause a considerable risk. So, it is very important to use it such as for the manufacturing of bricks or use as partial substitution of cement raw materials.

As can be seen in Table 4, the textile sludge is composed of high amounts of alumina (Al_2O_3) and silica (SiO_2) as compared to the other compounds. This chemical composition data indicates that the textile sludge has the potential to be used as a partial substitute of clay soil for making building materials such as bricks. However, it is hard to use it alone due to the less quantity of mineral oxides that do not fulfill the average amount of oxide requirements. The characteristics of good bricks is largely dependent on the main chemical constituents and respective proportions: silica (50-60%), alumina (20-30%), lime (2-5 %), ferric oxide (5-6%) and magnesia (<1%) [24].

The existence of these components plays a significant role in the property of bricks. The presence of silica prevents cracking, shrinking and warping of raw bricks. The occurrence of alumina imparts plasticity to earth so that it can be molded easily. Simultaneously, iron oxide acts as a flux to cause the grains of sand to melt and this helps to bind the particles together and it imparts red color to brick on burning [5].

The chemical composition of the sludge is very much related to the minerals found in clay but with a lower amount. As given in Table 4, the main components of textile sludge are CaO (2.56%), Al_2O_3 (21.4%), SiO_2 (16.1%), and Fe_2O_3 (2.32%). This shows that the textile sludge has similar components to clay, which means a likeness in terms of composition to clay, although not in percentage quantities. Conversely, as can be seen in the same table, the quantity of the silica content in the sludge is exceptionally low which is 16.10 to 18.5 % according to the chemical and XRF analysis. The test result implies that it has a much lower amount of silica than that in the standard range, i.e., 50 – 70 % in building materials.

Several researchers have described the great role of silica content in the strength of bricks. For instance, Hegazy et al. (2012), revealed that the strength of brick is highly dependent on the amount of silica in the raw materials which implies that the higher the silica, content the stronger are the bricks [25]. Moreover, the less amount of silica in the sludge indicates it lacks the binding property if it is used as an additive in building material. On the other hand, the quantities of the rest of the principal chemical compounds satisfy more or less the minimum percentage requirements. Also, the high value of the loss on ignition (L.O.I), with weight loss of approximately 51% indicates the availability of high volatile and organic content in the sludge [19].

The present study shows the same chemical compositions as reported by Rahman et al.[11]. However, it is not quite consistent with other results reported in different studies in the literature [10,12,26]. This might be due to the variation of the chemicals and other compounds utilized in the wastewater treatment plant and the manufacturing processes.

Therefore, the above results suggest that textile sludge is suitable to make bricks by partially replacing some percentage of the other materials such as clay material to get the required amount of chemical composition in the mixture.

Table 4: Chemical composition of textile sludge

Composition	Chemical analysis Content by weight (%)	XRF analysis Content by weight (%)
CaO	2.56	9.8
SiO_2	16.10	18.15
Al_2O_3	21.40	25.3
Fe_2O_3	2.32	3.12
MgO	1.51	3.11
SO_3	0.94	5.88
LOI	51.3	ND
Na_2O	ND	2.75
K_2O	ND	0.27

ND: not detected

3.2 Statistical analysis and optimization of bricks synthesis parameters

For statistical analysis and optimization of bricks synthesis parameters, a total of 13 experimental runs were carried out according to RSM-CCD. The results from bricks characterization, i.e., compressive strength, and water absorption, were used as study responses. Table 2 shows the experimental runs with the actual and predicted responses. To obtain the best model equation that would describe the relationship between the two study factors and the responses, the sequential model sum of squares model fitting was employed. Accordingly, the linear and quadratic model equations were selected for compressive strength and water absorption capacity, respectively. The two model equations can be written in terms of coded study factors: firing temperature (A) and sludge mix (B) as follows:

$$\text{Compressive strength} = 3.08 + 2.18 \text{ x } 10^{-3}A - 0.09B \quad (3)$$

$$\text{Water adsorption} = 76.738 - 0.118\text{A} - 0.592\text{B} - 4.650 \text{ x } 10^{-4}\text{AB} + 5.937A^2 + 0.052B^2 \quad (4)$$

The adequacies of these models were also investigated using the regression coefficient (R^2), which were found to be 0.9498 and 0.9971, respectively. These indicate that the model equations are adequate to predict the selected responses in the experimental range with 94.98 % and 99.71 % variability. respectively In other words, only 5.02 and 0.29 % of residual variability can be seen in the estimation of compressive strength and water absorption capacity, respectively. This is further confirmed from the actual and the predicted values that are in agreement as depicted in Table 2. The Pred R^2 show that the model equations for compressive strength and water adsorption give good predictions with 90.88 % and 97.88 % variability, respectively. In addition, the adj-R^2 of 93.98 % for compressive strength and 99.50 % for water absorption were in a reasonable agreement with Pred R^2 values i.e., the difference is less than 0.2. The degree of precision and reliability can be explained by the low values of coefficients of variable (CV) which were 2.58 % for compressive strength and 1.11 % for water absorption. Furthermore, adequacy precision for each response was found to be 31.025 and 76.906. Adequacy precision measures the signal to noise ratio. A ratio greater than 4 is desirable. The results indicated in this study show an adequate signal. Therefore, the two models can be used to navigate the design space.

The analysis of variance (ANOVA) for the suggested linear and second-order quadratic models shows F-values of 94.62 and 480.89 for compressive strength and water absorption, respectively. The P–values for the two responses also obtained are <0. 0001.These two results confirm that the adequacy of the model fits and the significance of each of the coefficients in the model equation [27].

Furthermore, the adequacy of the model was checked by constructing different diagnostic plots for the two responses as shown in Figures 1, 2, 3, 4, 5 and 6. The normal % probability plots of residuals for the responses were normally distributed, as they lie reasonably close to the straight line and show no deviation of the variance (Figures 1 and 2). Internally studentized residuals plots that were constructed to facilitate the satisfactory fit of the developed model and the plots (Figures 3 and 8) show that all the data points lie within the limits (±3). The predicted values obtained from the suggested models were quite close to the experimental values and lie reasonably close to the straight line and indicate the adequate agreement with real data (Figure 5 and 6).

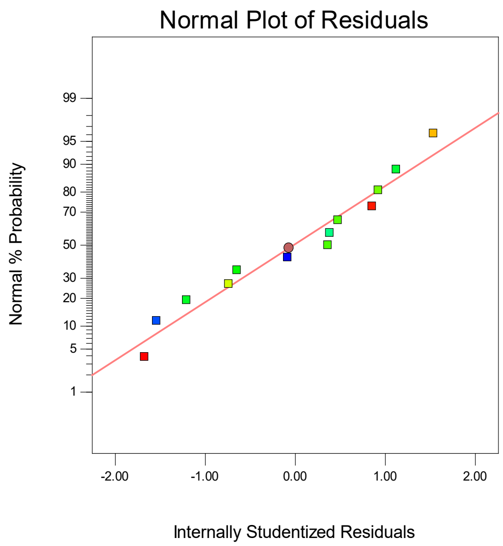

Figure 1. Normal plot of residual for compressive strength

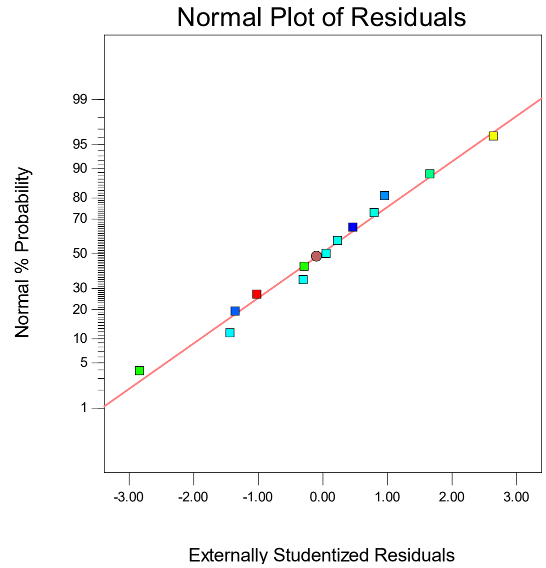

Figure 2. Normal plot of residual for water absorption

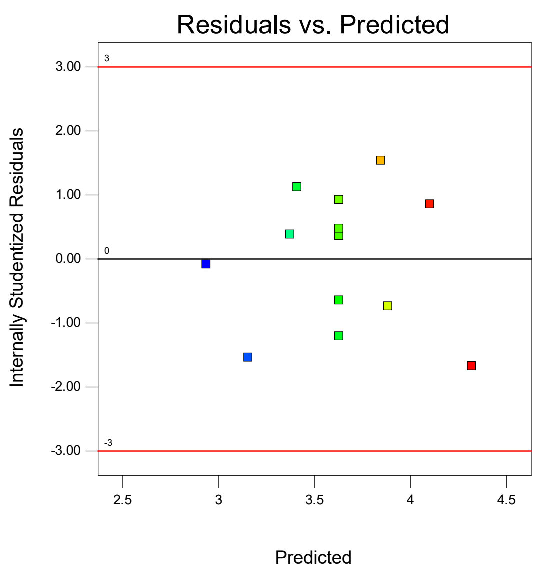

Figure 3. Residual vs. predicted response plot for compressive strength

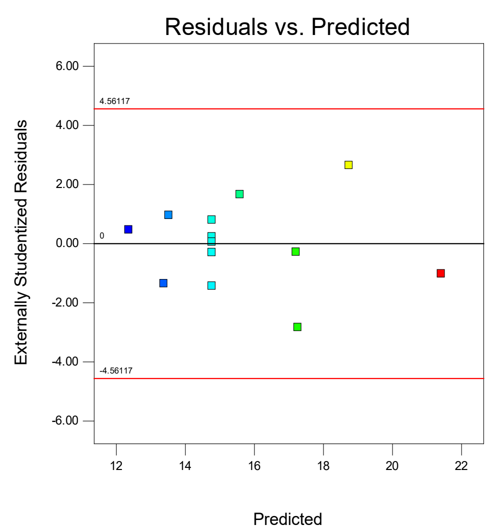

Figure 4. Residual vs. predicted response plot for water absorption

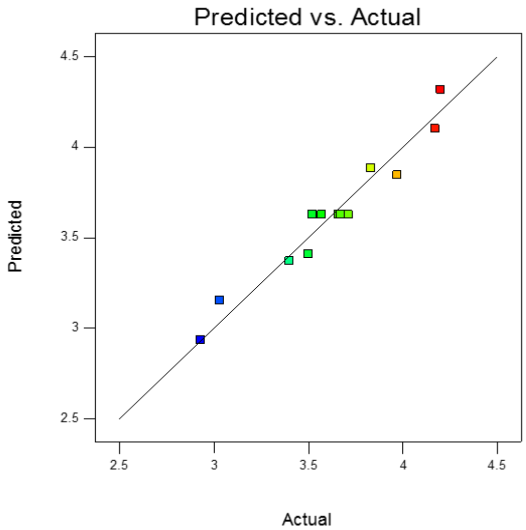

Figure 5. Actual and predicted values plot for compressive strength

3.3 Effect of sludge content on bricks compressive strength

Figure 7 shows effect of textile sludge mix proportion on the compressive strength of bricks. The mixing ratio of sludge has a great influence on the compressive strength of the bricks. As shown in the figure, compressive strength is found to be inversely proportional to the sludge content. This may be because the sludge has much less amount of silica and therefore an increase in sludge content creates low binding power with the clay [28].The study shows that the sludge content (10 %) gives quite high compressive strength (4.20 MPa) at 1000 ºC firing temperature. It is worth to note that the minimum compressive requirement of bricks which is 3.5 MPa according to ASTM is surpassed by all bricks prepared up to the sludge composition of 15% and fired at all temperatures investigated. In this study, the values of compressive strength obtained for 20 % of sludge mix at all firing temperature were below the minimum compressive strength requirement.

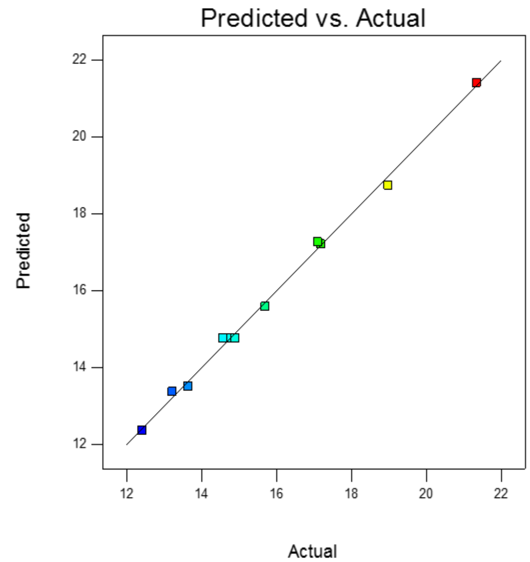

Figure 6. Actual and predicted values plot for water absorption

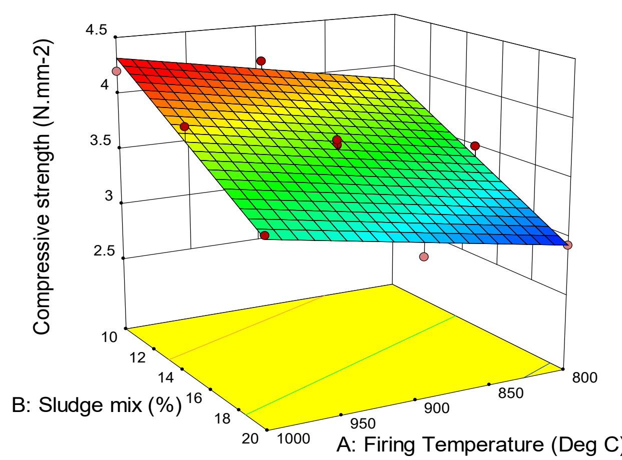

Figure 7. Three-dimensional response surface plots for compressive strength as a function of sludge mix and firing temperature

3.4 Effect of sludge content on water absorption

As can be observed from Figure8, water absorption increases with increase in sludge content. This is because of increased number of pores in the brick resulting from burning of organic matter present in the sludge. More than 21 % of water absorption was recorded for the sample prepared at 20 % sludge mix and firing temperature of 800 ºC. In general, the higher the percentage of sludge, the higher the water absorption becomes, resulting in lower quality bricks since the two important quality parameters, i.e., durability and resistance to the natural environment are inversely proportional to water absorption of the bricks [10].

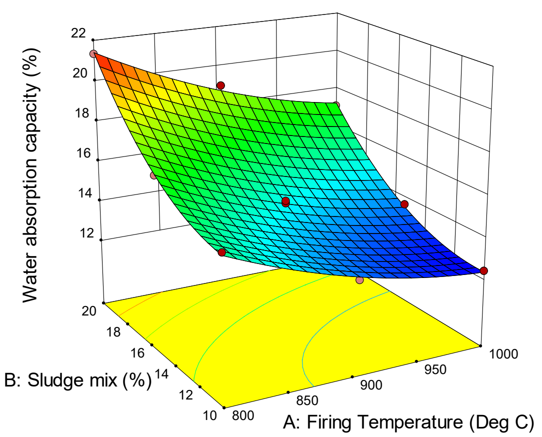

Figure 8. Three-dimensional response surface plots for water absorption as a function of sludge mix and firing temperature

3.5 Effect of firing temperature on bricks compressive strength

The burning process of bricks has a direct impact on the final product quality of the brick material because the firing process essentially involves the oxidation of organic matter, the transformation of inorganic components into less harmful compounds and the elimination of the pathogens that exist in the sludge to reduce public health impact. The mineral compositions are transformed to increase the durability and strength. During firing the minerals are fused and undergo chemical reactions forming complex compounds at high temperature. For this reason, firing temperature is an important factor that greatly affects the property of the final brick such as compressive strength.

Figure7 shows the effect of firing temperature on compressive strength in the temperature range of 800ºC-1000ºC.As can be observed from the same figure, the compressive strength is seen to increase with temperature for all the mixing proportions of the sludge. The compressive strength increased from 2.93 to 4.20 Mpa as the temperature increased and sludge content decreased from 20% to 10%. More specifically, the compressive strength of 10% sludge content fired at higher temperature nearly reaches the maximum compressive strength of 4.2 MPa.

Furthermore, the 20% sludge content fired at 1000°C was cracked and deformed its shape exceptionally. In general, during the firing process the atomic bonding of particles increase by the mechanism of diffusion creating a denser material and conversely, this leads the brick to shrink progressively [21].

3.6 Effect of firing temperature on bricks water absorption

Water absorption does not only depend on the proportion of sludge mix but also on firing temperature (Figure8). In this particular study, water absorption of the bricks was found to decrease with increase in firing temperatures for all sludge mix proportions. In general, water absorption is expected to increase at maximum sludge mix and firing temperature due to formation of void space during the baking process [28]. However, after a certain firing temperature these voids collapse and shrink and result in lower water absorption. As shown in the figure, for brick samples made at different sludge mix show a significant increment of water absorption from 12.4 to 21.33% when they were subjected to different firing temperatures. Generally, lower water absorption bricks are more durable than those with higher water absorption.

3.7 Optimization and verification of bricks synthesis parameters

Based on Derringer's desirability function approach for multiple response processes, the desired set of bricks synthesis parameters were determined through numerical optimization which searched the design space, using the two model equations created during analysis to find factor settings that meet the defined goals. To get the best optimum parameters, the compressive strength was targeted to be 3.5 MPa (according to ASTM minimum requirement), water absorption was set to be minimum, sludge mix set to be maximum in order to utilize more textile sludge and the firing temperature was selected to be in the range. Accordingly, the optimum synthesis parameters were found to be the proportion of sludge mix 18.66% and firing temperature of 1000 ºC with 0.802 % desirability to predict the compressive strength of 3.5 MPa and 16 % water absorption. Some researchers have suggested to use up to 30 % textile sludge to replace Portland cement in the preparation of building materials and reported that as the sludge mix is getting higher, the compressive strength of the brick drops gradually[8,21]. Based on the results obtained by Baskar et al. (2006), the addition of textile sludge up to 9% is effective enough to make brick material at a temperature of 800℃ and obtain a compressive strength of 3.54 MPa. Besides, according to Jahagirdar et al. (2013), textile sludge content of up to 15% was recommended to obtain values of the compressive strength exceeding 3.5 MPa. The water absorption also should be less than 20% in order to get more durable bricks[28].

To validate the predicted two response values, three samples were prepared under the selected optimum parameters and mean compressive strength and water absorption value of 3.87 ± 0.27 % and 15.12 ± 0.56 were obtained, respectively. The values are very close with the data obtained from numerical optimization analysis and the model equations can be potentially used to predict synthesis parameters in the same preparation conditions.

3.8 Leachate test

The textile sludge-based sample brick prepared at the optimum synthesis parameter was subjected for leaching test. Table 5shows the leachability result for the textile sludge-based bricks. The results indicate that the elements Tn, Cr, Ni, and Hg have shown relatively maximum concentrations in descending order whereas other metals such as Cd, As, Pb, Zn, and Cu have shown minimum leachability from the brick sample. However, as the test results show, the concentrations of all heavy metals were found within the allowable limits as given in the USEPA standard. This may be due to the phenomenon that some of the heavy metals in the sludge were transformed at the high firing temperature during sintering process, thus reducing the heavy metals inside the brick. The results indicated that the addition of textile sludge up to 18 -19 % composition into clay to produce bricks is possible and the heavy metals concentration was reduced significantly when incorporated into fired clay bricks. Therefore, this research shows the suitability of textile sludge as a partial substitute of clay for making bricks but recommended with quite moderate quantity which is up to 19 % and fired at high temperature (1000 ºC).

Table 5: Leachate analysis test results for sample bricks prepared at optimum synthesis parameter

Parameters		Content (mg/l)	USEPA Concentration limit (mg/l)
Copper	Cu	0.003	100
Iron	Fe	0.006	ND
Zinc	Zn	0.003	500
Nickel	Ni	0.048	1.3
Cobalt	Co	0.004	ND
Manganese	Mn	0.006	260
Chromium	Cr	0.053	5.0
Cadmium	Cd	0.001	1.0
Mercury	Hg	0.045	0.2
Tin	Sn	0.066	ND
Lead	Pb	0.003	5.0
Arsenic	As	<0.001	5.0
Boron	B	0.0295	ND

ND not detected

4. CONCLUSIONS

In the present study, the textile sludge-based synthesis parameters were investigated and statistically optimized using the RSM-CCD. The study has revealed that the statistical experimental method can be used as an excellent tool to identify the interaction effects of the individual synthesis parameters for bricks production. It was found that the compressive strength drops gradually as sludge proportion increases and increases progressively with firing temperature. Consequently, a good compressive strength result can be achieved at a higher temperature and smaller sludge proportion. Besides, the study has shown that the addition of sludge affects the water absorption to rise gradually with increase in sludge content. Under the optimized synthesis and firing condition, i.e., sludge mix of 18.66 % and firing temperature of 1000 ºC, 3.5 MPa comprehensive strength and water absorption of 16 % were predicted. Leachate analysis test shave shown minimum leachability of heavy metals. Based on the present findings, it can be concluded that utilization of textile sludge as partial substitute of clay in bricks production can potentially reduce textile sludge disposal and associated environmental problems.

ACKNOWLEDGMENTS

The authors are grateful to Industrial Parks Development Corporation of Ethiopia for facilitating the Textile Sludge collection from Hawassa Industrial Park Zero Liquid Discharge Facility.

CONFLICT OF INTEREST

The authors declare that they have no conflict of interest.

REFERENCES

[1] Gowdy J. "*Our hunter-gatherer future: Climate change, agriculture and uncivilization*," Futures, vol.. 115, 2020,pp.102888.

[2] Ali, S.H., Puppim J.A., Environ, D.O. and Lett, R.,"*Pollution and economic development : an empirical research*

review Pollution and economic development : an empirical research review",Environmental Research Letters, vol. 13, no, 12,2018,pp. 123003.

[3] Adane T, Adugna T, and Alemayehu E., "T*extile Industry Effluent Treatment Techniques*", Journal of Chemistry, vol. 2021,pp.1-14.

[4] Jahan, N, Tahmid, M, Shoronika, A.Z, and Farhia, A.,"*A Comprehensive Review on the Sustainable Treatment of Textile Wastewater: Zero Liquid Discharge and Resource Recovery Perspectives*", Sustainability (Switzerland), vol. 14,2022,pp.15398.

[5] Azanaw, A, Birlie, B, Teshome, B. and Jemberie, M., "*Textile effluent treatment methods and eco-friendly resolution of textile wastewater*", Case Studies in Chemical and Environmental Engineering, vol. 6, 2022,pp.100230.

[6] Yaseen,D.A. andScholz, M., "*Textile dye wastewater characteristics and constituents of synthetic effluents: a critical review*", International Journal of Environmental Science and Technology, vol. 16, 2019,pp.1193-1226.

[7] Zhang X, WangX.Q. and WangD.F. "I*mmobilization of heavy metals in sewage sludge during land application process in China: A review*", Sustainability (Switzerland), vol. 9, 2020,pp.1-19.

[8] Guha, A.K., Rahman, O., Das, S. and Hossain, S.,"*Characterization and Composting of Textile Sludge*", Resour Environ, vol. 5, 2015,pp.53–8.

[9] Abdel-Shafy,H.I. and Mansour,M.S.M., "*Solid waste issue: Sources, composition, disposal, recycling, and valorization*", Egyptian Journal of Petroleum, vol. 27, 2018,pp.1275-1290.

[10] Assi,A,Bilo, F, Zanoletti, A, Ponti, J. and Valsesia, A, La Spina, R, Depero, L.E, and Bontempi E."*Review of the reuse possibilities concerning ash residues from thermal process in a medium-sized urban system in Northern Italy*", Sustainability (Switzerland), vol. 12,2020,pp.1-21.

[11] Rahman, M.M., Khan, M.M.R., Uddin, M.T.andIslam M.A.,"*Textile Effluent Treatment Plant Sludge: Characterization and Utilization in Building Materials*", Arab J Sci Eng , vol. 42, 2017, pp.1435–1442.

[12] Patel, K., Patel, R.L. and Pitroda, J.,"*Technical Feasibility Study on Utilization of Textile Sludge as a Cement Substitute in Rubber Mould Paver Block*',' Int J Constr Res Civ Eng,vol. 3, 2017, pp.19–25.

[13] Liew, C.S., Yunus, N.M., Chidi, B.S., Lam, M.K., Goh P.S., Mohamad M., Sin, J.C., Lim J.W. and Lam S.S., "*A review on recent disposal of hazardous sewage sludge via anaerobic digestion and novel composting*", J Hazard Mater, vol. 423,2022,pp.126995.

[14] Iqbal, S.A., Mahmud, I. and Quader A.K.M.A.,"*Textile sludge management by incineration technique*", Procedia Eng,vol. 90, pp. 686–691.

[15] Kassahun, S.K., Zebene,K., Shin D.W., Park, S.S., Jung, W.Y. and Chung, Y.R.,"*Optimization of sol-gel synthesis parameters in the*

preparation of N-doped TiO_2 using surface response methodology", J Sol-Gel Sci Technol, vol.82, 2017, pp.322–334.

[16] Saeed M.O., Azizli K., Isa M.H., Bashir M. "*Application of CCD in RSM to obtain optimize treatment of POME using Fenton oxidation process*" J Water Process Eng , vol. 8, 2015, pp. 7–16.

[17] Antonopoulou M., Giannakas A. and Konstantinou I.,"*Simultaneous Photocatalytic Reduction of Cr(VI) and Oxidation of Benzoic Acid in Aqueous N-F-Codoped TiO_2 Suspensions: Optimization and Modeling Using the Response Surface Methodology*", Int J Photoenergy, 2012, pp. 1–10.

[18] Jahagirdar, S.S., Shrihari, S. and Manu B. "*Utilization of Textile Mill Sludge in Burnt Clay Bricks*", Int J Environ Prot, vol. 3, 2013, pp. 6–13.

[19] Xu H., Song W., Cao W., Shao G., Lu H. "*Utilization of coal gangue for the production of brick*" J Mater Cycles Waste Manag,vol. 19, 2017, pp. 1270–1278.

[20] Rahman A., Urabe T., Kishimoto N. and Mizuhara S., "*Effects of Waste Glass Additions on Quality of Textile sludge-based Bricks*" Environ Technol,Vol.36,pp. 37–41.

[21] Balasubramanian,J.,Sabumon,P.C.,Lazar,J.U. andIlangovan,R.,"*Reuse of textile effluent treatment plant sludge in building materials*",Waste Management, vol. 26, 2006, pp. 22-28.

[22] Maddumapatabandi, T.D., Silva W.R.M. and Silva K.M.N.,"*Analysis of textile sludge to develop a slow releasing organic fertilizer*", SAITM Res. Symp. Eng. Adv., vol. 2014, 2014, p. 79–82.

[23] Palanisamy V. "*Utilization of Textile Effluent Waste Sludge in Brick Production"* Int J Sci Basic Appl Res,vol. 4, 2011,pp.1–10.

[24] Johnson, O.A., Napiah, M., and Kamaruddin, I.,"*Potential uses of waste sludge in construction industry: A review"* Res J Appl Sci Eng Technol, vol.8, 2014,pp. 565–570.

[25] Hegazy, B.E.E., Fouad, H.A. andHassanain, A.M.,"*Brick Manufacturing From Water Treatment Sludge and Rice Husk Ash*",Aust J Basic Appl Sci, vol.6, 2012,pp. 453–61.

[26] Sandesh, N.U. andPrashanth,V.P.,"*A study on engineering properties of textile ETP sludge based cement concrete",* Int J Innov Eng Technol,vol.4, 2014,pp. 324-331.

[27] Rastegar, M., Shadbad, K.R., Khataee A.R. and Pourrajab, R.,"*Optimization of photocatalytic degradation of sulfonated diazo dye C.I. Reactive Green 19 using ceramic coated TiO_2 nanoparticles*", Environ Technol, vol.33, 2012, pp. 995–1003.

[28] Jahagirdar, S., Surathkal, S. and Manu, B.,"*Utilization of Textile Mill Sludge in Burnt Clay Bricks*", Int J Environ Prot, vol.3, 2013,pp. 6–13.

PROBABILISTICASSESSMENT AND FIELD TEST VERIFICATION FOR STRENGTH EVALUATION OF BRIDGE WITH DEFECTIVE GIRDER

Abrham Gebre [1,*], Esayas Gebreyouhannes[2], Yisihak Gebre[3]
[1, 2, 3] School of Civil and Environmental Engineering, Addis Ababa Institute of Technology, Addis Ababa University
[*]Corresponding author's Email: abrham_gebre@yahoo.com

ABSTRACT

The use of high-quality materials, regular inspection and testing of constituent materials, appropriate curing processes, and an acceptable overall construction methodology are all required for bridge construction. Failure to handle the aforementioned ways causes the bridge to operate poorly, jeopardizing its load-carrying capacity. As a result, determining the load carrying capacity of the bridge and assessing its safety are critical. This study investigatedthe performance of a defective girder of a Reinforced Concrete (*RC*) *bridge* (*located at km 69+937 along the Agulae-Berahle road segment*)*caused by failure of concrete to achieve the desired compressive strength. Various assessment methods were used to assess the strength of the existing defective girder. Following the uncertainty of random variables, a probabilistic assessment approach was used. A field load test was also used to correlate and verify the numerical result. The findings reveal that the bridge under investigation is safe against the design and legal loads specified in ERA Bridge Design Manual.*

Keywords: RC, deterministic approach, defective girder, probabilistic assessment, strength evaluation, uncertainty, random variables, load test

1 INTRODUCTION

The construction of a transportation network is critical for a country's development and requires significant investment. Bridges and culverts account for a significant portion of a highway project's cost. In line with this, proper construction of minor and major structures is critical, and special attention should be paid to avoid further damage throughout the operation phase. Bridge structure deficiencies are caused by design problems, poor construction quality, aging, excessive loads, maintenance negligence, and other factors. Assessing the safety of a bridge structure is a critical duty in bridge management that requires extra attention and caution. If bridge defects or construction problems are observed, load capacity of bridges will be reduced and reconstruction of these structures will consume extra time and money [1].

This study looked into performance assessment of a 20.50m defective reinforced concrete girder (bridge at km 69+937, Agula-Barahle road segment) caused by construction fault by which concrete of a lower grade than that specified in the specification has been used. The bridge was built in 2014, and a performance evaluation was conducted four years later as there was a defect on one of the interior girders (problem with concrete quality).The objective of this research was to investigate the safety level of a defective girder using numerical analysis and bridge load test. In the numerical analysis, rating factors and safety indices of the bridge were computed using deterministic and probabilistic approaches, respectively and the results were checked against the standard. For the probabilistic approach, uncertainties of variables were taken from experience and specifications. A field load test was also performed to verify the serviceability requirements of the bridge.

The analytical result was correlated with field load test and the results show that the bridge can carry the design and legal loads specified in the country's bridge design manual.

2 METHODS

2.1 Methods of Structural Assessment

Data acquisition and structural analysis are procedures for gathering necessary information about the structure's condition, which is used to access and evaluate the safety and serviceability margin where the failure zone can be estimated [2].

The deterministic approach is the most commonly used method of defining safety. It is entirely based on experience, and the safety measures are empirical in nature. Deterministic verification is characterized by simplifications and associated with those by conservative safety measures [2]. In the case of deterministic approach, all the mean values of the variables with appropriate factors stipulated in the codes are taken.

In practice, material properties, dimensions, loads, and so on, used in structural assessment have uncertainties. As a result, there is a need to consider the statistical variations of these random variables, which includes a probabilistic approach (reliability is the most reasonable approach), which allows for a more systematic determination of structural reliability [2].

In a probabilistic assessment, uncertainties and analysis variables for dead and live loads, as well as model uncertainty (NR) that accounts for error in the modeling process must be considered [3]. Furthermore, reduction of uncertainties using past experience, use of load and resistance calculation technique is possible to make the necessary decisions so that the assessment work can be completed properly [4]. The requirements to the safety of the structure are consequently expressed in terms of the accepted minimum reliability index (β) or the accepted maximum failure probability (P_f). In a general case, the probability of failure P_f is defined by the limit state function, $g(x) < 0$ and it is given in Eq. (1) [5]:

$$P_f = P\,(g(x)<0) \qquad (1)$$

where:

P_f is the probability of failure

$g(x)$ is the limit state function, design margin=$R(x)$-$S(x)$

$R(x)$ is the resistance of the section and $S(x)$ is effect of loads

For a given limit state function, the reliability index can be calculated using a direct integration method. However, determination of the safety index using the direct integration method becomes complex, especially if a number of random variables are involved (the probability integration is multidimensional). First Order Reliability Method (FORM) and the Second Order Reliability Method (SORM) are commonly used to ease the computational difficulties [5]. In most cases, empirical equations are used. In this study, as either of the random variables has log-normal distribution, the reliability index and the multiplication factor are estimated based on the expressions given in Eqs. (2) and (3), respectively [6].

$$\beta = \frac{\mu_R\left(1-k\frac{\sigma_R}{\mu_R}\right)\left[1-ln\left(1-k\frac{\sigma_R}{\mu_R}\right)\right]-\mu_s}{\sqrt{\left(\mu_R\left(1-k\frac{\sigma_R}{\mu_R}\right)\left(\frac{\sigma_R}{\mu_R}\right)\right)^2+\sigma_S^2}} \quad (2)$$

$$k = \frac{\bar{R}^e - r^*}{\sigma_R^e} \quad (3)$$

where:

β is the reliability index

μ_R and σ_R are mean and standard deviation for the resistance, respectively

$\mu_S$and $\sigma_S$are mean and standard deviation of total-load effect, respectively

k is a multiplication factor of the standard deviation

$\bar{R}^e$, σ_R^earemean and standard deviation for the resistance of the approximating normal distributions (equivalent normal parameters), respectively

r* is a design point on the failure boundary

2.2 Load Tests on Bridges

For existing bridges with large uncertainties, analytical methods have limitations, bridge load test is commonly used. It helps to determine issues that cannot be easily resolved by simple analysis [7]. A proof load test is one type of field test in which a load equal to the factored live load is applied. If the bridge can carry this load without signs of distress, the proof load test is found to be successful. A supplementary load test is also used for the assessment process and it is preferred as it involves applying a known load to the bridge [8].

2.3 Strength Evaluation

The strength evaluation of a reinforced concrete bridge with defective girder is discussed hereunder. Bridge data used in the assessment was obtained from the construction drawing (see Table 1).Design checking was also performed to ensure that the reinforcing bars used in the construction were adequate.

Table 1 Bridge data

Description	Values
Bridge span, L	20.50m
Area of main reinforcing bars	18 Φ32 in four layers
Transversal reinforcements	Φ12 c/c 130mm
Cylindrical compressive strength of concrete	16MPa
Yield strength of steel	400MPa
Girders spacing	2450mm
Web width	500mm
Girder depth	1450mm
Slab thickness	200mm

2.4 Design Review

The overall depth of the girder was checked with the design specification of AASHTO and ERA bridge design manuals (=0.07×20,500=1,435mm) and it was found out that it satisfied the minimum requirement. Web width of 500mm was used (greater than the minimum requirement, 250mm). The slab thickness was 200mm which was greater than the minimum requirement of 185mm [9, 10]. The reinforcement for the longitudinal interior defective girder using lower concrete strength was computed and is shown in Table 2.

Table 2Reinforcementsintheinterior girder

Design review result	Actual bridge detailing
17 ϕ32 in four layers (Main reinf.)	18 ϕ 32 in four layers
ϕ 12 c/c 150mm (stirrups)	ϕ 12 c/c 130mm

Overall, the findings of the design review clearly indicate that the defective girder was safe against both maximum flexural and maximum shear action with sufficient margin of safety. The adequacy of the defective girder bridge for the proposed load was comprehensively assessed and the summary report is presented here below. The design compressive strength of concrete was C30/25, however laboratory test result showed that the actual concrete grade was C20/16.

Strength evaluation of bridge is expressed in terms of rating factor (RF). It is the ratio of the available capacity of the bridge to the effect produced by the live load being investigated and it is given by Eq. (4) [8-10]:

$$RF = \frac{\varphi R_n - \gamma_{Di} D_i - \gamma_{DW} DW}{\gamma_{Li}(L_i + IM)} \tag{4}$$

where:
RF is rating factor
φR_n is nominal resistance
φ is resistance factor
D_i, DW, L_i are effect of dead, wearing surface and live loads, respectively
IM is an impact factor for the live-load effect
γ_{Di}, γ_{Dw} and γ_{Li} are load factors for dead, wearing surface and live loads, respectively

If the rating factor for legal loads exceeds 1.0, the bridge is said to be satisfactory for the legal loads and it is within the acceptable range for safety verification [8-10]. For the computation of effect of live load, a legal load type 3-2 with 32.5ton (Figure 1) given in ERA bridge design manual was used [9].

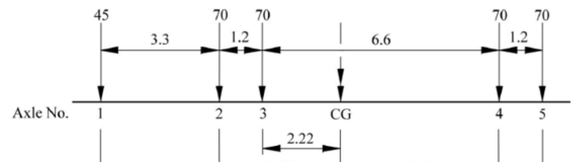

Figure 1 Truck type 3-2 axle load arrangement

The critical legal load placement (m) and axle load (ton) used for the assessment was obtained by influence line analysis. Using Response 2000 software (a reinforced concrete sectional analysis software using the modified compression field theory), the resistance of the defective girder in terms of bending moment was computed (f_y=400MPa and f_c'=16MPa). Figure 2 shows the cross-section of the defective RC girder.

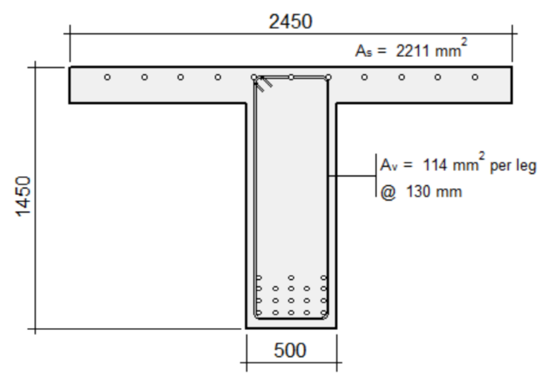

Figure 2 Cross section of an interior RC girder

In order to further investigate the load-deflection response, a nonlinear analysis was carried out on the defective girder. The analysis was conducted on COM3 platform with path and time dependent constitutive laws rooted in four-way fixed crack-approach for reinforced concrete. To reduce the computational time, the girder was modeled as half symmetry with the moving truck axle load over the bridge.

Using simple static calculations, nearly 60 % of the truck load was resisted by the defective girder for the considered truck position. As load distribution based on simple static analysis overestimates the load share of the defective bridge; however, FEM analysis was conducted to see the extreme condition to assure safety.The3D finite model of the girder is indicated in Figure 3. Here, it must be noted that, the differing values of compressive strength for the deck and the web regions was explicitly considered.

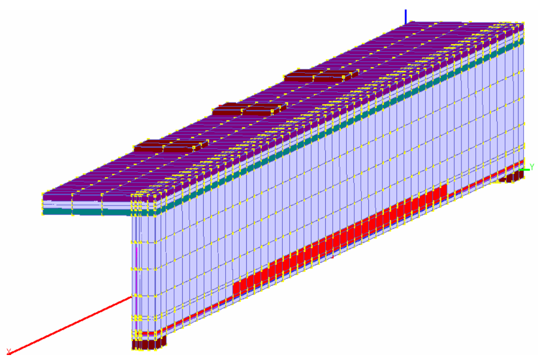

Figure 3FE model; half-symmetry

Rating factors for shear and moment considering design truck load and legal truck type 3-2 stipulated in ERA Bridge Manual [9] were calculated deterministically using Eq. (4). For such calculations, resistance factor of 0.9 was used. The load and impact factors used in the assessment were taken from bridge evaluation manuals [8-10]. Impact factors of 1.33 and 1.10 were used for design and legal load ratings case, respectively. As per Table 4.6.2.2.2b-1 and d-1 of AASHTO bridge design specification, the distribution factors for shear and moment were found to be 0.867 and 0.667, respectively and the effects of live loads were multiplied by these factors [10].

3 RESULTS AND DISCUSSIONS

3.1 Deterministic Assessment

Figure 4 shows the section capacity of the defective RC girder (output was obtained from Response 2000 software). The result of the 3D finite model (Figure 5) shows that the maximum shear capacity of the defective girder is 1540 kN (=2×770 kN).

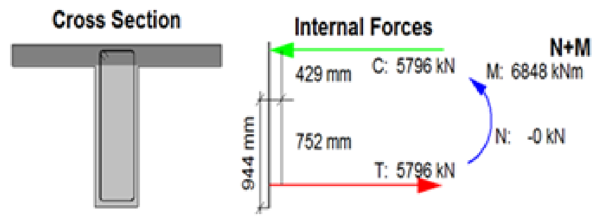

Figure 4 Section capacity

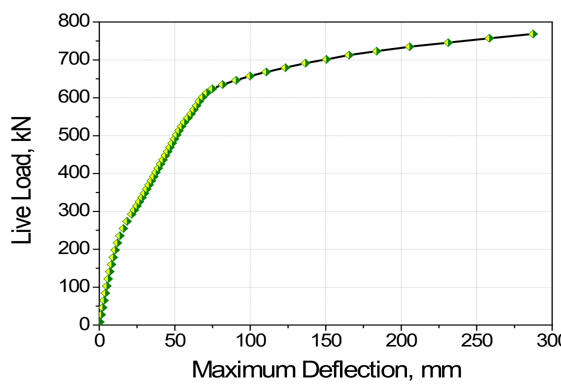

Figure 5Load-displacement diagram

Tables 3 and 4 show the rating factor of the defective girder. The rating factors of the bridge due to design and legal loads became 1.26 and 2.64 (shear force governs), respectively. As these rating factors are greater than one, the bridge under consideration is safe against design and legal loads. The corresponding available capacity of the existing bridge is 40 ton (=2.64×32.5).

Table 3 Rating factors for shear of the defective girder

Rating		Dead loadshear (kN)		Live load shear (kN)	Load factors			RF
		concrete section	wearing surface		concrete section	wearing surface	live load	
Design Load Level	Inventory	273.31	61.05	279.91 95.33*	1.25	1.50	1.75	1.26
	Operating				1.25	1.50	1.35	1.63
Legal Load	Truck Type 3-2			236.54	1.20	1.20	1.65	2.64

Table 4 Rating factors for moment of the defective girder

Rating		Dead load moment (kN-m)		Live load moment (kN-m)	Load factors			RF
		concrete section	wearing surface		concrete section	wearing surface	live load	
Design Load Level	Inventory	1,395.42	312.87	1,286.29 488.54*	1.25	1.50	1.75	1.43
	Operating				1.25	1.50	1.35	1.86
Legal Loads	Truck Type 3-2		80.32	993.96	1.20	1.20	1.65	3.42

* Effect of lane load

3.2 Probabilistic Assessment (Structural Reliability)

The deterministic values considered above were taken as mean values and the statistical distribution of random variables with corresponding coefficient of variations were obtained from standards, codes and manuals [2, 3, 12]. In this study, the shear capacity of a structure with deterministic value was considered as the reduction in shear capacity of the member by deterioration was very small [3]. For the bridge under consideration, as shown in Table 5,17 (n) statistical random variables with five groups have been considered.

Table 5 Statistical distribution of random variables

No.	Random variables	Mean values	CoV (%)	Std. dev.	Distribution
1	Statistical distribution of material properties				
1.1	Yield strength for flexural reinforcement steel (MPa)	400	5	20.00	Lognormal
1.2	Cylindrical compressive strength of concrete (MPa)	16.0	10	1.60	Lognormal
2	Statistical distribution of reinforcement bars				
2.1	Longitudinal bars (mm^2)	14,470	5	720.90	Normal
3	Statistical distribution of force effects				
3.1	Live loads	1.00	25	0.25	Normal
3.2	Dead loads	1.00	5	0.05	Normal
3.3	Overlay (wearing surface)	1.00	20	0.20	Normal
3.4	Analysis Variable for DL	1.00	5	0.05	Lognormal

No.	Random variables	Mean values	CoV (%)	Std. dev.	Distribution
3.5	Analysis Variable for LL	1.00	5	0.05	Lognormal
4	Statistical distribution of different factors				
4.1	Distribution factor for moment	0.667	2.5	0.016	Normal
4.2	Distribution factor for shear	0.867	2.5	0.022	Normal
4.3	Resistance factor	0.90	10	0.09	Normal
4.4	Model Uncertainty, N_R	1.00	4.6	0.046	Lognormal
5	Statistical distribution of bridge dimension				
5.1	Bridge Span (m)	20.5	0.05	0.01	Normal
5.2	Web width (mm)	500	0.5	2.50	Normal
5.3	Web depth (mm)	1450	0.5	7.25	Normal
5.4	Girder Spacing (mm)	2450	1.0	24.50	Normal
5.5	Slab thickness (mm)	200	0.5	1.00	Normal

For reliability assessment of the defective girder, 256 combinations of random variables of Latin Hypercube Sampling (LHS) were used [2]. For the computational analysis, a MATLAB code was prepared which enabled to compute the cross-section resistances, effect of loads, design margin, rating factors. It was also used to plot the corresponding probability density curves. The relationship between resistance and effects of loads for both bending moment and shear force are shown in Figures6 and 7, respectively. The RF for each case was computed and the scattered plot of RF for shear force and bending moment is shown in Figure8.

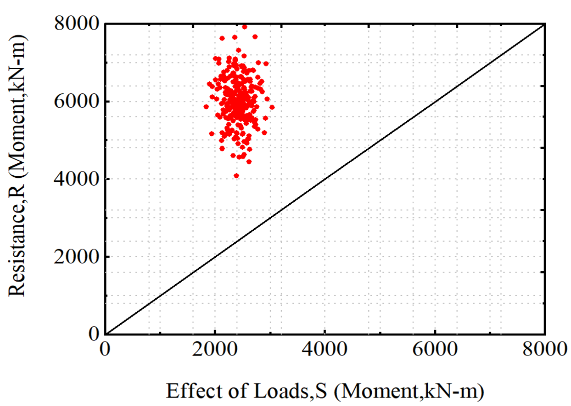

Figure 6 Distribution of moment resistance and effect of loads

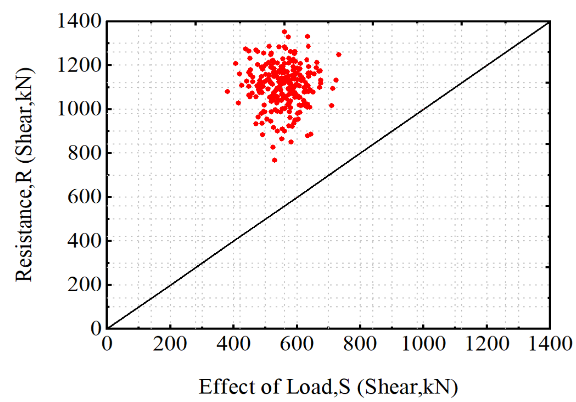

Figure 7 Distribution of shear resistance and effect of loads

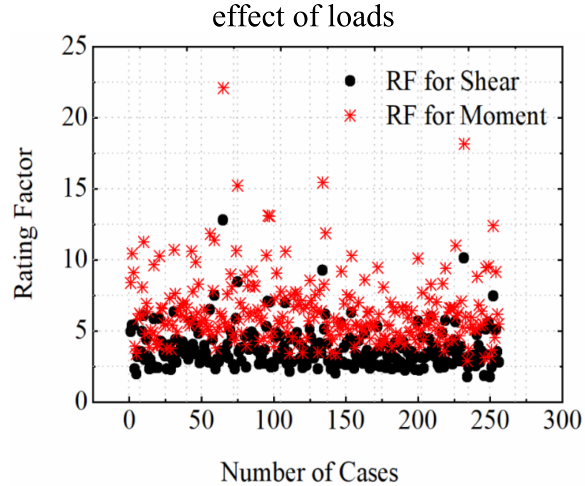

Figure8 Rating factors for shear force and bending moment

The probabilistic assessment results are summarized in Table 6. The mean values of rating factors for shear force and bending moment were found to be 3.71 and 6.41, respectively which are 40% to 80% higher than those obtained using the deterministic approach. Furthermore, the probabilistic distributions of bending moment and shear force are shown in Figures 9 and 10, respectively.

As shown in Table 6, the bridge's safety index was 5.08 (indicating that the unsafe region or failure region is about five standard deviations away from the mean) with a failure probability of 10^{-7} [2]. The result indicates that the bridge meets the standard (the safety index limit of 2.5) [10] and satisfies the minimum safety index limit set for newly constructed bridges (3.5 and above) [3]. Furthermore, the safety index of the bridge is greater than 2.80, corresponding to a rating factor of 1.0, indicating that the bridge is safe [3].

Table 6Design margin and safety index for shear and moment

Criteria		Resistance (φR_n)	Load (S)	Design Margin	Rating Factor	Safety Index
Shear	Mean	1,104.79	556.13	548.66	3.71	5.08
	Std. dev.	92.35	59.03	108.42		
	CoV (%)	8.36	10.62	19.76		
Moment	Mean	6,019.01	2,423.67	3,595.34	6.41	6.85
	Std. dev.	618.77	203.33	656.79		
	CoV (%)	10.28	8.39	18.27		

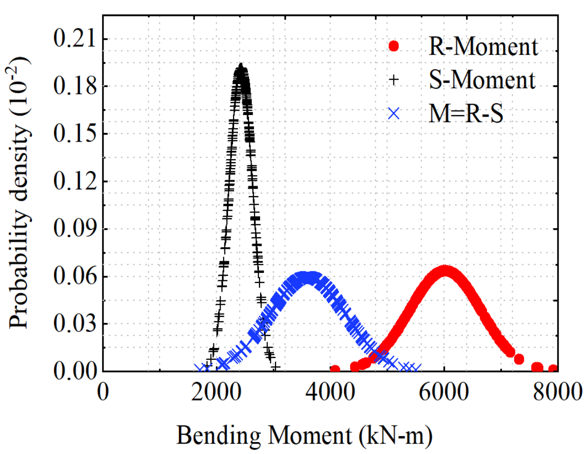

Figure 9 Probabilistic distribution of R, S and M for Moment

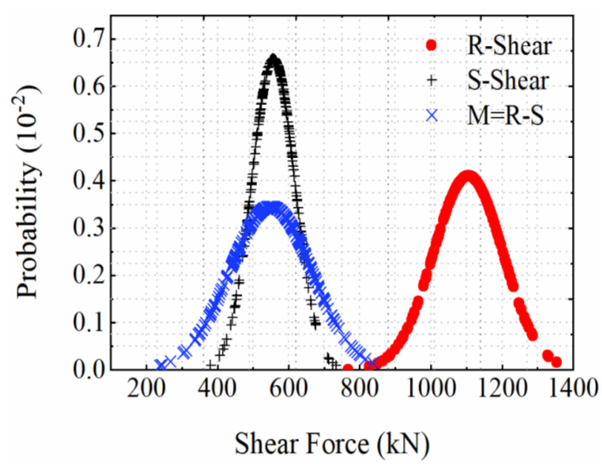

Figure10 Probabilistic distribution of R, S and M for Shear

3.3 Verification by Field Test

To verify the results obtained through the design review and a nonlinear Finite Element simulation of the defective girder, field test was conducted to ultimately assure the safety of the bridge. The verification included strength and durability aspects.

3.3.1 Field Test - Method

The field test was designed to assess the performance of the defective girder and solely targeted on the strength, stiffness, and geometry aspects. Test equipment (data Logger-for digital data acquisition-500 data points per second, 3 transducers, 3 dial gages, UPS-power storage, generator and so on) were mobilized.

3.3.2 Truck Loading Test

The truck loading test was mainly aimed to assess the strength and stiffness of the defective girder under moving load action of the loaded truck. The truck weighed 60.6 ton (Figure 11) and was made to pass on the bridge with its central axis aligned with the defective bridge. Three different speeds (5km/hr, 20km/hr and 40km/hr) were considered to assess any potential change in the response of the defective girder due to speed or impact. The load arrangement of the truck used in the load test is shown in Figure 12. The axle loads are given in tons and the axle spacings are given in meter.

For each loading case, measurements of deflection of the defective girder with its counterpart non-defective girder were recorded. Furthermore, the truck was made to pass with its edge wheel positioned at a distance of forty percent of girder spacing (=0.92m) from the curb [8, 9] and similar records were made as well. In addition to the deflection measurements, any possible formation, opening/closure of flexural and shear cracks were observed.

Figure 11 Truck used for loading test

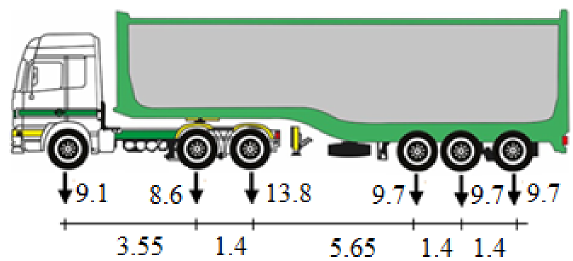

Figure 12 Axle load and spacing

The recorded mid-span deflection value while the truck was passing with its central axis coinciding with the alignment of the defective girder is shown in Figure 13. Mid-span deflection under moving load passages at 5km/hr; 20km/hr; 40km/hr; edge position with 5km/hr (non-sustained and sustained loads) is shown in Figure 14.

The three initial curves indicate the response for the running speeds of 5km/hr, 20km/hr and 40km/hr, respectively. The fourth curve indicates the response for the girder deflection with the trucks edge wheel positioned at 0.92m from the curb and at a running speed of 5km/hr. However, during the return of the third set of curves, the truck was allowed to stop when maximum mid span deflection was observed. This step was intentionally made in order to observe the effect of sustained load. The truck was sustained at this fixed position for nearly 60 seconds.

Figure 13 Set-up for truck loading test

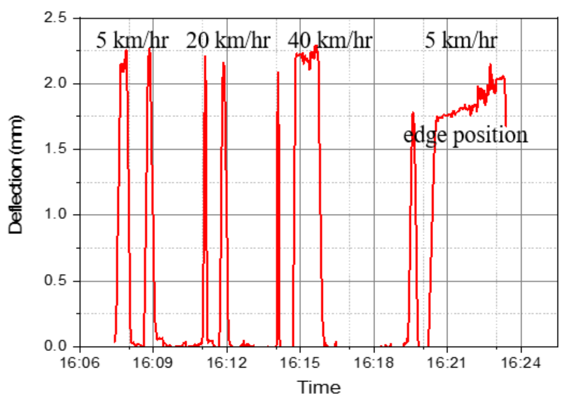

Figure 14 Mid-span deflection under moving load passages

As can be observed from the mid-span deflection of the defective girder (Figure 14), the maximum deflection was 2.3mm. For comparison, mid span deflection of the non-defective adjacent interior girder was simultaneously measured and the maximum mid-span deflection recorded was 1.9 to 2.0 mm. The last loading passage was made towards the edge of the curb and the corresponding deflection of the defective girder was observed to be 1.8mm. In addition, the truck was made to stop at the center and sustained for 60secs, resulting in a deflection of 2.2mm.

Overall, the defective girder is safe against stiffness and strength limits, with a maximum deflection of 2.3mm under the 60.6tons truck load, compared to the limit of 25.75mm. The actual recorded mid-span deflection was one-eleventh of the mid-span deflection limit, making the girder reasonably safe against serviceability and strength requirements.

3.4 Correlating Numerical Values with Field Load Testing

In some cases, prediction of load carrying capacity of bridges using conventional analytical load rating procedures possesses a lesser value than the load test result and depends on many factors. In line with this, uncertainty of analytical results depends on estimation of material properties, load distribution and impact factors, etc. Hence, conducting field test on bridges and correlating the result with the analytical value is necessary [7].

According to recent researches, when performance evaluation of bridges is determined based on field load test, the bridge load rating through field load test results can be estimated following AASHTO specification (analytical rating factor given inEq. (4)) and an adjustment factor is used to modify the rating factor [13]. Equation (5) provides an adjustment factor based on field test results [13].

$$RF_T = RF \times K \qquad (5)$$

where:

RF_T is load rating factor based on field test

RF is rating factor from Eq. (4)

K is an adjustment factor (without a load test, K=l. If the load test results agree with the analytical value, then K=1)

The adjustment factors were calculated using Eqs. (6) and (7) [13]:

$$K = 1 + K_a \times K_b \qquad (6)$$

$$K_a = \frac{\varepsilon_c}{\varepsilon_T} - 1 \quad (7)$$

where:

ε_T is maximum member strain measured during load test

ε_C is the corresponding theoretical strain due to the test vehicle and its position on the bridge

K_a is accounts for both the benefit derived from the load test

K_b accounts for the relationship between load test results and theoretical predictions

Equation (8) below gives the K_b factor:

$$K_b = K_{b1} \times K_{b2} \times K_{b3} \quad (8)$$

where:

K_{b1} ,K_{b2}, K_{b3} account for the type and frequency of follow-up inspections, the presence of special features like non-redundant framing and fatigue-prone details.

During the field load test, as strain gauges were not attached to the girder, the K_a factor was calculated based on deflections of the defective girder obtained by the test vehicle (T) and the rating vehicle (W). According to elastic analysis, the deflection of the defective girder caused by the rating vehicle (W) was computed as 6.81mm (in this case, gross moment of inertia of a section, $I=294.2\times10^9 mm^4$was used) and the maximum deflection of the bridge due to the test load was taken as 2.3mm (Figure 14). Using Eq. (7), the value of K_a was calculated to be 1.96.

K_b values were obtained from tables provided in [13] and read as K_{b1}=1.0 (for T/W>0.7), K_{b2}= 0.9 (routine inspection between 1 to 2 years) and K_{b3}= 0.7 (fatigue control without redundancy). Hence, the value of K_b became 0.63 (=1.0×0.9×0.7). Upon substitution, the value of$K$ became 1.24 (=1.96×0.63).

Thus, for the legal load, the modified rating factor, RF_T, for the bridge under consideration became 3.26 (=2.64×1.24). The modified rating factor of the bridge based on field test is in good agreement with the probabilistic method (*RF*=3.71). This shows that the bridge with defective girder is safe.

4 CONCLUSIONS

The load carrying capacity of the defective girder was evaluated through various approaches including design check, non-linear analysis, strength evaluation through legal load and truck load test. The deterministic approach was found as a conservative method of verification. The field test revealed that the bridge under investigation was safe against the test load with no damage or risk of collapse.

The results of the analysis indicate that the defective girder was safe against flexure as well as shear even if the compressive strength of concrete was reduced. The numerical evaluation of the bridge was also verified through load test and the modified rating factor was in good agreement with the probabilistic assessment. The safety index computed for the defective bridge satisfies the requirement for new bridges.

CONFLICT OF INTEREST

The authors declare that there is no conflict of interest.

ACKNOWLEDGMENTS

This study was undertaken in the School of Civil and Environmental Engineering, Addis Ababa Institute of Technology. The authors gratefully acknowledge Mr. Demiss Melaku for his professional assistance in conducting the field test.

REFERENCES

[1] Ethiopian Roads Authority (ERA), "*Standard Specification for Bridge Repair*", Addis Ababa, 2008.

[2] Rücker W.,Hille, F. and Rohrmann, R., "*Guideline for the Assessment of Existing Structures*", Final Report-F08a, pp. 48, Germany, 2006.

[3] National Cooperative Highway Research Program (NCHRP 292), "*Strength Evaluation of Existing Reinforced Concrete Bridges*", Transportation Research Board, Washington DC, 1987.

[4] William M. Bulleit, "*Uncertainty in Structural Engineering, Practice Periodical on Structural Design and Construction*", ASCE, February 2008, 7pages.

[5] James N. Siddall, "*Probabilistic Engineering Design"*, Retrieved from https://books.google.com.et/books?hl=en&lr=&id=mrwMrq-1G1YC&oi=fnd&pg=PA1&dq

[6] Rackwitz, R. and Fiessler, B., "*Structural Reliability under Combined Random Load Sequences*",Computers and Structures, Vol. 9, No. 5, 1978, pp. 489-494.

[7] National Cooperative Highway Research Program (NCHRP), "*Manual for Bridge Rating Through Load Testing*", Issue No. 234, Washington DC, 1998.

[8] American Association of State Highway and Transportation Officials (AASHTO), "*LRFD Bridge Design Specifications*", 4th edition, Washington, 2007.

[9]Ethiopian Roads Authority (ERA), "*Bridge Design Manual*", Addis Ababa, 2013.

[10] American Association of State Highway and Transportation Officials (AASHTO), "*The Manual for Bridge Evaluation*", 4th edition, Washington, 2013.

[11] Mohiuddin A. Khan, "*Bridge and Highway Structure Rehabilitation and Repair*", The McGraw-Hill Companies, Inc., New York, 2010.

[12] American Concrete Institute, ACI 214R-11, "*Guide to Evaluation of Strength Test Results of Concrete"*, Reported by ACI Committee 214, 2011.

[13] Abheetha, P. and Issam E. Harik, "*Bridge Load Testing Versus Bridge Load Rating*", Kentucky Transportation Center: KTC-19-16/SPR06-423-1F, pp. 78, June 2019.

ASSESSMENT OF DISTRIBUTED NON-LINEAR FIBER MODELS

Anur Oumer [1], Adil Zekaria[1,*]

School of Civil and Environmental Engineering, Addis Ababa Institution of Technology,
Addis Ababa, Ethiopia
*Corresponding author's email: anur.oumer@aait.edu.et

ABSTRACT

The study evaluates existing numerical nonlinear modeling techniques used in seismic analysis. Experimentally tested RC bridge column specimens have been taken as a case study and modeled in Open Sees finite element software. The study shows that the distributed force-based (FB) fiber models provide a more accurate result in capturing the nonlinear behavior of the RC bridge column that exhibits strain-hardening behavior. In contrast, the distributed displacement-based (DB) fiber models overestimate the ultimate capacity of the RC bridge column for sections exhibiting strain-hardening behavior. The study shows that for nonlinear analysis using distributed displacement-based (DB) fiber models, members should be divided into several elements to capture the inelastic response accurately. For the section exhibiting strain-softening behavior, both the distributed force-based (FB) and displacement-based (DB) fiber models are affected by localization issues. To overcome the localization issues, three-level of regularizations have been compared: 1) Applying regularization only to concrete, 2) Applying regularization only to steel 3) Applying regularization to concrete and steel materials.The level of regularizations was observed to have a significant effect in capturing the softening behavior, such as concrete crushing/spalling or rupture of reinforcing steel bars.

Keywords: *beam-column fiber models, Nonlinear-analysis, Strain-Hardening, Strain-Softening, Localization, Regularization*

1. INTRODUCTION

The advancement in computing technologies and the application of performance-based engineering design requires accurate and efficient computational nonlinear beam-column models. Based on their efficiency and computational cost, the nonlinear models used in the seismic analysis are classified into the (a) global model, (b) discrete finite element model, and (c) microscopic finite element models [1]. The study investigates the second class of models based on discrete finite element models. In discrete finite element models, two inelastic beam-column models are primarily adopted: (a) lumped plasticity and (b) distributed plasticity. The early approach to model lumped plasticity is by introducing zero-length nonlinear springs at both ends of the member. In these models, a hysteresis backbone curve is required to define the properties of the hinge.

The distributed plasticity models allow inelastic deformation to occur anywhere along the length of the beam-column elements. The axial-moment interaction can be captured automatically by integrating sectional force-deformation along the length of the element. The most common distributed plasticity models used in earthquake engineering are classical displacement-based and force-based beam-column elements [1, 2]. For the structures, in which failure is dominated by flexure, distributed plasticity has gained wide acceptance in earthquake engineering. However, softening or localization issues for such models are critical problems [3–5].

This paper investigates the localization issue with different material regularization techniques in distributed plasticity and suggests the best way to overcome mesh-dependent response. The effect of applying partial regularization only to concrete, only to steel or full regularization to both concrete and steel materials for structures exhibiting softening behaviour is investigated using force-based and displacement-based distributed plasticity models. Previous researches did not elaborate the significance of the application of partial localization and the consequence in capturing the post peak softening behaviour of reinforced concrete section.

2. REVIEW THE STATE OF ART

3.4. Fiber Based Distributed Plasticity Beam-Column Element

The fiber models are one of the recent techniques used to determine the inelastic responses of the beam-column elements by integrating nonlinear responses over the monitored cross-sections, as shown in Figure 1. The process can be achieved by discretizing the cross-section into a finite number of fibers. Each fiber contains constitutive laws of steel reinforcement, unconfined, and confined concrete materials, as shown in Figure 1 a. The assumption of the plane sections is taken into account by employing an Euler-Bernoulli beam theory, which ensures that the strains are distributed linearly across the cross-section [1]. The axial-moment interaction can be captured automatically by integrating sectional force-deformation along the length of the element.

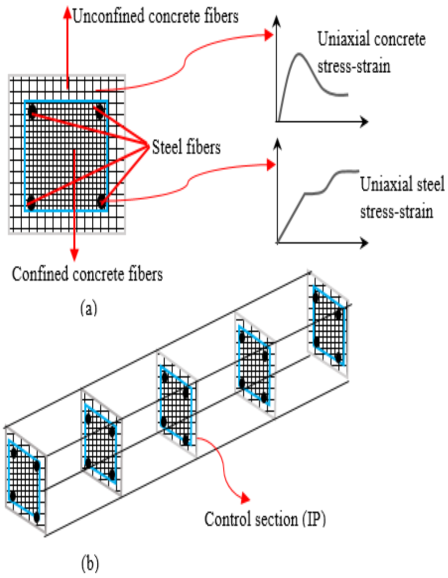

Figure 1. Distributed plasticity fiber-based beam-column element.

In the case of uniaxial bending the section stiffness matrix k_s can be evaluated numerically as follow:

$$k_s = \sum_{i=1}^{N_{IPs}} \begin{bmatrix} 1 & -y & z_i \\ -y_i & y_i^2 & y_i z_i \\ z_i & y_i z_i & z_i^2 \end{bmatrix} E_i w_i \qquad (1)$$

The section resisting forces s is calculated using the numerically integration as follow:

$$s = \begin{bmatrix} N \\ M_z \\ M_y \end{bmatrix} = \sum_{i=1}^{N_{IPs}} \begin{bmatrix} 1 \\ -y \\ z \end{bmatrix} \sigma_i w_i \qquad (2)$$

Where i is an integer counting from 1 to the number of integration points or (fibers) N_{IPs} And w_i is the weight of the integration scheme at i;E_i is the modulus of elasticity assigned to the integration point i.

2.1.1.Formulation of distributed displacement-based fiber models (DB)

The DB (displacement or stiffness-based) elements are the first distributed plasticity based on the classical stiffness method; thus, the models satisfy compatibility and equilibrium in an exact and approximate form, respectively. The models use a displacement interpolation function that assumes linear curvature and constant axial strain deformation to describe the nodal displacements. The element deformations are obtained directly from the shape function; hence iteration is required only at the structural level [1]. Figure 2 shows that N, M_1, and M_2 are element forces denoted by q, and u, θ_1, and θ_2 are element deformations represented by v in the basic system.

Figure 2. Basic forces of 2D beam-column element

$$u(x) = N(x)v \qquad (3)$$

Where u(x) is displacements at any point along the length of the beam-column element and $N(x)$ is a matrix containing the shape functions for the axial and transverse displacements.

$$\begin{bmatrix} u_1(x) \\ u_2(x) \end{bmatrix} = \begin{bmatrix} \frac{x}{L} & 0 & 0 \\ 0 & x - \frac{2x^2}{L} + \frac{x^3}{L^2} & -\frac{x^3}{L} + \frac{x^3}{L^2} \end{bmatrix} \begin{bmatrix} u \\ \theta_1 \\ \theta_2 \end{bmatrix} \qquad (4)$$

To ensure that the strains are distributed linearly across the cross-section, the first and second derivatives of the displacement shape functions must give constant axial strain and linear curvature, respectively, and are expressed as follows:

$$\begin{bmatrix} \varepsilon(x) \\ \kappa(x) \end{bmatrix} = \begin{bmatrix} \frac{\partial}{\partial x} & 0 \\ 0 & \frac{\partial^2}{\partial x^2} \end{bmatrix} \begin{bmatrix} u_1(x) \\ u_2(x) \end{bmatrix} \qquad (5)$$

The behavior of members near their ultimate resistance and the beginning of strain softening cannot be captured by the DB elements; hence multiple elements per member are needed to represent the inelastic response accurately [2,4,5].Most recently, Pantò et al.[6]have introduced a new Smart Displacement Based (SDB) beam element to improve the accuracy of the standard DB element."Smart" refers to an element's capacity to upgrade its displacement field following its current inelastic state[6].According to the authors, the new model gives a result comparable to the FB models. Furthermore, Pantò et al. [7]extended the model to a Fibre Smart Displacement Based (FSDB) beam element to account for the axial force-bending moment interaction. A strong equilibrium of the axial force along the beam element, which is not often achieved by standard DB beam elements, is demonstrated to be possible with the Fibre Smart Displacement Based (FSDB) beam element [7].Since those concepts are new and have yet to be incorporated in the most known finite element softwares, this study focuses only on the standard DB elements.

2.1.2. Formulation of distributed force-based fiber models (FB)

In the FB (force or flexibility-based) approach, the force interpolation functions are used as a shape function. The force-based method is based on an exact equilibrium solution within the basic system of a beam-column element. Section forces are calculated using interpolation within the basic system from basic forces, as shown in equation (6):

$$s(x) = b(x)q \qquad (6)$$

Where b(x) is force interpolation functions that provide constant and linear distribution of axial force and bending moment, respectively for a member without distributed element loads:

$$b(x) = \begin{bmatrix} 1 & 0 & 0 \\ 0 & -\left(1 - \frac{x}{L}\right) & \frac{x}{L} \end{bmatrix} \qquad (7)$$

The element state determination is more complex compared to the displacement-based fiber element. Element deformations in the basic system can be written as:

$$v = \int_0^L b^T(x)\ e(x)\,dx = \sum_{i=1}^{N_p} b_i^T e_i \omega_i \qquad (8)$$

The virtual force principle is used to derive the relationship between element deformations in the basic system v and sectional deformations e(x). Sectional deformation e(x) must be calculated from section forces s(x); however, in reality, this relation does not exist, but its inverse does[8, 9]. As a result, the section deformations are obtained by solving the nonlinear system of equations.

2.1.3. Localization issue in distributed fiber models

The term "localization" is well established in fracture mechanics, and various types of research are available regarding this topic. Experiment tests of compressive strength of different specimen sizes have shown that the post-peak stress-strain behavior of concrete is size-dependent. Jansen and Shah [10] conducted compressive tests for specimens with different slender lengths, and they found that the longer the specimen, the steeper the curves become. In computational mechanics, studies have shown that localization issues affect numerical models too; hence, this leads to the non-objective or mesh-dependent response, which results from the concentration of strain over a small finite element length or a single integration point.

Before developing and applying force-based beam-column elements, localization issues have been primarily studied in displacement-based elements. Still, there are several regularization techniques in the literature for this model. Among the earliest studies, Bazant et al.[11] correctly recognized that the localization issue in the displacement-based element is sensitive to mesh size and the mean tangential bending stiffness. Zeris and Mahin [12] were the first to explain that softening in FB elements has different features from DB approaches. Deformations localize over a single displacement-based element and single integration section in the DB and FB elements, respectively [13].

Even though several documented types of research on regularization techniques for DB are available, the works are more recent for FB beam-column elements. Coleman and Spacone [3] were the first who deeply investigated localization issues in FB beam-column model and applied the regularization techniques based on the constant fracture energy criterion to these models, which provides an objective response to the global force-displacement response. For sections undergoing softening, the FB element also fails to produce consistent and rational post-yielding global responses since the result is influenced by differences in the element mesh and the element's number of integration points. If too many integration points are employed, the element becomes unstable for softening sections [3, 5].

Coleman and Spacone [3] suggested a material regularization technique for FB models based on constant fracture energy criteria concepts to address mesh-dependent response. The authors modified the concrete model developed by Kent and Park [14] as shown in Figure. The ultimate strain is adjusted at the quadrature integration points; then, the strain-softening process begins. The shaded area is proportional to the energy released after the pressure's softening. The idea is that the concrete material models assigned to distributed-plasticity fiber sections are modified to have constant dissipated material energy during crushing. The following expression is proposed to express ε_{20}:

$$\varepsilon_{20} = \frac{G_{fc}}{0.6f_c' l_p} - \frac{0.8f_c'}{E_c} + \varepsilon_c \tag{9}$$

Where G_{fc} is the fracture energy of concrete in compression, f'c is the compressive strength of the concrete, ε_c is peak compressive strain of the concrete, E_c is modulus of elasticity, ε_{20} is compressive strain corresponding to 20% f'c and L_p is length of the plastic hinge, which acts as the characteristic length to overcome mesh-dependent response.

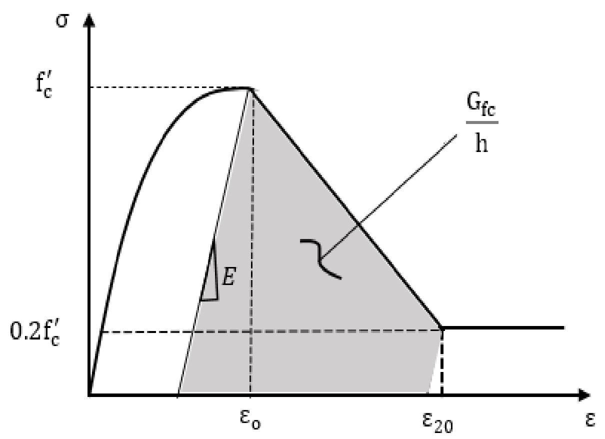

Figure 3. Kent–Park concrete stress–strain model with fracture energy in compression as shaded area.

The regularization technique proposed by Coleman and Spacone [3] was applied only to distributed force-based beam-column model. Pugh [15] recently extended the work to include displacement-based fiber models. After conducting experimental tests on several planar wall specimens, Pugh [15]expressed the crushing energy value in the specified strength of unconfined and confined concrete. Furthermore, he recommended using different crushing energy values for the force-based and displacement-based fiber beam-column models. He suggested the following values of unconfined crushing energy for the FB model:

$$G_{fc} = 2f_c' \text{(N/mm) (FB)} \tag{10}$$

Applying the concrete crushing energies developed for the force-based beam-column element to the displacement-based element produces an over-prediction of drift capacity Pugh [15] . Therefore, for the DB element, the unconfined crushing energy is:

$$G_{fc} = 0.56f_c' \text{(N/mm) (DB)} \tag{11}$$

The confined concrete crushing energy for both FB and DF models can be estimated as:

$$G_{fcc} = 1.7G_{fc} \tag{12}$$

Then Equation 9 can be written for the confined concrete properties as:

$$\varepsilon_{20c} = \frac{G_{fcc}}{0.6f'_{cc}L_{IP}} - \frac{0.8f'_{cc}}{E_{cc}} + \varepsilon_{oc} \tag{13}$$

Colemanand Spacone [3] recommended only applying material regularization techniques to the concrete material. However, this technique can be valuable only for sections subjected to high axial load, and failure is only due to concrete material crushing. If a member with widely spaced stirrups is subjected to high axial and cyclic lateral load, the section could face softening of concrete and localization of reinforcement bar. Reinforced concrete members at the critical section post-peak behavior of steel show strain hardening, whereas concrete exhibits strain softening. Even though steel shows hardening behavior, the section exhibits softening steel response and localizes at a critical section to confirm compatibility conditions[15,16]. Therefore, concrete and steel should be regularized because the section softening comes from the two fiber materials.

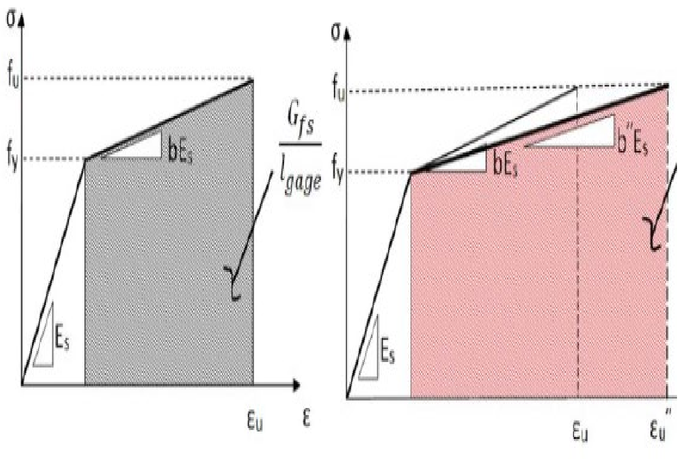

(a) Measured steel response (b) Regularized steel model

Figure 4. Stress-strain response histories for steel material [15].

The hardening energy, G_s for the simplified bi-linear steel stress-strain illustrated in Figure 4a can be defined as:

$$G_s = \frac{1}{2}(\varepsilon_{u,\exp} - \varepsilon_y)(f_u - f_y)L_{gage} \tag{14}$$

Where: $\boldsymbol{\varepsilon_{su}}$ is therupture strain, $\boldsymbol{\varepsilon_y}$ isthe yield strain, $\mathbf{f_u}$ isthe ultimate tensile strength and $\mathbf{f_y}$isthe yield strength. The ultimate rupture strain assigned to the steel material model in the analysis should be updated based on the length associated with the critical section or element for regularizing the steel material. Using the Equation 14 and Figure 4b, the strain at ultimate strength, ε_u, used in defining the regularized model can be calculated as:

$$\varepsilon_u'' = \varepsilon_y + (\varepsilon_{u,\exp} - \varepsilon_y)\frac{L_{gage}}{L_{IP}} \tag{15}$$

As the mesh becomes more refined and small L_{IP}, the hardening modulus of the reinforcing steel decreases, requiring larger strains to reach a particular post-yield stress level Pugh[15]. It should be noted that these formulations neglect the curved transition between the initial and post-yielding hardening slopes specified by steel material developed by Menegotto and Pinto[17]; nonetheless, this is a minor simplification that was proven to have minimal impact on numerical findings [15].The Gage length has been taken as 0.203 m, as suggested by ASTM A370[15,16]. After the ultimate strain is modified according to the gage length and length of the first integration section or element length, the post-yield hardening modulus must be modified based on the computed value for the maximum rupture strain of the regularized material [15, 16].

3. RESULTS AND DISCUSSION

3.4. Modelling Strategy

This section investigates the performance of the distributed force-based fiber models (FB) and displacement-based fiber models (DB) commonly used in earthquake engineering. The Open System for Earthquake Engineering Simulation, commonly known as Open Sees[18]finite element program, has been used to model a reinforced concrete bridge column downloaded from the PEER Structural Performance Database (2003). Material stress-strain relationships that describe the concrete and steel fibers should be adequately defined to capture the inelastic response of structures subjected to axial and lateral loading. To accurately simulate the bridge-reinforced concrete column specimens, the confined and unconfined concrete, denoted as Concrete02 in Open Sees, has been defined. The concrete Kent-Park model [14] shown in Figure 5was adopted to describe the stress-strain relation of concrete fibers. The monotonic compression envelope shown in Figure 5(a) has an initial parabolic envelope, a linear softening envelope, and an ultimate stress plateau. The confinement effect factor, K, can be determinedusing the formula proposed by Mander et al.[19]. For unconfined concrete fibers, the strain associated with 80% strength loss, f20u, was assumed to be 0.008. The ultimate strain capacity of the confined concrete can be calculated using Priestley et al.[20] expression as follows:

$$\varepsilon_{ccu} = 0.004 + 1.4\frac{\rho_s f_{yh} \varepsilon_{fs}}{f_{cc}} \quad (16)$$

As illustrated in Figure 5(b), Yassin assigned bilinear unloading and linear reloading branches to implement cyclic behavior on the monotonic compression envelope [15]. These hysteretic rules assume that tensile response happens immediately after complete compression unloading and consider stiffness degradation throughout both unloading and reloading. It is assumed that cracks will close suddenly; this can be seen by the quick shift in stiffness that occurs when compression is reloaded, as shown in Figure 5(b). Both the post-cracking softness and tensile strength can be controlled [15].

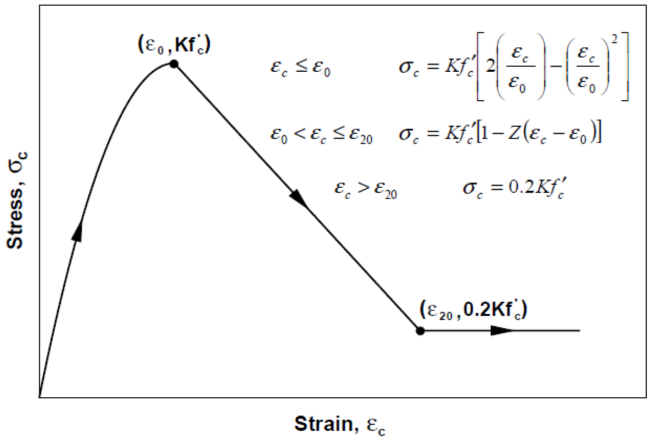

(a)

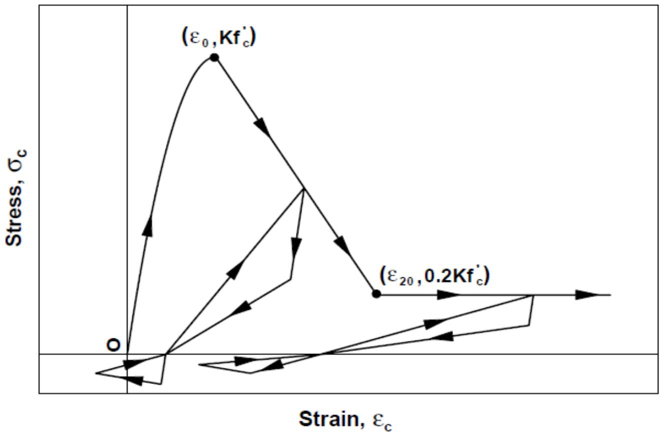

(b)

Figure 5Yassin/Modified Park-Kent (a) monotonic (b) Cyclic envelope[15].

A steel material, Steel-02, with a bilinear steel envelope, has been used to define the reinforcement bar. Cyclic reinforcing steel behavior is commonly modeled using the Menegotto-Pinto-Filippou [21], which includes isotropic strain hardening, as shown in Figure 6. This model represents steel behavior as a series of curved transitions between asymptotes defined by linear elastic and strain hardening properties. The curved transition allows for the representation of the Bauschinger effect. Model input parameters allow for control of cyclic stiffness deterioration.

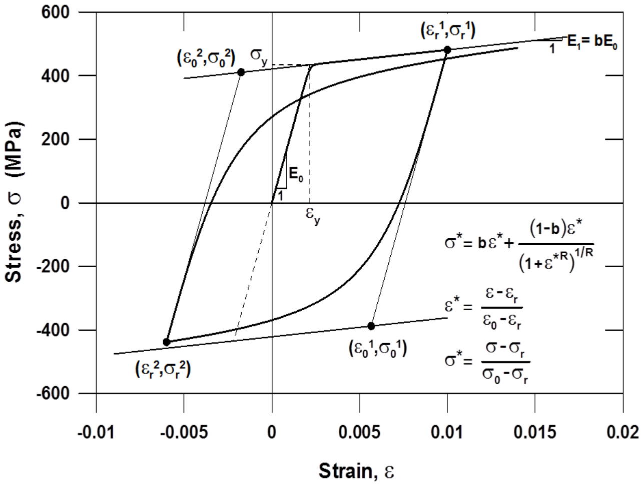

Figure 6Menegotto-Pinto-Filippou model [21].

3.4. Evaluation of DB and FB models under cyclic loading (Hardening)

Several researchers have identified that localization is not an issue for members exhibiting hardening behavior. The models are evaluated under members exhibiting strain-hardening behavior to verify these conclusions. Specimen A2 tested by Kunnath et al. [22]has been taken as a case study for a strain-hardening behavior.

The axial load, cyclic lateral load, and section discretization of specimen A2 are indicated in Figure 7. The properties of specimen A2 have been summarized in Table 1. Table 2 shows the material properties used for modeling the specimen in Open Sees finite element software.

Table 1 Properties of specimen A2 tested by Kunnath et al. [22].

Properties	Values
Concrete strength	29 (MPa)
Yield stress of stirrup	434 (MPa)
Yield stress of main bar	448 (MPa)
Diameter of the cross-section	305 (mm)
Height of the column	1372 (mm)
Test configuration	Cantilever
Axial load	200 (kN)
Diameter of the main bar	9.5 (mm)
Number of bars	21
Reinforcement ratio of the main bar	0.0204
Diameter of stirrup	4 (mm)
Hoop spacing, Sv	19 (mm)
Cover to center of hoop bar	14.5 (mm)
Reinforcement ratio of stirrup	0.94
Span-to-depth ratio	0.94
Axial load ratio	0.094

Table 2 Material properties in Open Sees of specimen A2 tested by Kunnath et al. [22].

Unconfined concrete(Concrete02)	
Maximum concrete strength (f_c')	29 Mpa
Peak strain (ε_{co})	$2\cdot\frac{f_{cc}}{E_{cc}}$
Crushing stress (f'_{c20})	$0.2\cdot f'_c$
Crushing strain (ε_{cu})	0.008
Confined concrete(Concrete02)	
Confinement factor (k)	1.62
compressive strength (f_{cc})	$k\cdot f'_c$
Peak strain (ε_{cco})	$2\cdot\frac{f_{cc}}{E_{cc}}$
Crushing stress (f_{cc20})	$0.2\cdot f_{cc}$
Crushing strain (ε_{ccu})	Equation 16
Reinforcement bar (Steel02)	
Yield strength(fy)	448 (mpa)
Modulus of elasticity (Es)	200000 (mpa)
Strain hardening	1%

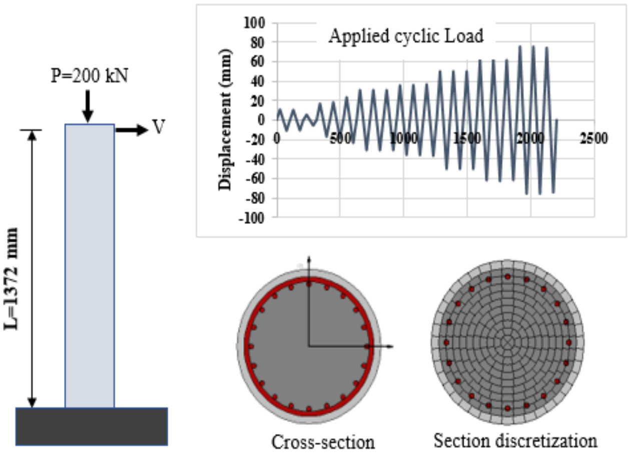

Figure 7Simulation of axial load, cyclic lateral load and section discretization of the specimen A2 tested by Kunnath et al. [22].

Strain-hardening behavior was considered because the column is subjected to a relatively low axial load of 200 kN (0.09fc′Ac), as shown in Figure 7. Furthermore, the hysteresis response obtained from the experiment has not shown any softening or degradation in strength. The materials have been discretized into many concrete and steel fibers to integrate the uniaxial material along the section, as seen in Figure 7. To simulate the load applied during the experiment in OpenSees, first, a downward constant axial force of 200 kN is applied vertically through the force control loading. Once the gravity analysis has been carried out, the cyclic lateral load is applied through the displacement control.

For the section exhibiting strain-hardening behavior, cyclic analysis was carried out using the DB and the FB beam-column fiber models. Because Neuenhofer and Filipe [2] suggest that more integration points do not improve accuracy in the DB model, in this research, the member was divided into several elements with two Gauss-Legendre integration points. However, increasing the number of integration points for the force-based element has a significant impact on the numerical result; as a result, a single element of the force-based model with several integration points is used.

As shown in Figure 8, when mesh refinement increases, the cyclic moment-curvature does not converge into the same solution because the DB element formulation assumes linear curvature, which is valid only for elastic. As seen in Figure 9, convergence is achieved fast in the global response; however, the ultimate curvature still varies significantly in the local response(see Figure 8). As shown in Figure 9, the DB with one element highly overestimates the actual response compared to DB with 4 and 10 elements per member. The ultimate base shear of the experimental result is 73.97 kN. With a 56.82% error, the maximum base shear utilizing 1 DB element per member is 116 kN. However, the ultimate base shear is 75.74 kN (with a 2.33% error) when the member was refined to 4 and 10 DB elements per member.

Analysis using the FB fiber models shows that the cyclic moment-curvature converges into a unique solution for strain-hardening behavior with increased integration points, as shown in Figure 10. The FB models accurately capture the hysteresis force-deformation shape using only one element per member with few integration points, as shown in Figure 11. The FB captured the hysteresis curve of force-deformation response better than the displacement-based model. The ultimate base shear obtained using the FB element is 74.08 kN (with a 0.14% error), which is almost the same as the experimental value. The reason is that the FB model satisfies equilibrium in an exact sense, whereas the DB is average.

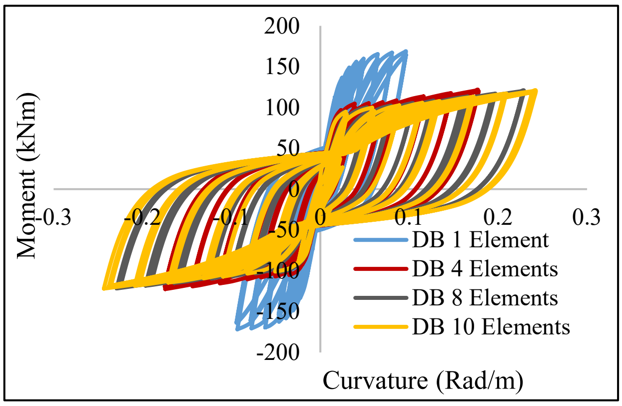

Figure 8. Hardening cyclic moment-curvature using DB (Specimen A2).

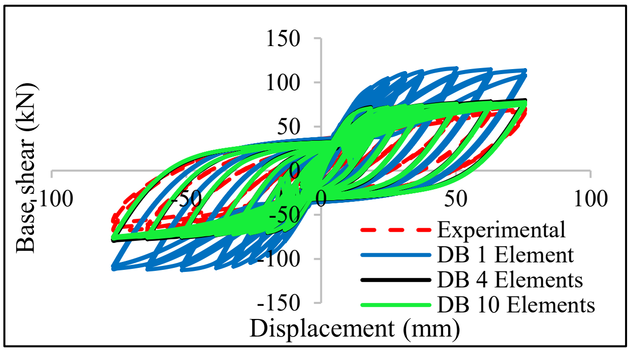

Figure 9. Hardening hysteresis response using DB (Specimen A2).

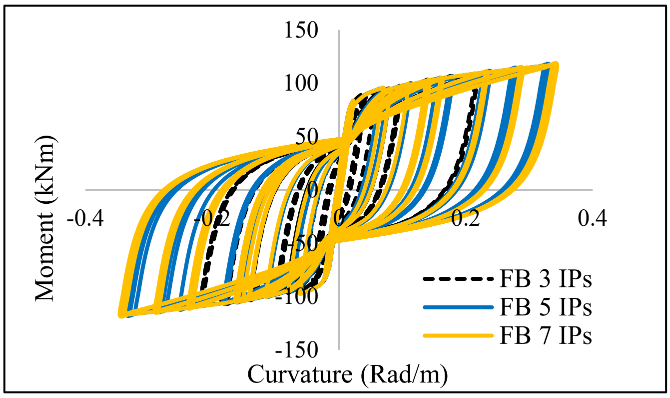

Figure 10. Hardening cyclic moment-curvature using FB (Specimen A2).

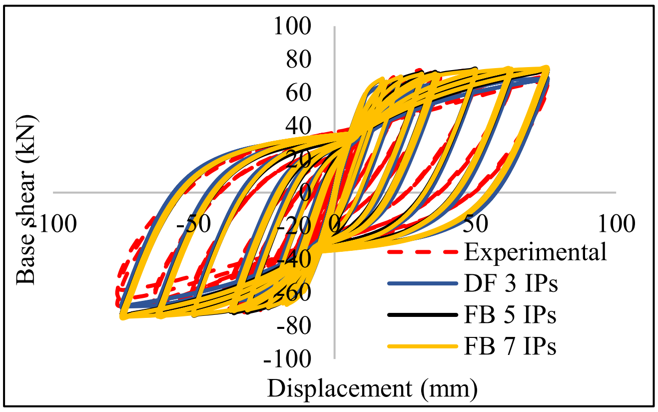

Figure 11. Hardening hysteresis response using FB (Specimen A2)

3.4. Evaluation of DB and DF models under monotonic loading (Softening)

Reinforced concrete columns that exhibit strain-softening behavior, specimen No. 3 in the tests by Wong et al. [23], and specimen FL3 tested byKowalsky et al. [24], have been taken as the case study to show the effect of softening behavior on the performance of the distributed-based fiber models. Specimen No. 3 and specimen FL3 are subjected to a high axial load of 1813 kN and 1780 kN, respectively. For specimen No 3, the experimental test showed significant concrete spalling and longitudinal bar buckling at a drift of 1.21% (9.7 mm) and 3.23% (25.9 mm), respectively. For the specimen FL3, the experimental test showed significant concrete spalling and longitudinal bar buckling at a drift of 2.79 % (102 mm) and 9.3 % (340 mm), respectively. For the push-over analysis, the loading method is carried out initially by applying a constant downward axial load through the force control loading. Then an increasing lateral monotonic load is applied through the displacement control. The Axial load, monotonic lateral load, and section discretization of specimen No. 3 are indicated in Figure 12. The actual properties of specimens

No. 3 and FL3 have been summarized in Table 3. **Table 4** shows the material properties used for modeling the specimens in Opeen Sees.

Table 3 Actual Properties of specimen No. 3 [23] and specimen FL3[24].

Properties	Specimen No. 3	Specimen FL3
Concrete strength	37 (MPa)	38.6 (MPa)
Yield stress of stirrup	300 (MPa)	445 (MPa)
Yield stress of main bar	475 (MPa)	477 (MPa)
Diameter of the cross-section	400 (mm)	457 (mm)
Height of the column	800 (mm)	3,656 (mm)
Test configuration	Cantilever	Cantilever
Axial load	1813 (kN)	1,780 (kN)
Diameter of the main bar	16 (mm)	15.9 (mm)
Number of bars	20	30
Reinforcement ratio of the main bar	0.032	0.0362
Diameter of stirrup	10 (mm)	9.5 (mm)
Hoop spacing, Sv	60 (mm)	76 (mm)
Cover to center of hoop bar	20 (mm)	30.2 (mm)
Reinforcement ratio of stirrup	1.42	0.92
Span-to-depth ratio	2	8
Axial load ratio	0.39	0.281

Table 4. Material properties in Open Sees of specimen No. 3 [23] and specimen FL3[24].

	Specimen No. 3	Specimen FL3
Unconfined concrete (Concrete02)		
Maximum concrete strength (f_c')	37 Mpa	38.6 Mpa
Peak strain (ε_{co})	$2 \cdot \frac{f_{cc}}{E_{cc}}$	$2 \cdot \frac{f_{cc}}{E_{cc}}$
Crushing stress (f'_{c20})	$0.2 \cdot f'_c$	$0.2 \cdot f'_c$
Crushing strain (ε_{cu})	0.008	0.008
Confined concrete (Concrete02)		
Confinement factor (k)	1.348	1.32
compressive strength (f_{cc})	$k \cdot f'_c$	$k \cdot f'_c$
Peak strain (ε_{cco})	$2 \cdot \frac{f_{cc}}{E_{cc}}$	$2 \cdot \frac{f_{cc}}{E_{cc}}$
Crushing stress (f_{cc20})	$0.2 \cdot f_{cc}$	$0.2 \cdot f_{cc}$
Crushing strain (ε_{ccu})	Equation 16	Equation 16
Reinforcement bar (Steel02)		
Yield strength(fy)	475 (Mpa)	477 (Mpa)
Modulus of elasticity (Es)	200000 (mpa)	200000 (mpa)
Strain hardening	1%	1%

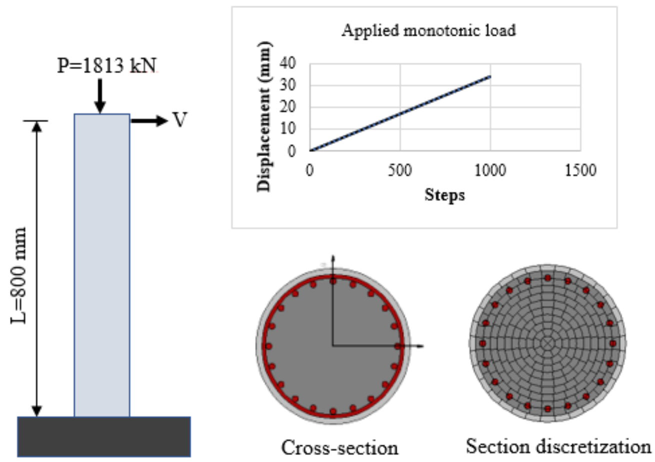

Figure 12. Axial load, monotonic lateral load and section discretization of specimenNo. 3.

A reinforced concrete column that exhibits strain-softening behavior was analyzed using FB and DB numerical models.

Figure 13-Figure 16 show the monotonic response of the member analyzed using the FB and DB models for both specimens. For the two specimens, the FB and DB numerical models showed two types of localization: first, linearly softening, which is the softening of concrete material that comes as the result of the crushing and spelling of concrete; second, a sudden drop in strength, which comes from the localization of the steel material (see

Figure 13-Figure 16). The analysis results have shown that mesh-dependent results underestimate the ultimate strength and drift

capacity of the columns. The softening rate in the DB model (see

Figure 15 and Figure 16) is slow compared with the FB (see

Figure 13 and Figure 14). On the other hand, the FB model's results began to soften with just one element (with 5 Ips), whereas the DB model experienced softening problems when the member was divided into eight or more elements (with 2 Ips).

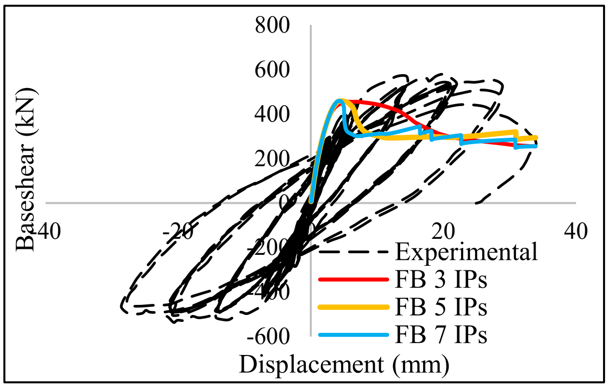

Figure 13. Monotonic response of specimen No. 3 using FB without applying material regularization.

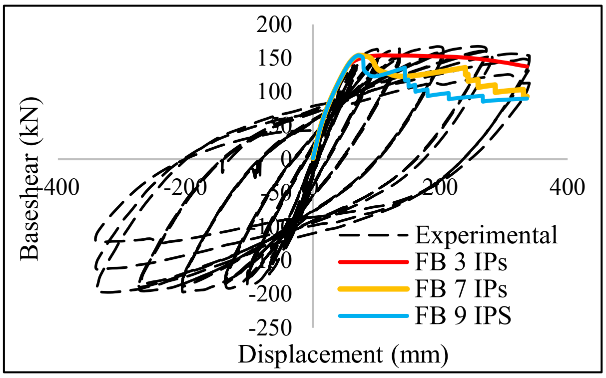

Figure 14. Monotonic response of specimen FL3 usingFB without applying material regularization.

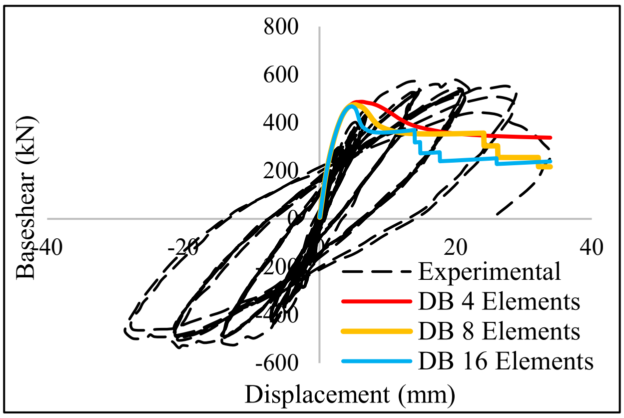

Figure 15. Monotonic response of specimen No. 3 using DB without applying material regularization.

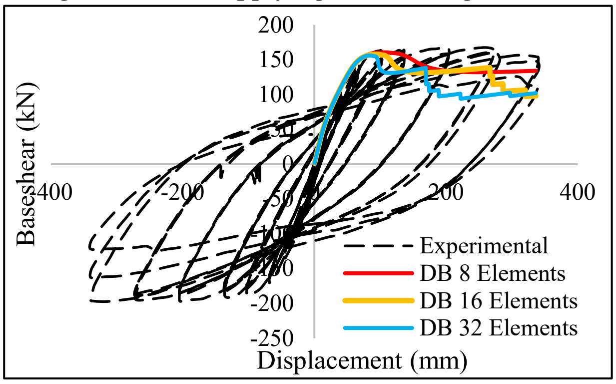

Figure 16. Monotonic response ofspecimen FL3 using DB without applying material regularization.

3.4. Investigation of partial and full material regularization in FB Model

Despite the fact that certain studies have suggested regularization be used for both steel and concrete materials, there hasn't been much discussion on the effect of the partial regularization techniques This section briefly discusses partial and complete material regularization techniques for fiber beam-column elements. Coleman and Spacone [3]recommended material regularization only for the concrete section that fails due to concrete crushing. Later on, Pughsuggested including regularization for steel material [15]. The ultimate strain was modified using Equation 13 to regularize concrete material. Adjusted fracture strain for steel material calculated according to Equation 15. The gauge length was assumed to be 203 mm, as recommended by ASTM A370m, and the maximum strain was taken as 0.09. In Open Sees, Min Max criteria have been considered for the steel, which enforces the stiffness and strength of the steel fibers to become zero when the compressive strain is reached. The estimated properties of the regularized material for FB and DB are summarized in Table 5 and Table 6. This paper does not present softening issues and regularization techniques at the local level.

Table 5 Regularized strains of the unconfined and confined concrete, steel ultimate rupture strain and strain hardening of specimen No. 3 for FB and DB models.

Force-based model (FB)					
No of Ips	LIP	ε_{c20}	ε_{cc20}	ε"	bs
3	133.3	0.027	0.034	0.136	0.006
7	40.0	0.085	0.109	0.447	0.002
9	19.0	0.177	0.227	0.936	0.001
Displacement-based model (DB)					
No of Elements	LIP	ε_{c20}	ε_{cc20}	ε"	bs
4	100	0.006	0.009	0.180	0.004
8	50	0.016	0.020	0.358	0.002
16	25	0.034	0.044	0.714	0.001

Table 6. Regularized strains of the unconfined and confined concrete, steel ultimate rupture strain and strain hardening of FL3 for FB and DB model.

Force-based model (FB)					
No of Ips	LIP	ε_{c20}	ε_{cc20}	ε"	bs
3	609.3	0.0071	0.0089	0.0316	0.0517
7	87.	0.0399	0.0511	0.2067	0.0074
9	50.7	0.0672	0.0864	0.3527	0.0043
Displacement-based model (DB)					
No of Elements	LIP	ε_{c20}	ε_{cc20}	ε"	bs
8	229	0.006	0.007	0.080	0.012
16	114.2	0.010	0.012	0.158	0.006
32	57.1	0.018	0.023	0.3141	0.003

Applying material regularization only for concrete failed to address the mesh-dependent response, as shown in Figure 17 and Figure 18. The ultimate drift capacity for FB with 3, 5, and 7 IPs is different. Specimen No 3. and FL3 showed the onset of a significant concrete spalling at a drift of 1.21% (9.7 mm) and 2.79 % (102 mm), respectively; therefore, regularizing only the concrete material tackles localization issues up to those drift levels. Furthermore, applying material regularization only to steel material failed to tackle the mesh-dependent response, as shown in Figure 19and Figure 20. However, this partial regularization successfully tackled the localization or sudden drop of strength (localization of steel) observed in the non-regularized response (

Figure 13-Figure 16). The most recent way is based on regularizing steel and concrete materials for fiber beam-column models. As shown in Figure 21 and Figure 22, the response using FB elements is objective for all integration points. Furthermore, the ultimate strength of the specimen No 3 obtained from the experiment is 578 kN, whereas the estimated base shear using non-regularized FB with 7 IPs was 465 kN, which has a 19.31% error. When regularization was applied for both materials, the ultimate strength was 508 kN, with a 12.56% error (see Figure 21). For the second specimen, FL3, the ultimate strength obtained from the experiment was 167.3 kN, whereas the estimated base shear using non-regularized FB with 7 IPs was 154.15 kN, which has a 7.86 % error. When both materials' regularization has been applied, the ultimate strength becomes 168.33 kN, with a 0.61 % error (see Figure 22). From the above results, it is seen that the localization issue

underestimates the maximum strength of the member subjected to high axial load. As illustrated in Figure and Figure 24, the DB element with regularized steel and concrete material produced an objective response for all types of mesh refinement. For column No 3, the estimated base shear using non-regularized DB with 16 elements is 472.612 kN, which is an 18.3 % error, whereas the ultimate strength is 501.83 kN for the fully regularized, with a 13.2 % error (see Figure). For the second specimen FL3, the ultimate strength of the column obtained from the experiment is 167.3kN, whereas the estimated based share using non-regularized DB with 16 elements is 155.8 kN, which has a 6.83 % error. For the fully regularized, the ultimate strength is 164.05 kN, which has a 1.94 % error (see Figure).

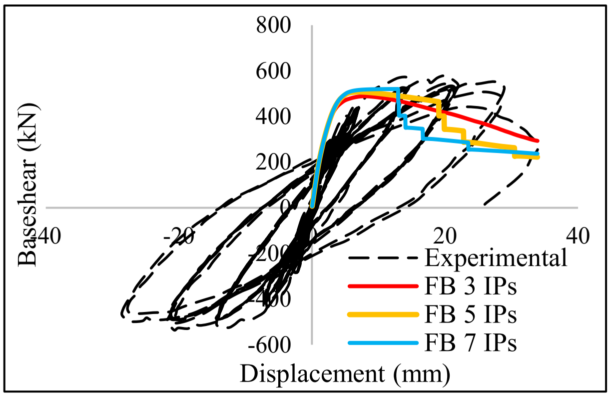

Figure 17. Monotonic response of specimen No. 3 using FB after applying material regularization only for concrete material.

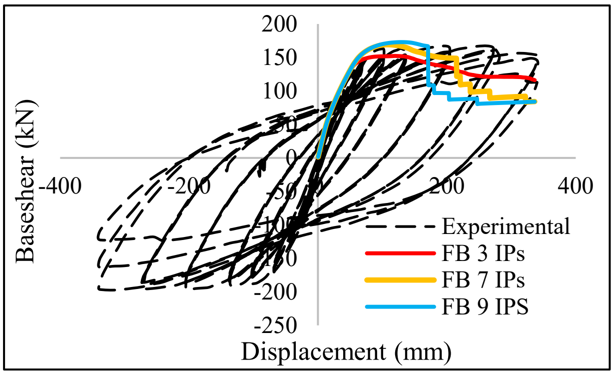

Figure 18. Monotonic response of specimenFL3 using FB after applying material regularization only for concrete material.

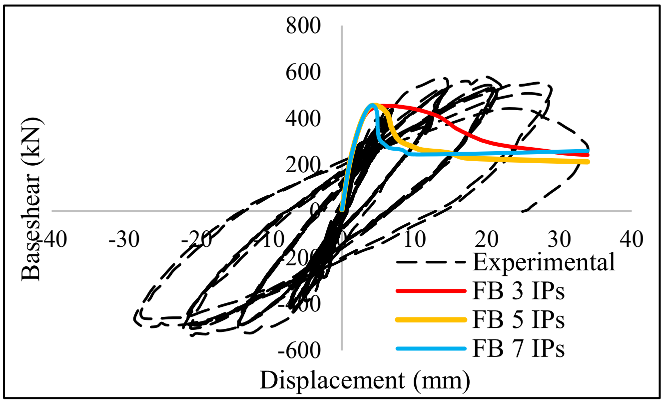

Figure 19. Monotonic response of specimen No. 3 using FB after applying material regularization only for steel material.

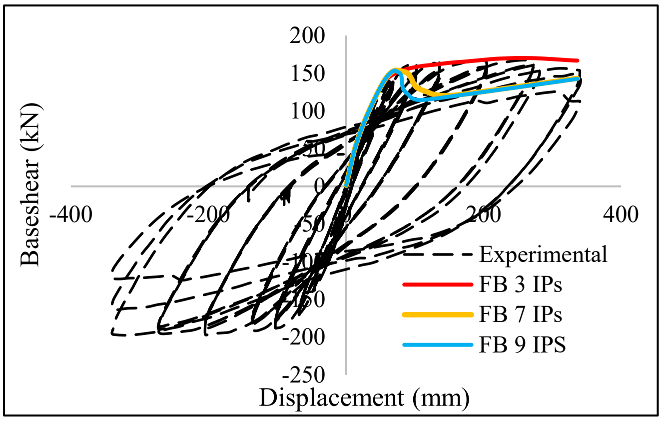

Figure 20. Monotonic response of specimen FL3 using FB after applying material regularization only for steel material.

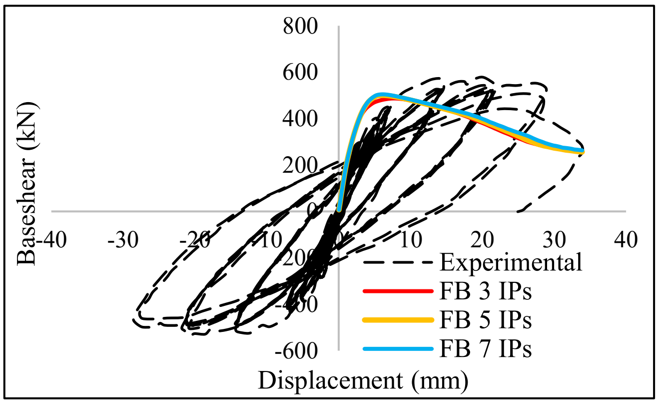

Figure 21. Monotonic response of specimen No. 3 using FB after applying material regularization for both concrete and steel materials.

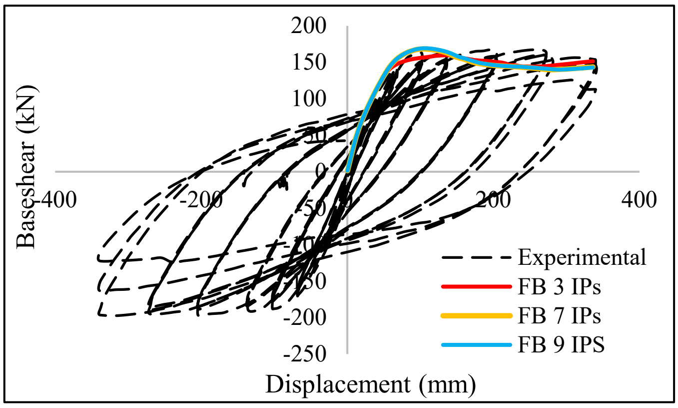

Figure 22. Monotonic response of specimenFL3 using FB after applying material regularization for both concrete and steel materials.

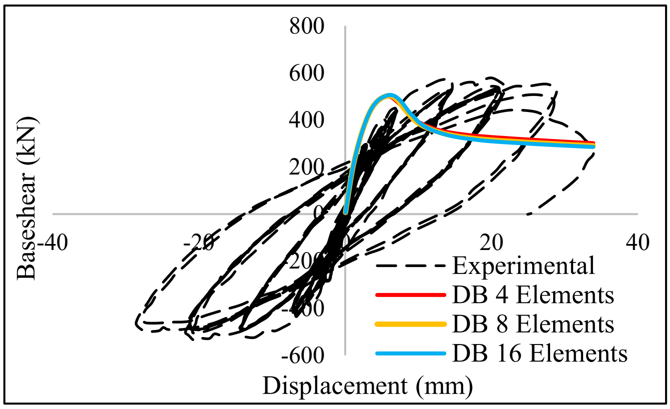

Figure 23. Monotonic response of specimen No. 3 using DB after applying material regularization for both concrete and steel materials.

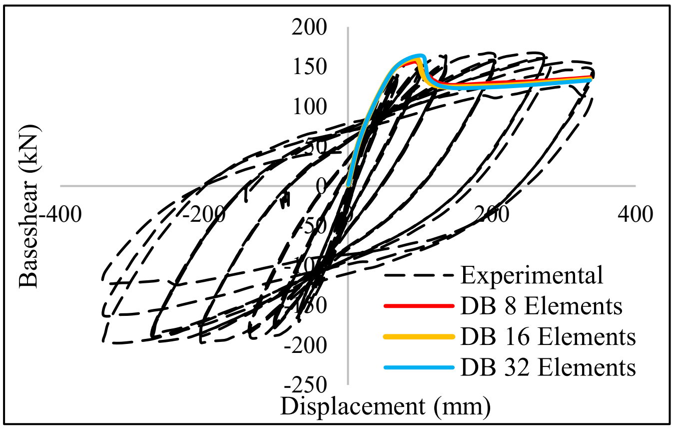

Figure 24. Monotonic response of specimen FL3 using DB after applying material regularization for both concrete and steel materials.

4. CONCLUSIONS

The research study offers the following results based on the experimentally tested cantilever columns for the section exhibiting strain-softening and strain-hardening behavior. For strain-hardening behavior, the distributed force-based fiber models with one element per member provide an accurate response. However, the distributed displacement-based fiber models require several elements per member to capture the actual inelastic response. Furthermore, in the distributed displacement-based fiber models, the rate of convergence in the local moment-curvature response is slow compared to the global force-deformation response. For sections exhibiting strain-softening behavior, both distributed force-based and displacement-based fiber models produce non-objective responses. The study identified two types of localization in the fiber models: linear softening and sudden loss of strength resulting from concrete softening and steel localization, respectively. Furthermore, if linear softening and sudden loss of strength are observed, it is recommended to employ regularization of steel and concrete materials to accurately capture the non-linear response.

CONFLICT OF INTEREST

The authors declare that there is no conflict of interest.

ACKNOWLEDGMENTS

The work described in this paper was prepared as a part of MSc thesis submitted in AAiT, AAU in 2019. The authors acknowledge the financial support from AAU and DBU.

REFERENCES

[1] Tauce,r F., Spacon,e E. and Filippou F., "*A fiber beam-column element for seismic response analysis of reinforced concrete structures"*, Report No. UCB/EERC-91/17, Earthquake Eng. Research Center, University of California at Berkeley, CA, December 2014, 1991.

[2] Neuenhofer, A. and Filippou, F.C., "*Evaluation of Nonlinear Frame Finite-Element Models*",Journal of Structural Engineering, vol. 123, no. 7, 1997.

[3] Coleman, E., and Spacone, J., "*Localization Issues in Force-Based Frame Elements*",Journal of Structural Engineering,vol. 127, no. 11, 2017, pp. 1257–1265.

[4] Calabrese, A., Almeida, J.P. and Pinho R., "*Numerical Issues in Distributed Inelasticity Modeling of RC Frame Elements for Seismic Analysis*",Journal of Earthquake Engineer*ing*, vol. 14, no. 51, 2010, pp. 38–68.

[5] Li, S., Zha,i C.H. and Xie, L.L., "*Evaluation of Displacement-Based, Force-Based and Plastic Hinge Elements for Structural Non-Linear Static Analysis*",Advances in Structural Engineering,vol. 15, no. 3, 2012, pp. 477–488.

[6] Pantò, B., Rapicavoli, D., Caddemi, S. and Caliò I., "*A smart Displacement Based (SDB) Beam Element with Distributed Plasticity*",Applied Mathematical Model,vol. 44, 2017, pp. 336–356.

[7] Pantò, B., Rapicavoli, D., Caddemi, S. and Caliò, I., "*A Fibre Smart Displacement Based (FSDB) Beam Element for the Nonlinear Analysis of Reinforced Concrete Members*",International Journal Non-Linear Mechanics,vol. 117, 2019.

[8] Filippou, F.C. and Fenves, G.L., "*Methods of Analysis for Earthquake- Resistant Structures", Earthquake Engineering: FromEngineering Seismology to Performance-Based Engineering",* Bozorgnia Y. and Bertero V. V., eds,Chap. 6, CRC Press, 2004, pp. 316–393.

[9] Kositić, S.M. and Deretić-Stojanović, B., "*FiberElement Formulation for Inelastic Frame Analysis*",Building Materials and Structures,vol. 59, no. 2, 2016, pp. 3–13.

[10] Jansen, D.C. and Shah, S.P., "*Effect of Length on Compressive Strain Softening of Concrete*",Journalof Engineering Mechanics, vol. 123, no. 1, 1997, pp. 25–35.

[11] Bazant, Z.P., Belytschko, T. and Chang, T.P., "*Continuum Theory for Strain-Softening*", Journal of Engineering Mechanics,vol. 110, no. 12, 1984, pp. 1666–1692.

[12] Zeris, C.A. and Mahin, S.A., "*Analysis of Reinforced Concrete Beam-Columns under Uniaxial Excitation*",Journal of Structural Engineering, vol. 114, no. 4, 1988, pp. 804–820.

[13] Scott, M.H. and Fenves, G.L., "*Plastic Hinge Integration Methods for Force-Based Beam–Column Elements*",Journal of Structural Engineering, vol. 132, no. 2, 2006, pp. 244–252.

[14] Kent, D.C. and Park, R., "*Flexural Members with Confined Concrete*",Journal of the Structural Division Proc. of the American Society of Civil Engineers, vol. 97, no. 7, 1971, pp. 1969–1990.

[15] Pugh, J.S., "*Numerical Simulation of Walls and Seismic Design Recommendations for Walled Buildings*", PhD dissertation, University of Washington, 2012.

[16] Ashtari, S., "*Evaluating the Performance-Based Seismic Design of RC Bridges*

According to the 2014 Canadian Highway Bridge Design Code", PhD Dissertation, University of British Columbia, 2018.

[17] Menegotto, M. and Pinto, P.E., "*Method of Analysis for Cyclically Loaded RC Plane Frames Including Changes in Geometry and Non-Elastic Behavior of Elements under Combined Normal Force and Bending*",Proceedings of IABSE Symposium on Resistance and Ultimate Deformability of Structures Acted on by Well Defined Repeated Loads, 1973.

[18] McKenna, F., Fenves, G.L. and Scott M.H., "*Open System for Earthquake Engineering Simulation*",University of California, Berkeley, 2000. http://opensees.berkeley.edu/

[19] Mander, J.B., Priestley, M.J.N. and Park R., "*Theoretical Stress-Strain Model for ConfinedConcrete*," Journal of Structural Engineering,vol. 114, no. 8, 1988, pp. 1804–1826.

[20] Priestley, M.J.N., Seible, F. and Calvi, G.M., "*Seismic Design and Retrofit of Bridges",* John Wiley & Sons, 1996.

[21] Fllippou, E., Popov, P. and Bertero, V.V, "*Effects of Bond Deterioration on Hysteretic Behavior of Reinforced Concrete Joints*", Earthquake Engineering Research Center, Report No. UCB/EERC-83/19, 1983.

[22] Kunnath, S.K., El-Bahy, A., Taylor, A. and Stone, W., "*Cumulative Seismic Damage of Reinforced Concrete Bridge piers*", Technical Report NCEER-97-0006, National Center for Earthquake Engineering Research, 1997.

[23] Wong, Y., Paulay, T. and Priestley, M., "*Response of Circular Reinforced Concrete Columns to Multi- Directional Seismic Attack*", ACI Struct J, vol. 90, no. 2, 1993, pp. 180–191.

[24] Kowalsky, M.J., Priestley M.J.N. and Seible, F., "*Shear and Flexural Behavior of Lightweight Concrete Bridge Columns in Seismic Regions*",ACI Structural Journal,vol. 96, no. 1, 1999, pp. 136–148

EFFECT OF TOXIC HEAVY METALS ON HUMAN HEALTH AT DOWNSTREAM IRRIGATION OF WASTEWATER TREATMENT PLANT: A CASE STUDY OF *KALITY* WASTEWATER TREATMENT PLANT, ADDIS ABABA, ETHIOPIA.

Johnny Girma 1[*], Asie Kemal [1], and Agizew Nigussie[1]

[1]*School of Civil and Environmental Engineering, Addis Ababa Institute of Technology, Addis Ababa University, Ethiopia*
** Corresponding Author: johnny.girma@aait.edu.et*

ABSTRACT

For several years, domestic wastewater from Addis Ababa's seven sub-cities has been treated at Kality domestic wastewater treatment plant. Despite being designed to treat domestic waste, certain industrial wastes were discharged into the treatment plant system via point and non-point sources, causing a number of problems. The effluent from the treatment plant was primarily used for irrigation by local farmers in the Akaki-Kality sub-city. To identify and quantify heavy and toxic heavy metals in treatment plant, samples were taken from effluent, irrigated soil, and vegetable plants to determine how they affect human health downstream, a cross-sectional study design was used. Liquid samples were collected from the Up flow Anaerobic Sludge Blanket reactor (UASB) reactor's inlet and outlet, trickling filter and secondary clarifier outlets, a soil sample from a cultivated field, and plant samples such as Habesha gommen and Kosta grown in the effluent. The presence and concentration of heavy and toxic heavy metals were determined in the samples, and the ability of unit processes such as the UASB, trickling filter, and secondary clarifier to remove toxic heavy metals was assessed. The laboratory tests revealed that majority of the toxic heavy metals were present in the samples analyzed (chromium, cadmium, arsenic, copper, lead, and manganese) and the unit processes were inefficient to remove theses metals.

Key Words: *Concentration, EPA, Toxic Heavy Metal, Trickling Filter, UASB*

1. INTRODUCTION

There are two types of biological processes with a high content of organic materials in wastewater treatment plants: aerobic and anaerobic processes[1]. Anaerobic processes use less energy and produce methane which can be used as a source of energy. The *Kality* domestic wastewater treatment plant employs an anaerobic process (the UASB reactor). For *Kality* domestic wastewater treatment plant the overall design removal for COD and BOD is 55%. Since the plant's inception, the plant's effluent has been used for irrigation. The practice of using treated effluent for irrigation will boost food production, which will support Addis Ababa's formal food production. Because the Addis Ababa population is growing at an alarming rate, and sub cities are expanding the residents are practicing using domestic wastewater treatment plant effluents for irrigation to support the people's livelihood. An increase in population should result in an increase in sectors such as agricultural production and irrigated lands, which rely on water resources for irrigation. These conditions have compelled farmers to irrigate with alternative water resources (i.e., blackish water, wastewater, and effluent water), thereby closing the gap between freshwater availability and crop demand [2]. Irrigation with treated municipal wastewater is an important component of global environmental strategies, and the scientific community is focusing more on it [3-5]. In a number of countries, treated wastewater is already regarded as a suitable water source for irrigation, primarily in agriculture and landscaping [6-8]. Despite the potential economic, social and environmental benefits of irrigation with treated municipal wastewater, the effects of reuse must be continuously monitored to ensure resource protection, soil health and particularly human health. Irrigation with treated wastewater produces a significant amount of biodegradable organic material (carbon and nitrogen), mineral macro and micronutrients (such as phosphorous, potassium, and magnesium), and toxic heavy metals (such as Molybdenum, Selenium, Boron, Chromium, Manganese, Lead, Arsenic, Cadmium and Copper) required for crop growth but affects human health beyond the recommended concentration [9]. To maintain soil quality, however, the possibility of trace pollutants, heavy metals, and salts accumulating in the soil must be considered. Heavy metal content in effluents can vary depending on treatment method (less or more intensive) and wastewater source (industrial, municipal, etc.). So, concentrations in the receiving system (soil, plant) must be monitored [10-12]. In contrast, long-term application of fully or partially treated or untreated wastewater may result in toxic heavy metal deposition in the soil [13]. Home and business effluents, drainage water, atmospheric deposition, and traffic-related emissions carried by storm water into sewage and/or irrigation systems carry a variety of pollutants and enrich urban wastewater with toxic heavy metals [14-16].

This study was conducted to identify the types of toxic heavy metals that exist in *Kality* domestic wastewater treatment plant effluent, downstream irrigated soil, and cabbages, as well as their effect on human health, and to compare their magnitude with the Ethiopian Guideline Ambient Environmental Standards, FAO/WHO, in order to determine the treatment efficiency of UASB reactor, trickling filter, and secondary clarifier in removing toxic heavy metals.

Eating food crops grown in wastewater-irrigated areas is one of the most important factors contributing to human pathogen exposure. Furthermore, growing crops for human consumption on wastewater-irrigated soil may result in trace metal uptake and buildup in edible plant parts, posing a risk to humans [17-19]. Heavy metals are extremely dangerous due to their non-biodegradability, long half-lives, and high bioaccumulation potential [20].According to several researchers, excessive accumulation of heavy metals and even important trace elements like Cu ,Cd, Mn , As ,Pb, and Zn in the human body can cause serious health problems [20-23]. Some heavy metals are required for human biological processes, but their consumption can have unanticipated negative effects on health and the physiological system, depending on the dosage (concentration) [24].Excessive heavy metal accumulation in agricultural soils as a result of wastewater irrigation may result in soil contamination as well as increased heavy metal uptake by crops, compromising food quality and safety [25].

According to [26], studies show that heavy metals, despite their beneficial health effects, act as carcinogenic agents. Dissolved forms of these metals enter the food chain via various means, including soil pollutants, water pollutants, and air pollutants, and eventually end up in humans, causing severe damage to the cellular system. Toxic metals pose health risks based on the concentrations of these metals in specific media and the length of exposure. Long-term and chronic exposure to hazardous metals, even at low levels, can cause health problems [27].

Heavy metal toxicity, according to Singh A et.al [28], can be classified into the following categories: nephrotoxicity, neurotoxicity, hepatotoxicity, carcinogenicity, cardiovascular toxicity, immunological toxicity, skin toxicity, genotoxicity, and Reproductive and developmental toxicity.

Lead has toxic effects on various organ systems, but those in the kidney are the most difficult. Acute lead nephropathy causes proximal tubular dysfunction, resulting in Fanconi-like syndrome Cadmium can also cause glucosuria, Fanconi-like syndrome, Phosphaturia, and aminoaciduria [29- 31].

Manganese is a necessary element that is involved in a number of physiological functions in the body. Acute exposure may have a neuro-protective effect by lowering apoptotic cellular death, but chronic exposure can result in dangerous illnesses such as Alzheimer's and Parkinson's disease [32]. When arsenic is consumed, it causes central nervous system cognitive impairment. It has also been linked to a variety of neurological disorders, including neurodevelopmental changes, and is associated with an increase in neurodegenerative diseases [33]. Arsenic exposure also has an impact on synaptic transmission and neurotransmitter balance [34].

Cadmium affects two human tissues: the renal cortex and the liver [35]. It accumulates in the liver during acute exposure and has been linked to a variety of hepatic dysfunctions. Cadmium alters the redox balance of cells, causing oxidative stress and hepatocellular damage [36]. Cadmium-induced hepatotoxicity, both acute and chronic, causes liver failure and thus increases the risk of cancer [37]. Arsenic poisoning increases the risk of cancer by binding to DNA-binding proteins and slowing the repair process [38].

Lead is a carcinogenic chemical that causes the DNA repair mechanism, cellular tumor-regulating genes, and chromosomal structure and sequence to be damaged. It interferes with transcription by removing zinc from certain regulatory proteins [39].

Cadmium is a carcinogenic and toxic metal [40]. Exposure to low to moderate levels of cadmium causes hypertension [41], diabetes ('Urinary Cadmium, Impaired Fasting Glucose, and Diabetes in the [42], carotid atherosclerosis [43], peripheral arterial disease [44], myocardial infarction and [45]. Cadmium has been linked to an increased risk of cardiovascular death in the general population of the United States in prospective studies [46].

2. MATERIALS AND METHODS

2.1 Study area

The *Kality* domestic wastewater treatment plant is owned by the Addis Ababa City Water and Sewerage Authority (AAWSA). It is located in Addis Ababa, Ethiopia, at 8°55' 11"N and 38°45'19"E. It is capable of handling a maximum flow rate of 100,000 m^3/day. The process includes a UASB front end, trickling filters, secondary clarifiers, and chlorination/dechlorination for disinfection before dumping into the river. The plant's catchment area was modeled, and 18 kilometers of additional sewer trunk mains were constructed [47]. The *Kality* wastewater treatment plant accounts for approximately 29% of the city's wastewater treatment coverage.

2.2 Study layout

A cross-sectional study was used to investigate heavy metal and toxic heavy metal concentrations in the *Kality* wastewater treatment plant, downstream irrigated soil, and vegetables during dry seasons.

2.3 Reconnaissance Survey

Before the official survey began, a reconnaissance survey was conducted. The preliminary data needed for sampling and sample transportation was assessed. The site description, vegetable varieties grown downstream of the treatment plant, and irrigated areas using the treatment plant's effluent were all documented.

2.4 Sample collection and preparation

Six specific sampling areas were selected based on vegetable availability, irrigation soil, and wastewater. For all samples, we used grab sampling techniques. Four water samples were collected from different treatment plant unit processing regions (sample-1: UASB reactor inlet, sample-2: UASB reactor outlet, sample-3: trickling filter outlet, sample -4: secondary clarifier outlet). A representative soil sample was collected from the irrigation area. Two types of plants were collected from the area where treatment plant effluent was used for irrigation. These points were chosen because we believed they would produce a better result.

2.4.1 Water samples

At various unit process locations, four water samples were collected from the treatment plant.

To avoid cross-contamination,1000ml of water was collected from each sampling station using pre-cleaned bottles. The locations of the samples were labeled. The water samples were kept cool in an icebox, and the time between sampling and analysis was kept to a bare minimum of 2hrs.

The optimum procedure for digestion of water and sediment samples was carried out for three hours at 250°C using 50 mL of water, 4 mL of HNO_3, and 1 mL of HCl. The digested volume remained at 25 ml after digestion, and was filtered in a 50 ml Erlenmeyer flask and refilled to volume.

2.4.2 Soil samples

A kilogram of soil was taken from the irrigation area. The sample was taken during the dry season to allow for easier soil-water mixing and to avoid inaccurate results caused by urea fertilizer and lime. To obtain an accurate result, the sample was made leaf-free. To avoid mixing with metal containers, the sample was stored in non-reactive containers in plastic bags. To avoid mixing of plant leaves and other materials; the sampling depth was set between 10 and 15 cm.

The soil sample was dried in an oven set to 30-40°C until it reached a constant weight. The dried sample was sieved with 2mm sieve size. The sample was ground to 9µm. The Coupled Plasma Optical Emission Spectrometry (ICP-OES) instrument was used for heavy metal analysis.

The sample (1g) was placed in a 50 mL crucible and treated with 10mL of concentrated HNO_3. To allow oxidation, the solution was placed on a hot plate for 30-45 minutes. Following cooling, 4 ml of 20% H_2O_2 was added, and the solution was reheated on a hot plate until the digest became clear and semi-dried. Before GF-AAS analysis, the suspension was filtered into a 50ml volumetric flask and diluted with deionized distilled water to the mark.

2.4.3 Plant Samples

During the dry season, farmers irrigate two types of widely consumed fresh vegetables cultivated with the *Kality* wastewater treatment effluent: Ethiopian Kale (*Habesh Gommen*) and Swiss chard (*kosta*).

Two plant samples were collected (each 500gram). Plants were collected from every corner of the plots to ensure that the samples were representative. The samples were carefully collected to avoid damaging, dead, or dying plant tissue. Before placing the samples in the bag, soil from the plant material was brushed off. To avoid cross-contamination, samples were collected in clean plastic bags separately. The plant samples were kept cool in an icebox.

In a "high form" porcelain crucible, 1.25g of sample was weighed. The sample was placed in the furnace, whose temperature was raised to 540°C . The sample was ashed for 6 hours and then wetted with distilled water before being dried on a hot plate with 5-10 ml of 6N HCl. To dissolve the ash, 10 mL of 1NHCl was added to the sample before the ash was dissolved. The sample was transferred to the ICP test tube.

2.5 Sample characterization

Total Cu, Pb, Cr, Cd, As, and Mn levels in digested water, soil, and vegetable samples were determined using Inductively Coupled Plasma Optical Emission Spectrometry (ICP-OES).

3. RESULTS AND DISCUSSION

3.1 Results

3.1.1 Water Sample

The major heavy metals found in the analysis of *Kality* domestic wastewater treatment plant effluent, irrigated soil, and plants were Iron, Manganese, Nickel, Cobalt, Copper, Zinc, Cadmium, Mercury, Lead, Arsenic, Boron, and Chromium.

Toxic heavy metals like Arsenic, Cadmium, Chromium, Copper, Manganese, and Lead were also discovered in the effluent, as shown in Table 1.

Table 1 Toxic heavy metals in water samples.

Toxic Heavy metals	(Sample-1) Concentration at the UASB inlet (mg/L)	(Sample-2) Concentration at the UASB outlet (mg/L)	(Sample-3) Concentration at the trickling filter outlet (mg/L)	(Sample-4) Concentration at the secondary clarifier outlet (mg/L)
Arsenic (As)	0.072±0.006	0.048±0.009	0.034±0.034	0.059±0.059
Cadmium (Cd)	0.053±0.001	0.053±0.005	0.036±0.002	0.056±0.004
Chromium (Cr)	0.145±0.002	0.103±0.011	0.075±0.012	0.073±0.055
Copper (Cu)	0.058±0.009	0.014±0.010	0.006±0.002	0.080±0.003
Manganese Mn)	1.215±0.005	0.800±0.003	0.578±0.005	0.441±0.003
Lead (Pb)	0.490±0.078	0.436±0.041	0.219±0.005	0.334±0.001

3.1.2 Soil Samples

The soil sample contained toxic heavy metals such as Arsenic, Cadmium, Chromium, Copper, Manganese, and Lead. Table 2 shows the mean concentrations of toxic heavy metals in the soil sample.

Table 2 Soil sample's mean toxic heavy metal concentration

Arsenic (As)	Cadmium (Cd)	Chromium (Cr)	Copper (Cu)	Manganese (Mn)	Lead (Pb)
8.760±0.140	**7.630±0.090**	41.287±0.866	**21.209±0.410**	929.67±12.3	119.6±3.400

3.1.3 Plant samples

Toxic heavy metals such as As, Cd, Cr, Cu, Mn, and Pb were found in plant samples. Plant samples like local cabbage (*Habesha Gommen*) and Swiss chard (*Kosta*) were found contained toxic heavy metals. The mean concentration of the toxic heavy metals concentrations are shown in the Table 3.

Table 3 Plant samples mean toxic heavy metal concentration

Heavy metals	Ethiopian Local Cabbage concentration (mg/L)	Swiss Chard concentration (mg/L)
Arsenic (As)	0.766±0.038	0.272±0.027
Cadmium (Cd)	0.189±0.014	0.008±0.046
Chromium (Cr)	1.193±0.092	0.327±0.042
Copper (Cu)	4.724±0.420	4.349±0.040
Manganese (Mn)	23.618±1.288	54.320±0.286
Lead (Pb)	2.784±0.373	0.559±0.045

3.2 Discussion

3.2.1 Water samples

The samples were analyzed for heavy metals and toxic heavy metals. Heavy metals such as Iron, Manganese, Nickel, Cobalt, Copper, Zinc, Cadmium, Mercury, Lead, Arsenic, Boron, and Chromium were found in all of the samples. Again, the samples were analyzed for the presence of toxic heavy metals. In all of the samples Arsenic, Cadmium, Chromium, Copper, Manganese, and Lead were found in the effluent as shown in the Table 4. Point and non-point sources were assumed as the possible sources of toxic heavy metals.

Table 4.Toxic heavy metals and their mean concentration in the water samples

Toxic Heavy metals	(Sample-1) Concentration at the UASB inlet (mg/L)	(Sample-2) Concentration at the UASB outlet (mg/L)	(Sample-3) Concentration at the Trickling filter outlet (mg/L)	(Sample-4) Concentration at the secondary clarifier outlet (mg/L)	Surface water quality standard by Guideline Ambient Environment Standard for Ethiopia	FAO/ WHO standard for irrigation water (mg/L)
Arsenic (As)	0.070±0.010	0.048±0.009	0.034±0.034	0.059±0.059	0.05mg/L	0.100
Cadmium (Cd)	0.050±0.001	0.053±0.005	0.036±0.002	0.056±0.004	5µg/l	0.010
Chromium (Cr)	0.150±.002	0.103±0.011	0.075±0.012	0.073±0.055	50µg/l	0.550
Copper (Cu)	0.058±.0100	0.014±0.010	0.006±0.002	0.080±0.003	5mg/L	0.017
Manganese (Mn)	1.215±.0100	0.800±0.003	0.578±0.005	0.441±0.003	0.3mg/L	0.200
Lead (Pb)	0.490±.080	0.436±0.041	0.219±0.005	0.334±0.001	0.05mg/L	0.065

As shown in Table 4, the UASB reactor has a removal efficiency of 33.3 percent for As, 0 percent for Cd, 28.9 percent for Cr, 75.7 percent for Cu, 34.2 percent for Mn, and 11.0 percent for Pb. The UASB reactor removal efficiency for toxic heavy metals such as As is higher than the surface water quality standard set by Ethiopia's Guideline Ambient Environment Standard (EPA), but it is lower for Cd, Cr, Cu, Mn, and Pb. Since the UASB reactor's primary use is for biological processes, it is inefficient at removing toxic heavy metals. According to FAO/WHO standards, the

UASB reactor is effective at removing toxic heavy metals such as As, Cr, and Cu, but it is ineffective at removing toxic heavy metals such as Cd, Mn, and Pb. The removal efficiency of toxic heavy metals (As, Cr, Cd, Mn, Cu, Pb) by trickling filters and secondary clarifiers is below the standard for both surface water quality guidelines and FAO/WHO. Despite the fact that the treatment plant's primary purpose is for biological processes, the removal of toxic heavy metals from domestic wastewater must be taken into account.

3.2.2 Soil Samples

Toxic heavy metal such as Arsenic, Cadmium, Chromium, Copper, Manganese, and Lead were found in the irrigated soil sample at downstream of *Kality* Wastewater Treatment Plant. Table 5 summarizes the results.

Table 5 Mean toxic heavy metal concentration in soil sample

Toxic Heavy metals	Concentration of toxic metal in Soil sample (mg/L)	Soil standard by Guideline Ambient Environment Standard for Ethiopia (mg/kg of dry wt.)	FAO/WHO standard for soil (mg/L)
Arsenic (As)	8.758±0.139	20.000	-
Cadmium (Cd)	7.627±0..096	0.500	3.000
Chromium (Cr)	41.287±0.866	20.000	-
Copper (Cu)	21.209±0.410	500.000	140.000
Manganese (Mn)	929.665±12.210	20.000	80.000
Lead (Pb)	119.610±3.301	40.000	84.000

Except for Cu and Pb metals, the mean concentrations determined by soil sample test analysis were found to be higher than the soil standard established by the Ethiopian Guideline Ambient Environment Standard (EPA) and FAO/WHO standards, as shown in the table 5. Since *Kality* WWTP's primary use is for biological processes, the existence of higher concentration of toxic heavy metals at downstream irrigated soils were expectable. Thus, other treatment facilities were required to reduce their concentrations to an acceptable level based on the standard.

3.2.3 Plant samples

Local Cabbage (Habesha Gommen) and Swiss chard (kosta) plant samples were analyzed for toxic heavy metals such as As, Cd, Cr, Cu, Mn, and Pb. Table 6 summarizes the findings.

Table 6 Mean heavy metal concentration of plant sample

Heavy metals	Ethiopian Local Cabbage concentration (mg/L)	Swiss Chard concentration(mg/L)	FAO/WHO standard for plant (mg/L)
Arsenic (As)	0.766±0.038	0.272±0.027	-
Cadmium (Cd)	0.189±0.014	0.008±0.046	0.020
Chromium (Cr)	1.193±0.092	0.327±0.042	5.000
Copper (Cu)	4.724±0.420	4.349±0.040	40.000
Manganese (Mn)	23.618±1.288	54.320±0.286	500.000
Lead (Pb)	2.784±0.373	0.559±0.045	0.300

The mean concentrations of As, Cd, and Pb certain toxic heavy metals in local cabbage and Swiss chard plants were higher than the FAO/WHO. Owing to the fact that the WWTP did not have unit processes for the removal of toxic heavy metals.

4. CONCLUSIONS

The presence of (toxic) heavy metals in treatment plant effluent, irrigated soil, and vegetable plants were investigated in this research. The ability of unit processes such as the UASB reactor, trickling filter, and secondary clarifier to remove toxic heavy metals was determined. Heavy metals such as Iron, Nickel, Cobalt, Zinc, Mercury, and Boron were found in all of the samples tested. Majority of toxic heavy metals such as Chromium, Cadmium, Arsenic, Copper, Lead, and Manganese were also found in the samples. Furthermore, the mean concentrations of these chemicals in effluent, soil, and cabbage plants were compared to Ethiopian Ambient Environmental Standards and FAO/WHO Standards. Majority of the mean concentrations of toxic heavy metals in the effluent, irrigated soil samples, and vegetables were found to be above values set in these standards. Though the UASB reactor removes some toxic heavy metals, its removal efficiency is determined to be less than the standards. Likewise, laboratory results showed that trickling filters and secondary clarifiers were ineffective in removing toxic heavy metals. Thus, individuals exposed to the consumption of vegetables irrigated by the plant's effluent have a significantly higher risk of developing illnesses such as nephrotoxicity, neurotoxicity, hepatotoxicity, carcinogenicity, cardiovascular toxicity, immunological toxicity, skin toxicity, genotoxicity, etc. It is recommended to include chemical processes like hydration, chemical precipitation, adsorption and heavy metal settlement processes in the *Kality* Wastewater Treatment Plant in order to minimize the effect of toxic heavy metals on those who use the effluent for irrigation.

CONFLICT OF INTEREST

The authors declare that there is no conflict of interest.

ACKNOWLEDGEMENTS

The authors would like to acknowledge students Abenezer M, Dawit M. and Burkitawit T. for data collection and taking the samples to laboratory for analysis. Furthermore, I would like to thank all workers at *Kality* WWTP.

REFERENCES

[1] Gómez, R.R., " *Upflow anaerrobic sludge blanket reactor: modeling"* Licentiate thesis, Royal Institute of Technology, Sweden, 2011.

[2] Amer, K.H., *"Corn crop response under managing different irrigation and salinity levels*", Agric Water Manag, vol. 97, no. 10, 2010, pp. 1553-1563. doi:10.1016/j.agwat.2010.05.010

[3] Campi, P., Navarro, A., Palumbo, A.D., Mastrangelo, M. and Lonigro, A., *"Bioenergy productivity of sugar beet irrigated with reclaimed wastewaters*", Italian Journal of Agronomy, vol. 10, no. 3, 2015, pp. 155-159. doi:10.4081/ija.2015.652.

[4] Intriago, J.C., López-Gálvez, F., Allende, A., et al., *"Agricultural reuse of municipal wastewater through an integral water reclamation management*", J Environ Manage. vol. 213, 2018, pp. 135-141. doi:10.1016/j.jenvman.2018.02.011

[5] Chaoua, S. Boussaa, S., El Gharmali, A. and Boumezzough, A., "*Impact of irrigation with wastewater on*

accumulation of heavy metals in soil and crops in the region of Marrakech in Morocco", J Saudi Soc Agric Sci. vol. 18, no. 4 pp. 429-436, 2019. doi:10.1016/j.jssas.2018.02.003

[6] Toze, S., "*Reuse of effluent water - Benefits and risks*", Agric Water Manag.; vol. 80, (1-3 spec. iss.), pp. 147-159, 2006. doi:10.1016/j.agwat.2005.07.010

[7] Becerra-Castro, C., Lopes, A.R., Vaz-Moreira, I., Silva, E.F., Manaia C.M. and Nunes, O.C., "*Wastewater reuse in irrigation*: *A microbiological perspective on implications in soil fertility and human and environmental health*", Environ Int. vol. 75, 2015, pp. 117-135. doi:10.1016/j.envint.2014.11.001

[8] Vivaldi, G.A., Camposeo, S., Lopriore, G., Romero-Trigueros, C., Salcedo, F.P., "*Using saline reclaimed water on almond grown in Mediterranean conditions": Deficit irrigation strategies and salinity effects*", Water Sci Technol Water Supply, vol. 19 no. 5, 2019, pp. 1413-1421. doi:10.2166/ws.2019.008

[9] Pedrero, F., Camposeo, S., Pace, B., Cefola, M., Vivaldi, G.A., "*Use of reclaimed wastewater on fruit quality of nectarine in Southern Italy*", Agric Water Manag. vol. 203(January), 2018, pp. 186-192. doi:10.1016/j.agwat.2018.01.029

[10] Siebe, C., Fischer, W.R., "*Effect of long-term irrigation with untreated sewage effluents on soil properties and heavy metal adsorption of leptosols and vertisols in Central Mexico*", doi:10.1002/JPLN.1996.3581590408

[11] Wuana, R.A. and Okieimen F.E., "*Heavy Metals in Contaminated Soils: A Review of Sources, Chemistry, Risks and Best Available Strategies for Remediation*", ISRN Ecol., 2011, 120. doi:10.5402/2011/402647

[12] Kiziloglu, F.M., Turan, M., Sahin, U., Kuslu, Y., and Dursun, A., "*Effects of untreated and treated wastewater irrigation on some chemical properties of cauliflower (Brassica olerecea L. var. botrytis) and red cabbage (Brassica olerecea L. var. rubra) grown on calcareous soil in Turkey*", Agric Water Manag. vol. 95, no. 6, 2008, :pp. 716-724. doi:10.1016/j.agwat.2008.01.008

[13] Elgallal, M., Fletcher, L., and Evans B., "*Assessment of potential risks associated with chemicals in wastewater used for irrigation in arid and semiarid zones: A review*", Agric Water Manag. vol. 177: , 2016, pp. 419-431. doi:10.1016/j.agwat.2016.08.027

[14] Shah, M.T., Ara J., Muhammad, S., Khan, S. and Tariq S., "*Health risk assessment via surface water and sub-surface water consumption in the mafic and ultramafic terrain", Mohmand agency, northern Pakistan*", J. Geochemical Explor., vol. 118, 2012, pp. 60-67., doi:10.1016/j.gexplo.2012.04.008

[15] Zia, M.H., Watts, M.J., Niaz, A., Middleton, D.R.S. and Kim, A.W., "*Health risk assessment of potentially harmful elements and dietary*

minerals from vegetables irrigated with untreated wastewater, Pakistan", Environ Geochem Health. vol. 39, no. 4, 2017, pp. 707-728. doi:10.1007/s10653-016-9841-1

[16] Woldetsadik, D., Drechsel, P., Keraita, B., Itanna, F., Erko, B. and Gebrekidan, H., "*Microbiological quality of lettuce (Lactuca sativa) irrigated with wastewater in Addis Ababa, Ethiopia and effect of green salads washing methods*", Int J Food Contam. vol. 4, no. 1, 2017. doi:10.1186/s40550-017-0048-8

[17] Rattan, R.K., Datta, S.P., Chhonkar, P.K., Suribabu, K. and Singh, A.K., "*Long-term impact of irrigation with sewage effluents on heavy metal content in soils, crops and groundwater - A case study*", Agric Ecosyst Environ. vol. 109, no. 34, 2005, pp. 310-322. doi:10.1016/j.agee.2005.02.025

[18] Xue, Z.J., Liu, S.Q., Liu, Y.L. and Yan, Y.L., "*Health risk assessment of heavy metals for edible parts of vegetables grown in sewage-irrigated soils in suburbs of Baoding City, China*", Environ Monit Assess. vol. 184, no. 6, 2012, pp. 3503-3513. doi:10.1007/s10661-011-2204-6

[19] Ahmad, K., Ashfaq, A., Khan, Z.I., Muhammad, K. and Niaz, Z., "*Health risk assessment of heavy metals and metalloids via dietary intake of a potential vegetable (Coriandrum sativum L.) grown in contaminated water irrigated agricultural sites of Sargodha, Pakistan*", Hum Ecol Risk Assess, vol. 22, no. 3, 2016, pp. 597-610. doi:10.1080/10807039.2015.109563

[20] Oliver, M.A., "S*oil and human health: A review*", Eur J Soil Sci. vol. 48, no. 4, 1997, pp. 573-592. doi:10.1111/j.1365-2389.1997.tb00558.x

[21] Järup, L., "*Hazards of heavy metal contamination*", Br Med Bull. vol. 68, 2003, pp. 167-182. doi:10.1093/bmb/ldg032

[22] Luo, C., Liu, C., Wang, Y., Camposeo, K. and Romero M., "*Heavy metal contamination in soils and vegetables near an e-waste processing site, south China*", J Hazard Mater, vol. 186, no. 1, 2011, pp. 481-490. doi:10.1016/j.jhazmat.2010.11.

[23] Kim, Y.J. and Kim, J.M., "*Arsenic Toxicity in Male Reproduction and Development*", Dev Reprod, vol. 19, no. 4, 2015, pp. 167-180., doi:10.12717/dr.2015.19.4.167

[24] Tchounwou, P.B., Yedjou, C.G., Patlolla, A.K. and Sutton, D.J., "*Molecular, Clinical and Environmental Toxicicology*", Environmental Toxicology, vol 101, 2012. doi:10.1007/978-3-7643-8340

[25] Muchuweti, M., Birkett, J.W., Chinyanga, E., Zvauya, R., Scrimshaw, M.D. and Lester, J.N., "*Heavy metal content of vegetables irrigated with mixtures of wastewater and sewage sludge in Zimbabwe: Implications for human health*", Agric. Ecosyst. Environ, 2006,vol. 112, no. 1, pp. 41-48. doi:10.1016/j.agee.2005.04.028

[26] Kim, J.J., Kim, Y.S. and Kumar, V., "*Heavy metal toxicity: An update of*

chelating therapeutic strategies", J Trace Elem Med Biol. vol. 54(May), 2019, pp. 226-231. doi:10.1016/j.jtemb.2019.05.003

[27] Mahalakshmi, M., "*Characteristic levels of heavy metals in canned tuna fish*", J Toxicol Environ Heal Sci. vol.4, no. 2, 2012, pp. 43-45. doi:10.5897/jtehs11.079

[28] Singh, A., Sharma, R.K., Agrawal, M. and Marshall, F.M, "*Health risk assessment of heavy metals via dietary intake of foodstuffs from the wastewater irrigated site of a dry tropical area of India*", Food Chem Toxicol, 2010, vol. 48, no. 2, pp. 611-619. doi:10.1016/j.fct.2009.11.041

[29] Nolan, C. V. and Shaikh, Z.A., "*Lead nephrotoxicity and associated disorders: biochemical mechanisms*", Toxicology', vol. 73, no. 2, 1992, pp. 127-146. doi:10.1016/0300-483X(92)90097

[30] Hazen-Martin, D.J., Todd, J.H., Sens, M.A. and Okieimen ,A., "*Electrical and freeze-fracture analysis of the effects of ionic cadmium on cell membranes of human proximal tubule cells*", Environ Health Perspect, vol. 101, no. 6, pp. 510-516, 1993. doi:10.1289/ehp.93101510

[31] Reyes, J.L., Molina-Jijón, E., Rodríguez-Muñoz, R., Bautista-García, P., Debray-García, Y. and Namorado, M.D.C., "*Tight junction proteins and oxidative stress in heavy metals-induced nephrotoxicity*", Biomed Res Int. 2013. doi:10.1155/2013/73078

[32] Goldhaber, SB., "*Trace element risk assessment: Essentiality vs. toxicity*", Regul Toxicol Pharmacol., vol. 38, no. 2, 2003, pp. 232-242.doi:10.1016/S0273-2300(02)00020-X

[33] Garza-Lombó, C. Pappa, A., Panayiotidis, MI., Gonsebatt, M.E. and Franco, R., "*Arsenic-induced neurotoxicity: a mechanistic appraisal*', J Biol Inorg Chem. vol. 24, no. 8, 2019, pp. 1305-1316. doi:10.1007/s00775-019-01740-8

[34] Tolins, M., Ruchirawat, M., Landrigan, P., "*The developmental neurotoxicity of arsenic: Cognitive and behavioral consequences of early life exposure*", Ann Glob Heal. vol. 80, no. 4, 2014, pp. 303-314. doi:10.1016/j.aogh.2014.09.005

[35] Bernard, A., "*Renal dysfunction induced by cadmium: Biomarkers of critical effects*", Bio Metals., vol. 17, no. 5, 2004, pp. 519-523.doi:10.1023/B:BIOM.0000045731.75602.b9

[36] Zalups, R.K., "*Evidence for basolateral uptake of cadmium in the kidneys of rats*", Toxicol Appl Pharmacol, vol. 164, no. 1, 2000, pp. 15-23. doi:10.1006/taap.1999.8854

[37] Hyder, O., Chung, M., Cosgrove, D. and Liu, C., "*Cadmium Exposure and Liver Disease among US Adults*", J Gastrointest Surg, vol. 17, no. 7, 2013, pp, 1265-1273, doi:10.1007/s11605-013-2210-9

[38] Uter, W., Werfel, T., White, I.R. and Johansen, J.D., "*Contact allergy: A*

review of current problems from a clinical perspective", Int J Environ Res Public Health, vol. 15, no. 6, 2018. doi:10.3390/ijerph15061108

[39] Silbergeld, E.K., Waalkes, M. and Rice, J.M., "*Lead as a carcinogen: Experimental evidence and mechanisms of action*", Am J Ind Med, vol. 38, no. 3, pp. 316-323, 2000. doi:10.1002/10970274(200009)38:3<316::AID-AJIM11>3.0.CO;2-P

[40] Addis Ababa Water and Sewerage Authority (AAWSA), "*Wastewater Masterplan* ", vol.1, 2002.

[41] Tellez-Plaza, M., Navas-Acien, A., Crainiceanu, C.M. and Guallar, E., "*Cadmium exposure and hypertension in the 1999-2004 National Health and Nutrition Examination Survey (NHANES)*", Environ Health Perspect, 2008, vol. 116, no. 1, pp. 51-56.doi:10.1289/ehp.10764

[42] Schwartz, G.G., Il'Yasova, D. and Ivanova, A., "*Urinary cadmium, impaired fasting glucose, and diabetes in the NHANES III*", Diabetes Care, vo.. 26, no. 2, 2003, pp. 468-70. doi:10.2337/diacare.26.2.468

[43] Messner, B., Knoflach, M., Seubert, A. and Okieimen, A., "*Cadmium is a novel and independent risk factor for early atherosclerosis mechanisms and in vivo relevance*", Arterioscler Thromb Vasc Biol., vol. 29, no. 9, 2009, pp. 1392-1398. doi:10.1161/ATVBAHA.109.19008

[44] Navas-Acien, A., Selvin, E., Sharrett, A.R. Calderon-Aranda, E., Silbergeld, E. and Guallar, E., "*Lead, cadmium, smoking, and increased risk of peripheral arterial disease*", Circulation, vol. 109, no. 25, pp. 3196-3201. doi:10.1161/01.CIR.0000130848.18636.B2

[45] Peters, J.L., Perlstein, T.S., Perry, M.J.,McNeely, E. and Weuve, J., "*Cadmium exposure in association with history of stroke and heart failure*", Environ Res., vol. 110, no. 2, 2010, pp. 199-206. doi:10.1016/j.envres.2009.12.0

[46] Tellez-Plaza, M., Guallar, E., Howard, B.V. and Okieimen M.N., "*Cadmium exposure and incident cardiovascular disease*", Epidemiology, vol. 24, no. 3, 2013, pp. 421-429. doi:10.1097/EDE.0b013e31828

ASSESSMENT OF CONTROLLED BLASTING TECHNOLOGY EMPLOYED AT ADDIS ABABA RIVERSIDE GREEN PROJECT-FRIENDSHIP SQUARE

Wang Yang[1], Tewodros Gemechu[2*] and Su Wu[1]

[1] China First Highway Engineering Co. Ltd.

[2]School of Civil and Environmental Engineering, Addis Ababa Institute of Technology, Addis Ababa University, Addis Ababa, Ethiopia

*Corresponding author: tewodros.gemechu@aait.edu.et

ABSTRACT

This research paper presents an assessment of the planning and execution of controlled blasting operations that took place as part of the Addis Ababa Riverside Green Development Project. The application of liquid CO_2 fracturing blasting technology in the prevention and control of rock burst in the project shows that it reduces the stress concentration of rock burst system and transfers energy to the deeper part, and there is no open fire in blasting. Assessment results showthat there were only minimal to negligible vibrations recorded on the day of the blasting. Photo analysis techniques reveal that the rock fragmentation output was of acceptable quality. There was no interference with other operations, and the operation gave reproducible results with minimized entry into sensitive locations. Productivity performance assessment indicate that 200,000 m^3 of hard rock material has been excavated and hauled away in just 21 days which can be labeled as a very efficient performance.

Key words: Controlled blasting, Presplitting Method, Continuum rock masses, Performance assessment

1. INTRODUCTION

The Addis Ababa Riverside Green Development Project integrates landscape, architecture, municipal administration, roads, water conservancy and gardens. The project is located in the "heart" of Addis Ababa City surrounded by landmark buildings such as Prime Minister's Office, Presidential Office, Parliament Building, Sheraton Hotel, etc. Due to the sensitive construction location of the project, environmental problems such as construction dust, noise pollution, impact on traffic and disturbance to residents should not occur.

The rock excavation of the project was about 200,000 m^3, which was the key process of the project. As the project was adjacent to many important institutions, in the middle of densely populated area with intense traffic, conventional blasting operations could not be carried out. Therefore, the project has adopted special static blasting to ensure the blasting safety and construction safety and solve the neck sticking process.

Rock splitting operations still rely heavily on drilling and blasting. The drawback of the drill and blast method is that, if not done carefully, it can occasionally cause uncontrollable cracks as well as micro cracks in both the block and the leftover rock. The propagation of such effects might induce undesirable outputs such as uncontrolled deformation, unfavorable site amplification of seismic events, over excavation, unfavorable sound and vibration, etc. To this end, controlled blasting techniques are employed in the world to circumvent these problems and control the output. Such was the case for the project in question. This research generally aimed to assess and characterize the controlled blasting operations that took place as part of the Addis Ababa Riverside Green Development Project.

Blasting operation in sensitive areas requires special attention to their effects on the surrounding environment. A sudden change in the geometry of the rock mass along with blast induced ground vibration may lead to slope stability problems. Fly rock and throw of blasted materials downwards the valley sides may endanger nearby habitants. Air blast (noise) and ground vibration generated from blasting operation could scare inhabitants of the area causing trauma and unwanted turmoil. All these problems can be tackled amicably, if the blast design is made meticulously, explosive is chosen properly, and safety-concerns are dealt with proper care and guidance of experts working either at the same mine or from outside agency. This paperpresents a case study of a controlled blasting operation that was successfully carried out, which potentially makes it the first well-documented case in Ethiopia.

The basic steps in blast engineering are design, implement and observe the outcome of a blast (Fig. 1). The primary goals of rock blasting are to shatter the strata in order to achieve the desired yield with minimal adverse effects. Though side effects such as ground vibrations, noise, and fly rock cannot be fully avoided, they can be reduced by employing appropriate explosives, initiating devices, and blast design in certain geo-mining settings. Higher intensity of unwanted results indicates improper utilization of explosive energy in the fragmenting process, as the total amount of energy released by unit quantity of explosive is constant[1].

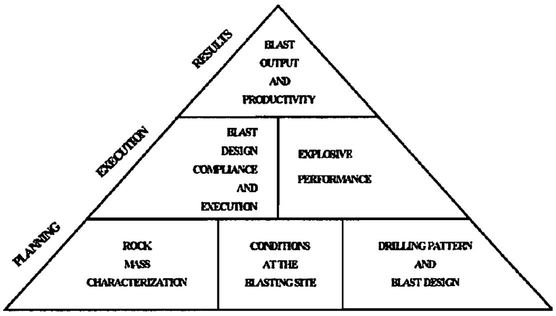

Figure 1 Blast optimization pyramid [2]

Block production and block splitting still rely heavily on drilling and blasting. The drawback of the drill and blast method is that, if not done carefully, it can occasionally cause uncontrollable cracks as well as micro cracks in both the block and the leftover rock. When compared to other procedures, recovery by this method is poor. In order to achieve the desired results, efforts have been made to establish controlled crack growth. There is a great deal of interest in preventing fractures in undamaged brittle materials for a variety of practical uses, such as controlling over break and fragmenting rocks[3]. Generating stress concentrations along those favored paths is one technique to achieve controlled fracture propagation along certain directions while preventing growth along other ones.

Controlled blasting has two senses of meaning and applications. In one sense, controlled blasting means controlling of ground vibration, fly rock and air overpressure (noise) within safe limit. On the other hand, controlled blasting means minimization of over-break and under-break beyond the boundary of the excavation area. The first one is generally applied when blasting operation is to be conducted near residential structures/buildings or another sensitive environment. The latter is applied both in surface as well as underground to obtain smooth and stable final excavation wall. Proper selection of blast design parameters and systematic blasting operation is crucial for controlled blasting operations. Blasting operation in ecologically fragile hilly areas requires special attention to their effects on the surrounding environment. A sudden change in the geometry of the rock mass along with blast induced ground vibration may lead to slope stability problems. Fly rock and throw of blasted materials downwards the valley sides may endanger nearby habitant located at the foothill and close by areas. Excessive propelling of fragmented rock caused by the explosive energy is called fly rock. Inadequate burden, improper stemming, deviation in drilling, excessive powder factor, unfavorable geological conditions (e.g., open joints, weak seams, cavities, etc.), too much delay timing, and back break are considered the main causes of the fly rock [4, 5]. Air blast (noise) and ground vibration generated from blasting operation could scare the fauna of the area causing birds and wildlife to migrate to other areas. All these problems can be tackled amicably, if the blast design is made meticulously, explosive is chosen properly, and safety-concerns are dealt with proper care and guidance of experts working either at the same mine or from outside agency [6].

Controlled blasting techniques produce the macro crack in a desired direction and eliminate micro crack in the remaining rock. Macro crack development in desired direction is required for extraction of dimensional stone and at the same time, there is need to reduce micro crack development in the block and remaining rock. Blasting techniques have been developed to control over-break at excavation limits. Some techniques are used to produce cosmetically appealing final walls with little or no concern for stability within the rock mass. Other techniques are used to provide stability by forming a fracture plane before conducting any production blasting. On permanent slopes for many civil projects, even small slope failures are not acceptable, and the use of controlled blasting to limit damage to the final wall is often required. The principle behind these methods is that closely spaced parallel holes drilled on the final face are loaded with a light explosive charge that has a diameter smaller than that of the hole [7].

There are four methods of controlled blasting, and the one selected depends on the rock characteristic and the feasibility under the existing conditions. The four methods are line drilling, cushion blasting, smooth-wall blasting, and presplitting (also pre-shear) [8].

When the rock is reasonably competent, smooth-wall blasting techniques can be used to take advantages in underground applications. Horizontal holes are charged with small-diameter, low-density decoupled cartridges strung together and by providing good stemming at the collar of the hole. Charges are fired simultaneously after the lifters. If the rock is incompetent, smooth-wall blasting may not be satisfactory [9]. Cushion and presplitting blasting are the most commonly used methods, with the main difference between the two beings that in cushion blasting, the final row holes are detonated last in the sequence, while in pre-shearing, the final line holes are detonated first in the sequence. Cushion blasting method is a control technique which is used to cleanly shear a final wall after production blasting has taken place. In cushion blasting method, the cushion holes are loaded with light, well-distributed charges. The sole purpose of a cushion blast is to create a smooth, stable perimeter. It offers no protection to the wall from the production blast [7]. Presplitting consists of creating a plane of shear in solid rock on the desired line of break. It is somewhat similar to other methods of obtaining a smoothly finished excavation, but the chief point of difference is that presplitting is carried out before any production blasting and even in some cases before production drilling [6]. Presplitting utilizes a detonation before the production blast in terms of lightly loaded and closely spaced drill holes. The purpose of presplitting is generating a fracture plane across which the radial cracks from the production blast cannot travel. Secondarily, the formed fracture plane may be smooth and allow the use of steeper slopes with less maintenance. Presplitting should be thought of as a protective measure to keep the final wall from being damaged by the production blasting [9].

2. MATERIALS & METHODS

The research design adopted for this specific project is qualitative study setting. A desktop study of relevant literature and data were conducted. All relevant literature on controlled blasting and geology of Addis Ababa were assessed. Qualitative methods are especially useful in situations when historical data was not available.

Majorly secondary data has been utilized in this study. The available geological data has been analyzed using a software called Roc Science to determine the strength of the underlying material. This information was then used to check whether the planning and execution of the blasting operation was up to the required quality. The performance of the controlled blasting operation has been reported in terms of ground vibrations, rock fragmentation and assessment of productivity. Seismograph readings were consulted to check the level of vibration induced because of the blasting operations while photo analyses technique were adopted to qualitatively assess the productivity.

For the assessment of controlled blasting operations, the controllable variables, non-controllable variables and expected outcomes used for objective assessment are highlighted in Figure 2.

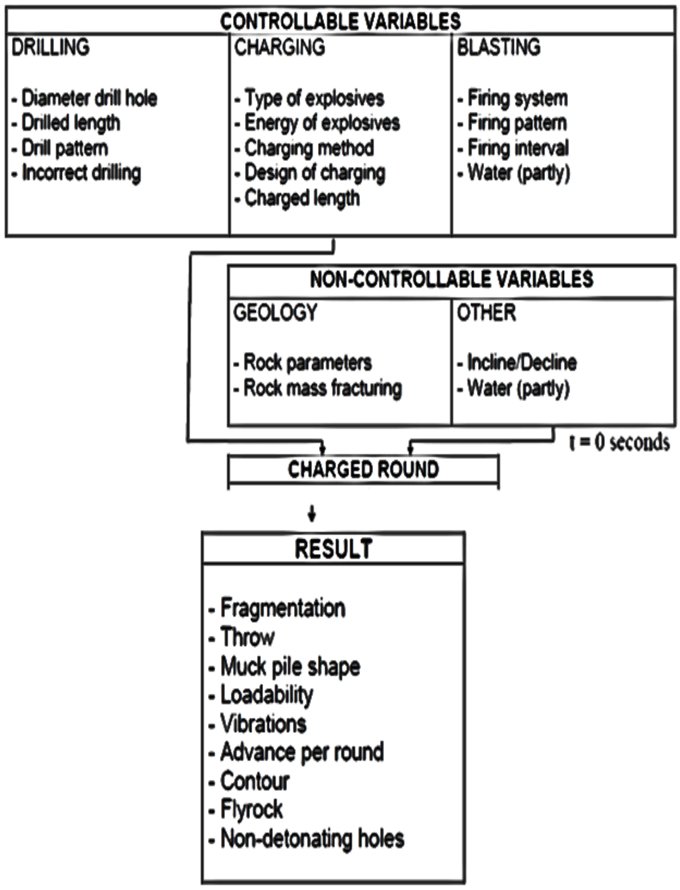

Figure 2 Summary of controlled blasting operation variables

3. RESULTS & DISCUSSION

3.1 Pre-blasting and blast initiation

Rock Mass Characterization

Rock samples were collected during several site visits. The sample that is less fractured is used to uni-axial compression test. The rocks that are very fractured and could not be used to perform the conventional compression test were used in the point load test whose outputs are summarized in Table 1.

Table 1 Rock mass characterization

Parameter	Value
Rock mass type	Basalt
Intact rock material constant, mi	17±4
Modulus of Elasticity of the intact rock, Ei	50GPa
Uniaxial compressive strength of the intact rock, UCS	80MPa
Poisson's ratio, ν	0.2

The Generalized Hoek-Brown (H-B) criterion better simulates the rock mass situation in this project. From Roc Data analysis the reduced value for intact rock constant mb and the Hoek-Brown criteria Conditions at the Blasting Site

Drilling of rock was carried out using Jackhammers driven by air compressors for shallow depth rock and intermediate excavations & hydraulic wagon drills for other as required. Rock and intermediate excavation area was determined and approved by the Engineer.The total hard rock excavation is 200,000m^3 out of this 17,000 m^3 is basalt and sound rock, which is very difficult to excavate using jackhammer excavator and control blasting, was applied.

Drilling Pattern and Blast Design

Controlled blasting methods are used to control blast induced effects such as, over-break, fractures within remaining rock walls and ground vibrations etc. In construction industries, blasting is the predominant method for fragmentation of consolidated mineral deposits. Controlled blasting methods are used to control adverse impact such as: - over-break, reduce ground vibration, reduce fractures within remaining rock walls, reduce noise, reduce dilution

For our purpose among the various techniques of controlled blasting such as line drilling, trim (cushion) blasting, smooth (contour or perimeter) blasting, pre-splitting etc., were considered in selecting and employing various parameters of blast design; using modern technology such as precise timing delays, varied density of explosives product by using bulk explosives; muffle blasting at very critical and congested areas. In the end, pre-splitting techniques was adopted since this method is essential to determine the radii of cracking zones.

constants s and a have been imported into the Rock Soil model to complete the material property of the rock mass [10].

As it is possible to determine the radii of cracking zones around the blast hole, we can use this principle to determine the extent of the damaged zone in the rock mass surrounding the excavation. As first, the damaged zone extent depends on the explosive pressure in the contour blast holes. It is well known that contour blast holes are placed closer and charged with less explosive than other blast holes in the blasting pattern. Therefore, if blast holes are charged less, the length of the tension cracks around the excavation decreases and vice versa. The shape of the damaged zone depends on the excavation cross section and its shape is the same as the shape of excavation cross section, but it is offset for the radius of the damaged zone. Depending on how much rock mass is jointed, we can differ two possible situations. The first situation is when primary block size is larger than the maximum length of the blast induced radial cracks in zone r4. In this case, pressure wave that induces radial cracks is not limited by pre-existing joints in rock mass and radial cracks may reach their maximum length. Therefore, for this situation, the extent of the blast damaged zone is equal to the maximum length of the radial cracks in cracking zone r4.

Damaged zone extent and shape of the damaged zone around the excavation depends on the blasting pattern, cross section of the excavation and the structure of rock mass (primary block sizes). One should imagine rock mass as a set of interlocked monolith blocks that are separated by pre-existing rock joints. In this manner rock blocks may be considered to be an elastic part of rock mass and their plasticization is done through the blasting process when blast induced radial cracks are formed. It is well known that discontinuities as joints and fractures in rock mass limit pressure wave propagation and therefore may limit propagation of radial cracks induced by explosive charge. This also means that pre-existing joints and fractures define the extent and shape of the blast damaged zone around the excavation, as explosive charge will break only the rock block in which it is placed. In other words, pre-existing joints define domain for pressure wave propagation. Numerical investigations, using distinct element modelling, on radial crack and pressure wave propagation in jointed rock mass are presented by Aliabadian, and Sharafisafa [11].

It's well known that contour blast holes are placed closer and charged with less explosive than other blast holes in the blasting pattern. Therefore, if blast holes are charged less, the length of the tension cracks around the excavation decreases and vice versa. The shape of the damaged zone depends on the excavation cross section and its shape is the same as the shape of excavation cross section, but it is offset for the radius of the damaged zone. Depending on how much rock mass is jointed we can differ two possible situations. The first situation is when primary block size is larger than the maximum length of the blast induced radial cracks in zone r4. In this case pressure wave that induces radial cracks is not limited by pre-existing joints in rock mass and radial cracks may reach their maximum length. The second situation is when the primary block size is smaller than the maximum length of blast induced radial cracks. In this case, pressure wave propagation is being limited by pre-existing joints in rock mass, and therefore blast-induced radial cracks are limited in their length by pre-existing joints. It is obvious that more jointed rock masses are less subjected to blast induced damage and vice versa. The size of the blast damaged zone, in this case, depends primarily on maximum distance between pre-existing joints in rock mass, or primary block size.

Field Monitoring and Control

As it is already known, there are plenty of methods for assessment of blast-damaged zones. Also, there is a lack of precise methods for assessing the extent and quantification of these zones. Many of the existing methods are empirical and highly case dependent, while on the other hand, theoretical methods have limited applicability. An important part of the new rock breakage theory is presented, making it possible to estimate the length and density of the tension (radial) cracks caused by explosive charge initiation.

Specifically our site is very critical site due to the fact that it is at heart of important historical and high value establishments. The project is located in the "heart" of Addis City surrounded by landmark buildings such as Ethiopian Prime Minister's Office, Presidential Office, Parliament Building, Sheraton Hotel, etc. Due to the sensitive construction location of the project, environmental problems such as construction dust, noise pollution, impact on traffic and disturbance to residents cannot occur.

- East direction →Sheraton =400m far
- East direction → Ethio- telecom tower=168m far
- West direction→ Asphalt road =324m
- North direction → Fence of the National palace=108m far
- South direction → Buildings =270m far

Based on the above distances and direction of the locations, we decided the direction of blasting and blasting damaged zone. The direction of the blasting was south west and maximum blasting damaged zone was decided to be less than 108m.

Type of rock from geological classification was basalt rock or very hard rock. From the theoretical calculation based on the type of rock, the excavation/blast-induced damaged zone (EDZ/BDZ) were calculated as follows.

For the distance 2-3 m, D=0.8, r4=2.16m,

GSI bdz=GSIurm-10 where; GSI bdz= value of blasted damaged zone
GSI urm= value of undisturbed rock mass
GSI bdz = GSI urm-10 = 65 – 10 = 55m

Drainage of Large Holes

It has been made sure that the large holes contain no water when the round is blasted. By giving the large holes an eccentricity at the bottrom of the holes equivalent to 3% upward slope, the holes will be self drained. Other cut holes are given the same eccentricity at the bottom of the holes.

Drilling

When designing a drilling, the cut and the contour holes are placed first. Then invert holes and the row nearest the contour are placed. Finally, the easers are placed. Finally, the easers are placed. The easers closest to the cut must allow necessary rock expansion. Hence the maximum burden must not be exceeded. The holes in the rest of the stopping area are then placed from the contour towards the cut. The eccentricity at the bottom of the hole for the different holes must be taken into consideration when deciding burden and spacing. The confinement at the bottom of the holes must be checked.

Placing the cut in the cross section has an influence on the fragmentation, consumption of explosive, the shape on the muck pile and load ability. If the cut is placed high in the cross section, the throw will increase. The fragmentation is better, but the consumption of explosives increase. A low placed cut results in poorer fragmentation and less consumption of explosives. The rock pile is well graded, but can be difficult to load because the rock is packed as most of the holes in the round throw downward. It is common to put the cut symmetrical about the vertical tunnel axis. It is sometimes placed towards one of the walls because some drilling jumbos have blind sectors. Considering rational drilling is very important when the cut is placed and the drilling patter determined. Distributing the drilling between each of the drilling machines is necessary to optimize the total drilling time. Rational charging implies that the cut can be reached from the invert.

Charging

Liquid CO_2 fracturing blasting technology is mainly used in coal mines to increase the permeability of coal seams and gas extraction efficiency. It is rare to apply liquid CO_2 fracturing blasting technology to rock burst prevention and control. Compared with the traditional explosive technology, the liquid CO_2 fracturing technology has no open fire and can be relatively safe in the process of blasting, and the pressure relief effect is remarkable. The CO_2 cracker is mainly composed of a filling valve, a heating pipe, the main pipe, a sealing gasket, a shearing piece, and an energy release head. The structure and damage range of the CO_2 cracker are presented in Figure 3 and Figure 4, respectively.

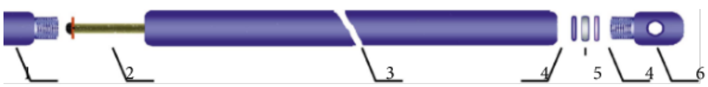

Figure 3 Structure of CO_2 cracker.

Key: 1 -Filling valve; 2 -Heating pipe; 3 -Main pipe; 4 -Sealing gasket; 5 -Shearing piece; 6 -Energy release head.

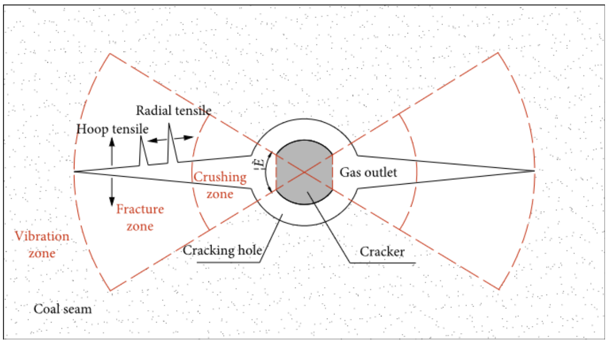

Figure 4 Sketch map of damage range of CO_2 cracker

3.1.8 Initiation of Blasts

Time delays have historically been utilized to regulate the orderly flow of material via the free faces, as we have described, or to restrict the amount of explosive that may be discharged at once, which lowers the intensity of ground vibration. With the introduction of electronic initiation, a new era in which we could better utilize physics began. Time delays have historically been offered in 25 ms increments, which is suitable for the purposes for which they have been employed.

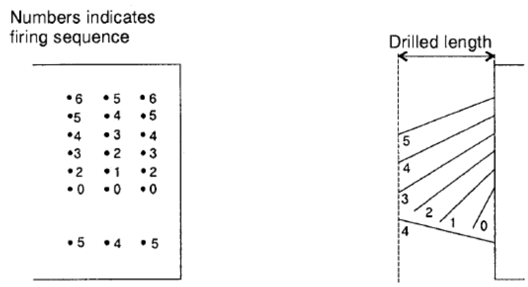

Figure 5 Fan cut, the right-hand section as seen from above

Explosive Product Performance

The working principle of liquid CO_2 fracturing blasting is described below.

When the temperature of liquid CO_2 is lower than 31°C or the pressure is greater than 7.35 MPa, it usually exists in liquid form. When the temperature of liquid CO_2 is higher than 31°C, it begins to gasify. Taking advantage of the phase transition characteristics of CO_2, liquid CO_2 was filled in the main pipe of the cracker, and the heat pipe was rapidly excited by the detonator. Liquid CO_2 was instantly gasified and expanded to generate high pressure. When the pressure reached the ultimate strength of the constant pressure shearing piece, the shearing piece was broken, and the high-pressure gas was released from the energy release head and then acts on the coal and rock mass, thus realizing the directional fracturing blasting on the coal and rock mass (Figure 4). The crushing zone, fracture zone, and vibration zone were formed successively from the center of the explosion position, so as to complete the pressure relief.

3.2 Blast Output and Productivity

Ground Vibrations

Most of the explosive energy in a blast is absorbed in the process of breaking the rock. One effect of the remaining energy is to cause air shocks and shock waves in the surrounding rock. This may cause considerable damage if the blast is fired close to vital installations and the round is not carefully designed.

The amount of energy which is transferred through the rock depends on the character of the rock mass and the effect of the blast. On a free surface as in the case of this project, the following types of waves from a blast may easily be recognized.

1. Longitudinal waves (Primary or P-Waves) causing oscillation of particles in the direction of wave propagation
2. Transversal waves (Secondary or S-Waves) causing particle oscillation perpendicular to the wave propagation direction.
3. Surface waves, of which Rayleigh waves (R-waves) are the most important. The particles have a retrograde

At the planning stage of the blast the assumption is normally made that the vibrations can be represented by harmonic oscillations. For harmonic oscillations (sinusoidal waves), the following relationship exists between vibration velocity (v), maximum amplitude (A) and frequency (f); and between vibration acceleration (a), maximum amplitude and frequency:

$$v = 2\pi \cdot f \cdot A \quad (1)$$
$$a = 4\pi^2 \cdot f^2 \cdot A \quad (2)$$

Vibration velocity, v, is the distance per time unit (i.e. mm/s) which a surface particle has travelled around its point of equilibrium. Vibration velocity, v, is the distance per time unit (i.e. mm/s) which is a surface particle has travelled around its point of equilibrium. This velocity is different from the seismic velocity, which in hard rocks is normally in the order of 4500-6000 m/s for P-waves.The resultant wave has a wide range of different frequencies, depending on ground conditions, distance, detonator characteristics, etc. In most hard rocks the dominant frequencies are in the range of 10-100Hz.

The planning of a blast is in many cases based on empirical equations of the following type:

$$v = k.\frac{Q^{\frac{1}{2}}}{R} \quad (3)$$

where: v = vibration velocity
k = “k-value”
Q = weight of simultaneously detonating charge
R = distance from detonation

The k-value is not constant, but a parameter dependent on ground conditions and distance from the blast. As a part of general planning procedure, small-scale test detonations are carried out to evaluate the k-value. The next step is then to calculate the maximum permissible charges as a function of distance from the blast using this k-value and the maximum vibration velocity allowed.

Most criteria used for defining “allowable vibrations” are based on critical values of v, a of A. When critical values are defined, it is important to bear in mind that human beings are particularly sensitive to vibrations. For instance, at a frequency of 50 Hz an amplitude of only 2 µm is easily recognized by human beings, while the critical value for building damage is 200 µm or more.

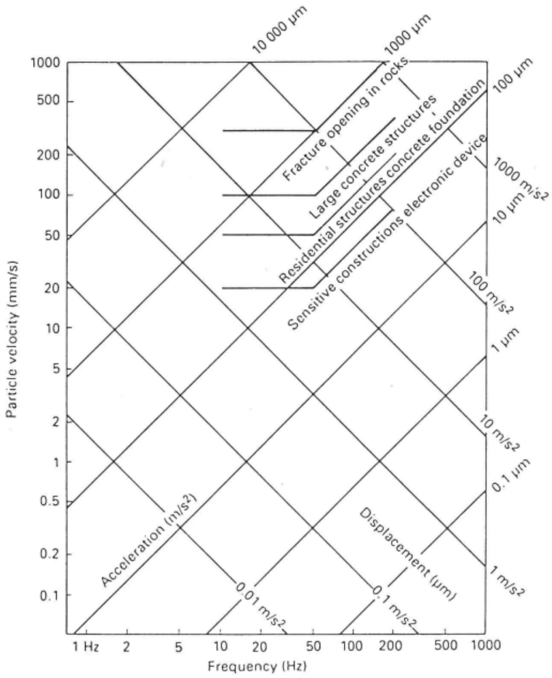

Figure 6 General criterion used as first indication of damage risk [12]

Assessment of Productivity

Estimated output for a drilled hole depth 2.6m and 10 holes

Output of 2.6m dilled hole=2.6*.7=1.82m

Therefore; - Area =3*3 = 9m^2

Volume= 1.82*9 = 16.38m^3

Daily output for 100holes =<u>819m^3</u>

Total working days = 17000/819 =21days

4. CONCLUSIONS

Seismograph readings from the site monitoring indicate that there were only minimal to negligible vibrations recorded on the day of the blasting. Photo analysis techniques also revealed that the rock fragmentation output was of acceptable quality. There was no interference with other operations, gave reproducible results, and minimized entry into sensitive locations.

Controlled blasting has been proven to prevent fly rock to occur. The application of liquid CO_2 fracturing blasting technology in the prevention and control of rock burst in the project shows that it reduces the stress concentration of rock burst system and transfers energy to the deeper part, and there was no open fire in blasting process, which has a good pressure relief effect. It can be concluded that the project can be set a role model for future projects that may involve excavation of hard rock in sensitive locations.

CONFLICT OF INTEREST

Wang Yang and Su Wu are employees of China FirstHigh way Engineering Co. Ltd.

Tewodros Gemechu declares no conflict of interest.

ACKNOWLEDGEMENTS

The authors would like to thank Office of the Prime Minister of Ethiopia and Addis Ababa Institute of Technology for all the help they extended for the successful realization of this paper.

5. REFERENCES

[1] Singh, S.,"*New trends in drilling and blasting technology*", International Journal of Surface Mining, Reclamation and Environment vol. 14, no. 4,2000,pp. 305-315.

[2] Sastry, V., "*Rock blasting technology: the way forward*," Recent Advances in Rock Engineering (RARE 2016), pp. 606 - 611, 2016.

[3] Fourney, W., "*Mechanisms of rock fragmentation in by blasting*", Compressive rock engineering, principles, practice and projects,1993.

[4] Monjezi, M., Amini Khoshalan, H., and Yazdian Varjani, A., "*Prediction of flyrock and backbreak in open pit blasting operation: a neuro-genetic approach*", Arab J Geosci, vol. 5, 2012, pp. 441–448.

[5] Monjezi, M., Yazdian Varjani, A.B., Reza, Sayadi, A. andBahhrami, A., "*Prediction and controlling of flyrock in blasting operation using artificial neural network*", Arab J Geosci,vol. 4, 2011, pp. 421–425.

[6] Fourney, W., Dally J. and Holloway, D. "*Controlled blasting with ligamented charge holders*", International Journal of Rock Mechanics and Mining Sciences &Geomechanics,vol. 15, no. 3,1978, pp. 121 - 179.

[7] Cho, S.H., Nakamura, Y., Mohanty, B., Yang, S.H.and Kaneko, K. "*Numerical study of fracture plane control in laboratory-scale blasting*", Eng Fract Mech,vol. 75, 2008, pp. 3966–384.

[8] Sharafisafa, M. andMortazavi, A. "*A numerical analysis of the presplitting controlled blasting method*", in 45th US Rock Mechanics / Geomechanics Symposium, San Francisco, CA,

USA, 2011.

[9] Rathore, S.S. and Bhandari, S., "*Controlled fracture growth by blasting while protecting damages to remaining rock*", Rock Mech Rock Engng,vol. 40, no. 3, 2007, pp. 317–326.

[10] Hoek, E., Carranza-Torres, C. and Corkum, B., "*Hoek-Brown failure criterion,*" in *NARMS-TAC Conference*, Toronto, 2002.

[11] Aliabadian, Z., and Sharafisafa, M. "*Numerical modeling of presplitting controlled method in continuum rock masses*," *Arab J Geosci,* 2014.

[12] Nilsen, B. and Thidemann A., *"Rock Engineering",* Trondheim: Norwegian Institute of Technology, 1993.

CAPACITY ANALYSIS OF SELECTED MAJOR INTERSECTIONS ON THE ROUTE AUTOBUS TERA - KALITY BUS STATIONS AND MITIGATION MEASURES

[1]Abel Kebede Bekele , [1]Tamru Tilahun Habteyes

[1]School of Civil and Environmental Engineering, Addis Ababa Institute of Technology (AAiT), Addis Ababa University, Addis Ababa
Corresponding Author's email: Abelkebede2015@gmail.com

ABSTRACT

Engineering mitigation measures were proposed in order to improve the existing levels of service for major intersections. The adjustment to the existing cycle time, delineation of movements on existing lane configuration and geometric modifications to observe the improvements on the respective levels of service were among the proposed mitigation measures. It was hypothetically believed that there exist short comings on the route Autobus Tera - Kality bus stations from congestion and level of service points of view. Subsequently, four signalized intersections were selected based on statistical outputs of mixed type of questionnaire. They were then analyzed by using software tool (SIDRA) so that the outcome could be used as a source of information and data for transport sector organizations and academic reference. Accordingly, the level of service of Eliana hotel site improved from level F to D & the average delay from 167.3 seconds to 54.7 seconds and level of service of Immigration site improved from level F to E & the average delay from 435.5 seconds to 68.7 seconds. Moreover, level of service for both Harambae and Saris Adey Ababa sites improved from F to D & the average delay from 642.6 seconds to 54.2 seconds and from 865.1 seconds and 49.13sec respectively.

Key words: *Level of Service, Delay, Major Intersections, SIDRA*

1 INTRODUCTION

The Addis Ababa city transport policy has the general objectives of providing safe, efficient, comfortable, affordable, reliable and accessible transport service for the urban dwellers, enabling the sector to provide socio-economic development, good governance, improve the livelihood of the society and adopt environmental protection of the city and enhancing the status of the city as international seat, by introducing seamless traffic flow through modern traffic management system [1]. In order for the above policy objectives to be achieved, continuous assessment of performance at transport infrastructures must be carried out. The route considered for this research runs from north to south of the city and crosses 5 sub cities namely Addis Ketema, Arada, Kirkos, Nifas Silk Lafto and Akaki Kality sub cities. The three measures of effectiveness commonly used to evaluate signalized intersection operations are, capacity and volume-to-capacity ratio, delay and queue [3]. Level of Service (LOS) is considered as a performance measure. It is computed for the automobile, pedestrian, and bicycle travel modes. It is useful for describing intersection performance to elected officials, policy makers, administrators, and the public. Capacity is defined as the maximum rate at which vehicles can pass through a given point in an hour under prevailing conditions. Delay is defined as the additional travel time experienced by a driver, passenger, or pedestrian. Control delay is used as the basis for determining LOS. Intersection control delay is generally computed as a weighted average of the average control delay for all lane groups based on the amount of volume within each lane group [4]. The signal timing of an intersection plays an important role in its operational performance. Key factors include effective green time, clearance interval, loss time, cycle length and progression [5].

Many of the intersections especially in the capital city, Addis Ababa were found to be operating in low LOS with higher delays [6 – 9]. Similarly, various capacity analysis and study of traffic intersections had been made in major cities of countries in the world and found out that many of the intersections were with level of service F. The researches also pointed out engineering mitigations such as geometric modifications, cycle time optimization and dedication of lanes for traffic movements which could possibly improve the site levels of service [10 – 12].

Researches had been conducted in analysis of intersections located in major cities of Ethiopia. The researchers analyzed the level of services, delay and environmental problems of major intersections. However, only few researches showed the comparison of suggested mitigation measures with the existing conditions [6].

The present work has analyzed the existing conditions at the major intersections and unlike the previous researches conducted, it proposed three engineering mitigation measures (cycle time optimization, delineation of movements and geometric modifications) for all the four major intersections there by comparing and contrasting the level of improvements with the existing conditions and to each proposed mitigations so that the most applicable and economic approach in view of short term and long term plan can be inferred and applied to solve the engineering problems prevailing at the major intersections.

2 MATERIALS AND METHODS

Primary sources of data like questionnaire and field data recording were used for analysis based on statistical estimations of sample size required. The data were then analyzed using the software tool Signalized & Unsignalized Intersection Design and Research Aid (SIDRA) [2].

2.1 Study Area

The study areas for this research were located in Addis Ababa, specifically, the major signalized intersections on the route from Autobus Tera to Kality Bus stations namely Eliana Hotel/ Banco Di Roma, Immigration, Ethiopia hotel/ Harambae and saris Adey Ababa signalized intersections.

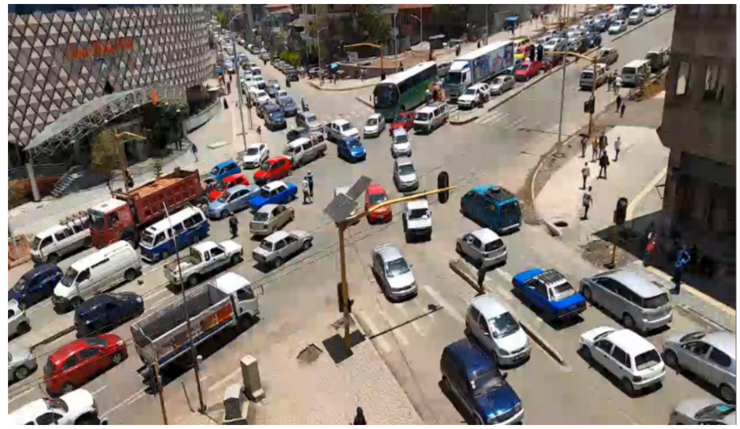

Figure 1 Study area of Eliana Hotel signalized Intersection

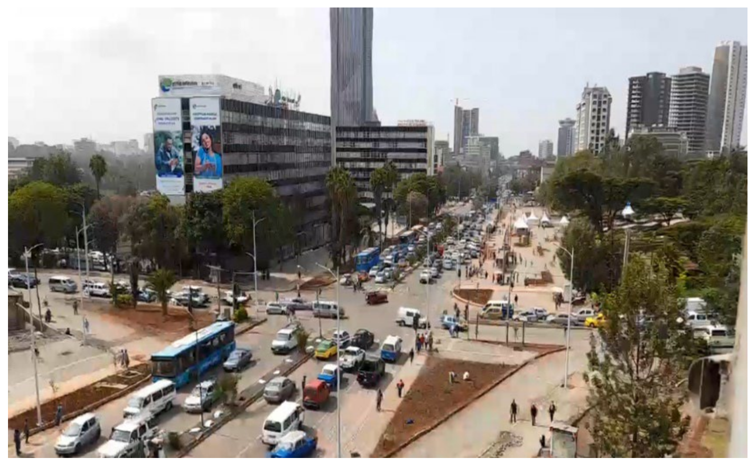

Figure 2 Immigration signalized intersection

2.2 Data Gathering

2.2.1 Questionnaire

In developing the questionnaire, the respondent's status including gender distribution, age, driving license level and experience in years was used because these data provide an oversight to the driver's capability to understand situations related to driving.

The statistical calculation of sample size for questionnaire distribution was determined from Cochran's formula (1) with infinite population size and found to be 70 with 90% confidence interval and no previous data is available [p=q=0.5].

$$N = (Z^2 * pq)/e^2 \quad (1)$$

Where N = sample size
P= is the estimated proportion of an attribute that is present in the population (0.5 if no previous data is available)
q = 1-p
e= margin of error
Z= Z score

The road users who participated were public transport and private vehicles drivers who have used the route most frequently. The road users selected were drivers because these test samples experience the urge to attain the travel reliability and were exposed to performance measurements like delay and queue at intersections along the route.

A pilot survey was conducted before making the main questionnaire distribution and it was found out that the English version of the questionnaire needed to be changed to Amharic (local language) due to communication barrier with the respondents. Moreover, responses which had faulty responses such as unspecified experience year, driving license level and unmarked intersection were discarded.

2.2.2 Video recording

Video recording was used for the research in order to gather reliable primary source of traffic volume data for the vehicles and pedestrians.

2.3 Data Analysis

2.3.1 Software tools

For this research SIDRA Intersection 8 plus was used for performance analysis of selected major intersections due to its versatility and non-complexity. Unlike other software packages, the HCM Setup in SIDRA intersection offers various extensions on the capabilities HCM offers. The Parameter settings option in the software provides the capability to use HCM 2010 delay & v/c method of analysis for site and pedestrian level of service analysis and selection of specific performance measures like capacity, delay, queue, degree of saturation, etc.

2.3.2 Intersection and Movement Definitions

The standard right option was selected under the software setup menu to meet the driving rule in the country. The intersection type was selected as at-grade intersection from signals option under site tab. The standard classes included for the analysis procedure were light vehicles and heavy vehicles with ids LV and HV, respectively

2.3.3 Lane Geometry and grade

The lane geometry and editor option were used to input number, arrangement and geometric properties for the approach lanes, exit lanes and strip islands. The other lane property is the grade for lanes and it was calculated based on the elevation difference of approach and exit lanes of the intersection.

2.3.4 Lane Length and lane movements

In the lane length option, the approach distance was taken as the mid-block distance between two intersections in the approach travel direction on an intersection leg while exit distance was taken as the mid-block distance between two intersections in the exit travel direction on an intersection leg.

The lane movements' option specifies the proportion of flow for the flow directions on the approach lanes. The movements were setup based on the lane discipline for the respective approach legs.

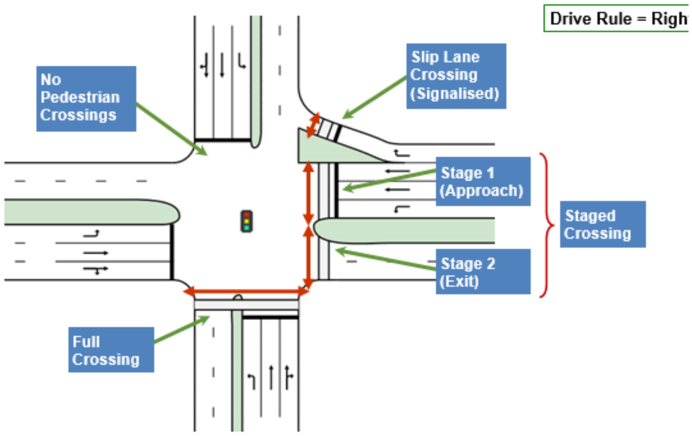

Figure 3 Pedestrian movement definitions and description

2.3.5 *Vehicular Volumes, Vehicle movement and volume data*

The volumes option was used to input the vehicles volume for the respective approaches of the signalized intersection considered. There are three options to feed the volume data namely;

Separate - where the volume of light vehicles and heavy vehicles were fed and total volume were calculated and displayed.

Total and % :- where total volume and percentage of vehicle class is fed and the remaining class percentage were calculated and displayed.

Total and vehicles - Total volume and volumes for Movement Classes other than Light Vehicles are specified.

2.3.6 *Parameter settings*

This setting contained the general options, model parameters, cost and fuel & emissions inputs. The general option tab was used to specify the site level of service method, target and pedestrian level of service target and performance measure.

2.3.7 *Phasing and Timing*

This setting included the sequence selector, sequence editor, phase and sequence data and timing options. The sequence option provided a choice between variable phasing, two phase, split phasing or leading left turn phasing while the timing option provided choices between practical cycle time, optimum cycle time user given cycle time and user given phase times.

2.3.8 *Stochastic Analyses of Queues*

Using a stochastic approach to analyze queues considers the fact that certain traffic characteristics such as arrival rates are not always deterministic. Arrivals at an intersection are deterministic or regular only when approach volumes are high. Arrival rates tend to be random for light to medium traffic. Thus, the stochastic approach was used to determine the probability that an arrival would be delayed, the expected waiting time for all arrivals, the expected waiting time of an arrival that waits, and so forth.

This method was applied at the Saris Adey Ababa intersection since it is composed of vehicular traffic movement and Light Rail Transit (LRT).

Regarding the queue performance, it was considered with Random arrival and Random service with single channel for the left turns of each approach and through movements of the East – West approach since there exists only 1 entry and exit lane for the movements. Hence the que performance was taken as M/M/1 (∞, FIFO). Based on the above conditions the average delay was calculated from:

$$\boldsymbol{D} = \frac{\mathbf{1}}{\mu - \boldsymbol{\lambda}} \qquad (2)$$

Where D is average delay and μ & λ are service rate and arrival rate respectively

3 RESULTS AND DISCUSSIONS

3.1 Questionnaire results

Based on the distributed Questionnaire the following four out of the nine major intersections were ranked with higher congestion as shown in the Table 1. The respective percentages of replies are also indicated.

Table 1 Selected Intersections for analysis based on questionnaire response

No	Major Intersection	Percentage
1	Saris Adey Ababa	95.70%
2	Immigration	72.90%
3	Ethiopia hotel/ Harambae	67.10%
4	Eliana Hotel/ Bancodiroma	61.40%

3.2 Existing levels of service

3.2.1 Eliana Hotel/Bancodiroma site

The hourly vehicle's volume distribution with the peak hours being 11:45-12:45 am and 4:15-5:15 pm was 3676 and 3907 vehicles respectively and the movements gradually decrease onwards.

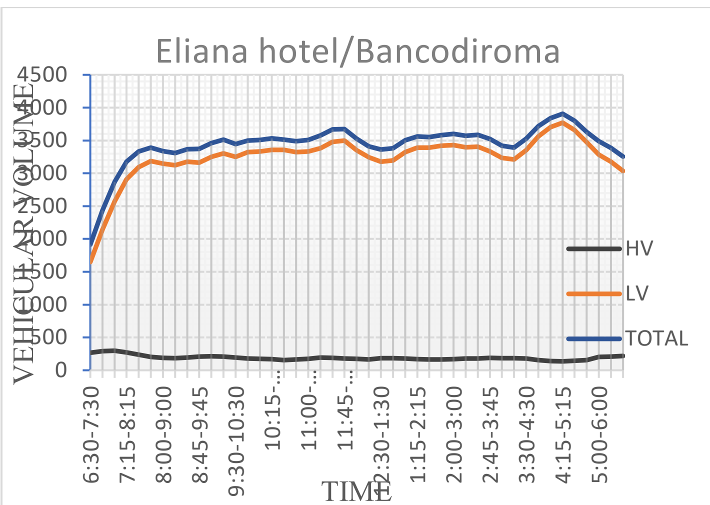

Figure 4 Eliana Hotel site hourly Volume distributions

The right turns at each leg of the intersection were with level of service A because all the signal phases were not right protected and allowed turn on red on each approach leg.

Moreover, the level of service of the intersection was F. This was mainly because of the capacity difference at which the intersection could operate and the arrival volume during the peak hour volumes. Majority of the approaches were with degree of saturation greater than one and closer to one. Especially Betemengist approach had the maximum degree of saturation. In addition to this, the average delay for the East – West direction had higher delay values which indicated poor performance of the intersection.

The Churchill through movements were with level of service C with the average delay of 25.9 seconds. The left turn of Piassa approach was level of service E with average delay of 73.4 seconds. The remaining movements except the right turns were with level of service F with average delay of greater than 80 seconds. The average delays in the four directions for pedestrians were greater than 60 seconds which exceeded tolerance level and hence there was high likelihood of pedestrian risk-taking to make crossings.

3.2.2 Immigration site

The hourly vehicular volume distribution of the site was with multiple peak hours. The highest vehicular volume was recorded between 11:30 am and 12:30 pm with 4283 vehicles which slightly differed from an hour before, 10:45-11:45 am with volume of 4209 vehicles.

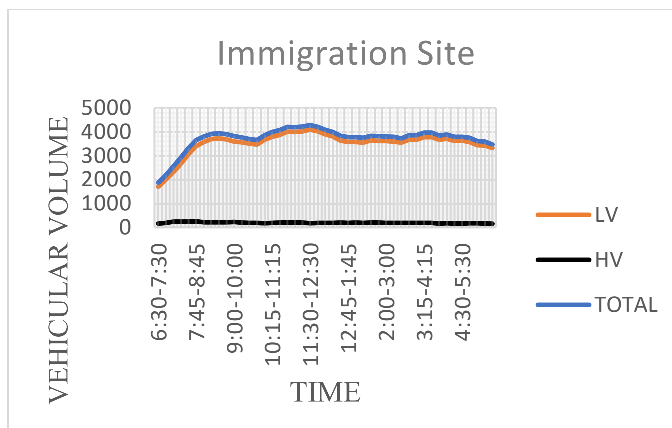

Figure 5 Immigration site hourly Volume distributions

The average delay, especially for the Bherawi approach and the Tikur Anbessa approach were higher. Hence, the intersection's performance was with level of service F and average delay of 435.6 seconds. The left turns of south-north direction were with level of service E with average delays of 71.7 and 60.1 seconds, respectively. The average delays in the four directions for Pedestrians were greater than 60 seconds which exceeded the tolerance level and hence there was high likelihood of pedestrian risk-taking to make crossings.

3.2.3 Ethiopia Hotel/Harambae site

The hourly vehicular volume distribution had multiple peak hours. The highest vehicular volume was recorded between 02:45pm and 03:45 pm with 3702 vehicles. The next highest volumes were recorded between 9:00-10:00 am, 8:15-9:15 am and 10:45-11:45 am with the respective volumes of 3402, 3381 and 3376 vehicles. The characteristic of the vehicular movement drastically changed in the afternoon after attaining its peak of the day.

Figure 6 Harambae site hourly Volume

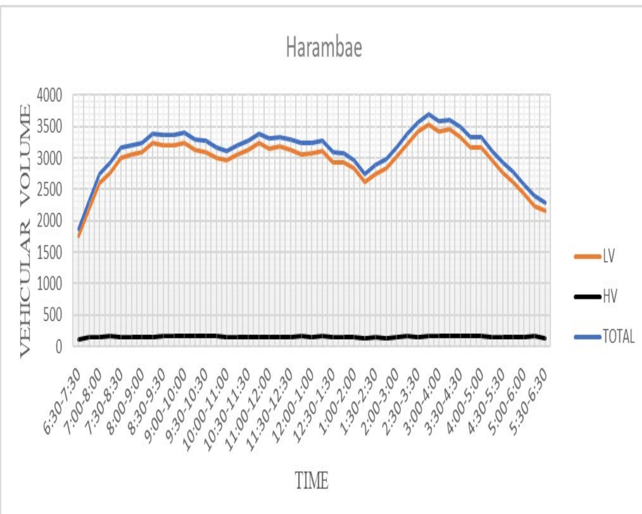

distributions

The right turns at each leg of the intersection were with level of service B because even though the intersection signal was not right protected and allows turn on red on each leg, the average delays exceeded 10 seconds. The left turns of all the approaches were with level of service E due to the average delay which lied between 55 and 80 seconds. The intersection level of service was F with average delay of 642.6 seconds. The pedestrian level of service of the intersection was also F because of the average delay the pedestrian experience. The average delays in the four directions namely P1 up to P4 were greater than 60, around 80 seconds, which exceeded the tolerance level and hence there was high likelihood of pedestrian risk-taking to make crossings.

3.2.4 Saris Adey Ababa site

Saris Adey Ababa signalized intersection was different from the above discussed intersections in that the intersection had LRT route along the South – North direction of the intersection. The clearance time was calculated from the difference between the train arrival detection time (Arrival time) and the time the train fully clears the intersection (Departure time). The arrival difference was obtained by taking the difference between the time a train is detected/arrived at the intersection and the time the next train arrives/detected at the intersection from either of the South –North approach. Based on these it was seen that the average time for a train to clear the intersection was 29 seconds, while the average time for arrival interval was 6minutes and 30 seconds.

Table 2 Frequency of trains' arrival time

Designation	Arrival Time interval	Freq
A	00:00:06 < t =< 00:05:00	42
B	00:05:00 < t =< 00:10:00	45
C	00:10:00 < t =< 00:15:00	17
D	t > 00:15:00	3
	Total	107

The distribution of hourly volumes for Saris Adey Ababa site are shown in figure 7, where it can be seen that the hourly volume was more or less uniform after it peaked between the time 8:30 am and 9:30 am and then decreased starting from 4:00 and 5:00.

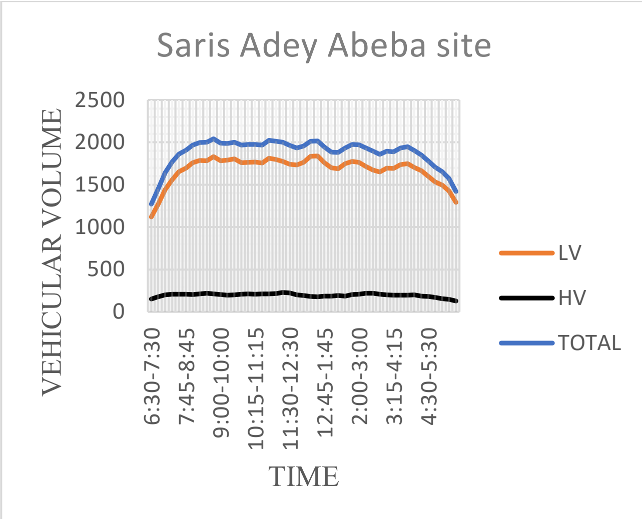

Figure 7 Saris Adey Ababa hourly Volume distributions

The Saris Adey Ababa signalized intersection was with level of service F with an average delay of 756 seconds.

Table 3 Time occupied by the LRT

Description	Time/no
Average train Clearance time [A]	00:29
Average Train Arrival time [B]	06:30
Number of Arrivals in 1hr. [C]=60sec /[B]	9.23 ≈ 10
Time occupied by the LRT 1 hr. [D]=[A]*[C]	04:46

The time occupied by the train in an hour was found to be 4 minutes and 24 seconds during its arrival and departure in peak hour. The average train clearance time was determined by averaging the clearance times recorded in the field data.

Table 4 Average delay from the LRT clearance time

	Average Delay due to Light Rail transit (LRT)					
	Arrival Rates (Veh/hr)			**Average Delay (sec)**		
South Approach	Left	Through	Right	Left	Through	Right
	230	405	54	16	0	0
North Approach	Left	Through	Right			
	190	400	86	19	0	0
West Approach	Left	Through	Right			
	248	67	26	15	54	0
East Approach	Left	Through	Right			
	98	134	121	37	27	0
			Total	166	**≡ 2 min 46 sec**	

Delay incurred by the LRT during its clearance of the intersection was determined by the stochastic queue analysis and is shown in the table above.

3.3 Engineering mitigations

The proposed engineering mitigations for the signalized major intersections were cycle time adjustment with updated volume, delineation of movements and geometric modification of the approaches and site.

3.3.1 Eliana Hotel/Bancodiroma site

With varied cycle times in order to improve the intersection, there was no significant improvement obtained at the site during the peak hour due to the higher volume of traffic at the intersection. With an increase in cycle time the Piassa approach tended to improve yet the intersection level of intersection remained F.

At complex intersections where the correct path through the intersection may not be immediately evident to drivers, pavement markings may be needed to provide additional guidance. In this case, assigning through movements to the right turns of each approach has a significant improvement on the level of service of individual lanes as well as the intersection. The movement performance measure, average delay was also improved significantly for Betemengist and Somalitera approaches with 986 to 74 seconds and 645 to 76 seconds on average respectively.

Table 5 Improvement for cycle time and delineation adjustments for Eliana hotel intersection

Adjustment	Intersection LOS	Avg. Delay
None (Existing)	F	167.3 sec
Cycle time (157sec)	F	262.3 sec
Cycle time + Delineation	E	58.8 sec

The geometric improvement made for analysis at the Eliana Hotel site was the addition of a single lane along the East – West direction approaches and exits. The geometric improvement was then coupled with delineation of through movements to the right turn movement in the South – North (SN) direction and assigning through movements to both the right and left turn movement in the East – West (EW) approaches. The reason for doing so was the variation on the degree of saturation and delay between the SN and EW directions when using the conventional movement assignments.

Table 6 improvement for adjustments for Eliana hotel intersection

Adjustment	Intersection LOS	Avg Delay
None (Existing)	F	167.3 sec
Cycle time (157 sec) + Delineation	E	58.8 sec
Geometric + Delineation (150 sec)	D	54.7 sec

3.3.2 Immigration site

The cycle time optimization for this site was preceded as analyzing incremental cycle times with a difference of 10 seconds. This was made because the site exhibits a very low performance and hence even the optimization was incapable of improving the level of service of each approach as well as the intersection as whole whenever the cycle time is increased excessively. The level of service for the South – North direction increases while down pressing heavily the other direction, East – West. Likewise, the reverse happens when the cycle time was reduced below the existing cycle time. The statistical approach used was the application of regression using the practical spare capacity for graphical plot simplicity because of its integer number format rather than using fraction as in the degree of saturation. The purpose was to obtain balanced spare capacity from the left and through movements of all the approaches and obtain the corresponding cycle time from best fitting curve by regression.

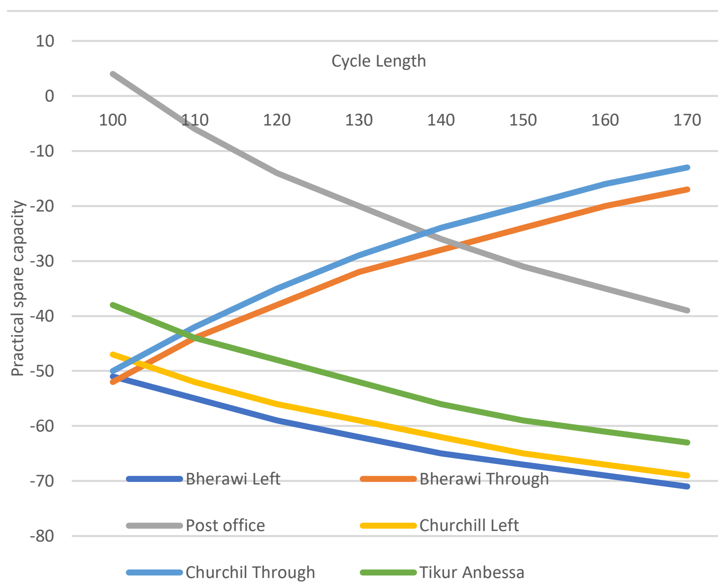

Figure 8 Plot for practical spare capacity vs Cycle time for immigration site

Figure 8 above shows four of the movements named Bherawi left turn, Churchill left turn, Tikur

Anbessa and Post office both movements exhibited a decrease in spare capacity hence increase in degree of saturation while the Churchill through and Bherawi through movements increase in spare capacity hence reduced degree of saturation.

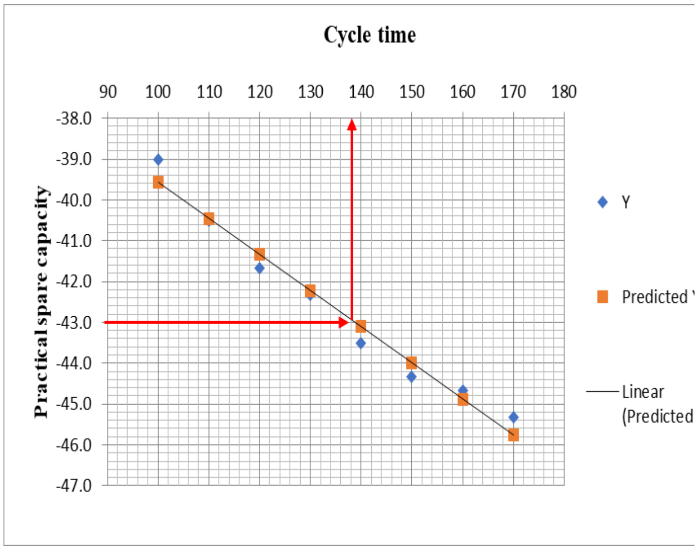

Figure 9 curve fitting plot for cycle time (sec) and average practical spare capacity (vehicle)

Based on the above analysis tool, the optimum cycle time was found to be 138 seconds which corresponds to the total average practical spare capacity of 43 vehicles. The statistical parameters of the data analysis are R squared value is 0.97 with confidence level of 95%. The p value was 6.85×10^{-06} which is less than 0.05 which showed the test is statistically significant. From these values the cycle time could be adjusted to 138 seconds though the level of service remains very poor. This adjustment added only 3 second to the existing condition.

The delineation of movements on the Immigration site was made by assigning the through movements of all the approaches onto the right turns. The right turns were with level of service A due to the reason of turn on red. Hence delineating the through movements will share some proportion of the through movement volumes and increased the level of service. The degree of saturation for through movements of all the approaches was improved. For instance, the Bherawi approach decreased from 1.63 to 0.833% and Churchill approach from 1.43 to 0.9%. Likewise, the post office and T/Anbessa approaches improved from 1.37 to 0.83 and 1.87 to 1%, respectively. The average delays for all the approaches were improved; the delay on Bherawi approach decreased from 1189 to 41 seconds and from 1612 to 146 seconds on the T/Anbessa approaches along the through movements. The left turns' delays were increased as the degree of saturation for the South -North directions decreasing the level of service.

The addition of a single lane on the East – West direction only alongside the delineation of movements and the adjusted cycle time improved the level of service for all approaches except the left turns of the South – North direction. The degree of saturation for the Bherawi and Churchill approaches decreased from 1.6 to 0.8% and 1.43 to 0.9% respectively while the average delay decreased significantly from 1189 to 43 seconds and 830 to 47 seconds respectively. Likewise, the degree of saturation for Post office and Tikur Anbessa approaches decreased from 1.37 to 0.5% and 1.9 to 0.5% respectively. The average delay decreased from 728 to 55 seconds and 1612 to 60 seconds.

Table 7 LOS comparisons and Geometric improvement phase times' description for Immigration site

Adjustments	Intersection LOS	Avg Delay
None (Existing)	F	435.5 sec
Cycle time only	F	838.9 sec
Cycle time + Delineation	E	78.3 sec
Geometric + Delineation	E	68.7 sec

3.3.3 Ethiopia Hotel/Harambae site

The optimization of existing cycle time for Harambae site was done through iteration. Analyzing the intersection by changing the existing phasing sequence the optimum cycle time would be 160 seconds. Increasing of the cycle time after 160 seconds would make the right turns of the approaches with level of service A and the west approaches to Level of service of E whereas the remaining approaches and overall level of service of the intersection remain F. The degree of saturation for the lanes on each approach did not show significant difference from the existing condition, while the degree of saturation for pedestrian movements significantly decreased. We can see that the pedestrian movement along the Stadium approach (P3) improved from 0.507 to 0.463 and the delay from 81.8 seconds to 74.8 seconds. The average delay was decreased from the existing level for the through and right turns. The average delay in seconds of Stadium approach for through and right turn were 1818.9 and 10 seconds in the existing condition while reduced to 623 and 3.5 seconds, respectively after the cycle time was optimized.

When delineating the through movements on the respective right turn movement lanes, the overall level of service improved to level D from existing level F. The optimum cycle time also decreased to 120 seconds from the optimization and decreased from the existing cycle time of 174 seconds. The degree of saturation for all the approaches decreased like in Stadium and Bherawi approaches from 2 to 0.8. Likewise, the delay in pedestrian movements decreased from 82 to 54 seconds which was Level of service E and the delay approaches tolerance level, risk-taking behavior was likely.

Table 8 LOS for Delineation of movements for Harambae site

Adjustments	**Intersection LOS**	**Avg. Delay**
None (Existing)	F	642.6 sec
Cycle time (160)	F	193.3 sec
Cycle time (120) + Delineation	D	54.2 sec

The land use of Harambae area was majorly business area surrounded by large newly constructed buildings such as Commercial bank of Ethiopia and another nearby newly planned construction site. Moreover, the geometric improvements (addition of lanes) shall consider the impact of the intersection on the neighboring intersection such as Bherawi signalized intersection, Post office signalized intersection, Immigration signalized intersection, Legehar signalized intersection and Filwha T-section unsignalized intersections detailed network model analysis should be done prior to effecting the geometric improvements.

3.3.4 Saris Adey Ababa site

The traffic types in Saris Adey Ababa intersection included vehicular movements from the four approaches, LRT along the South – North direction and pedestrian movements.

Figure 10 Traffic type demonstrations in Saris Adey Ababa intersection

Since the Saris Adey Ababa intersection constitutes the LRT it was proposed for semi actuated signal for the operation in order to control the vehicular movements with respect to the arrival of the train.

Table 9 LOS comparisons and phase times' description for actuated signal at Saris Adey Ababa site

Adjustment	**Intersection LOS**	**Avg. Delay**
None (Existing)	F	756 sec
Actuated signal design	D	48.5sec

In addition to designing and optimizing the existing nonoperational traffic signal, another mitigation measure could also be applied which avoids the traffic conflicts with the rail transit. Based on the engineering remedies taken in other parts of the city like CMC Michael overpass (over LRT), Global Lancha overpass (over LRT) and Gerji overpass (Over highway) the engineering mitigation proposed for this intersection was similarly to construct an overpass in the direction of East – West approaches.

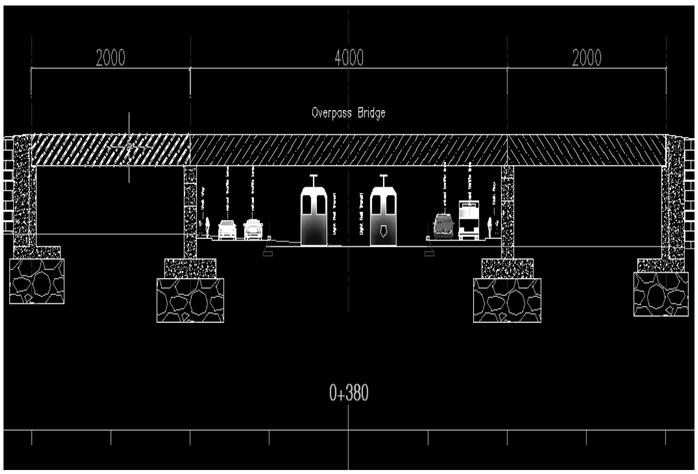

Figure 31 Traffic movement types after construction of Overpass Bridge

The proposed over pass design will modify the total number of lanes in both directions of the East – West approach from 4 lanes to 6 lanes keeping the number of lanes in the South – North direction to 4. Moreover, this proposed overpass is with a width of 12 meters where 9 meters of turning lanes are provided at each side of the bridge totaling to 30 meters of clear span on the East – West direction of the approach. The number of lanes for the right turners from the South – North approaches will be 2 in order to accommodate the left turn movements of these approaches as they shall use the overpass bridge to turn without a conflict with the rail transit.

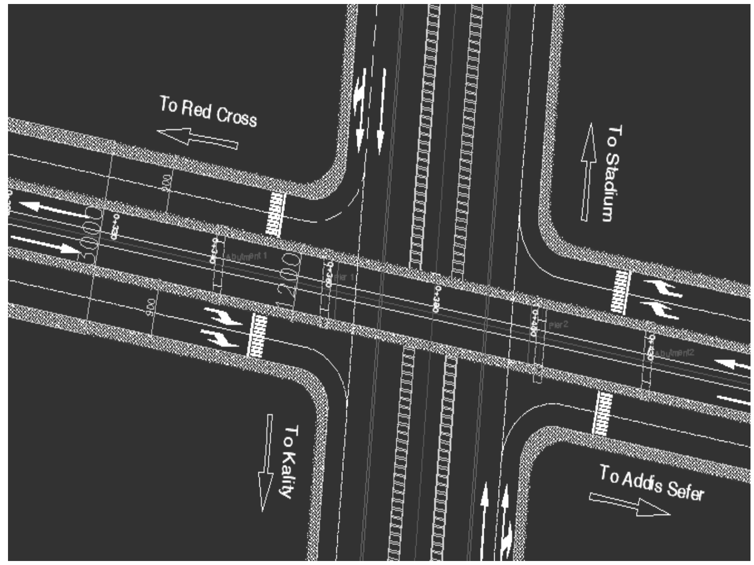

Figure 42 Plan view and dimensions of Overpass Bridge

4 CONCLUSIONS

Based on the above outcomes in the results and discussions sections and the proposed engineering mitigations for existing problems the following conclusions are made.

Regarding the Eliana hotel/ Bancodiroma site while most of the approach lanes remained in poor level of service according to the existing condition analysis. The delineation of movements with optimization of the cycle time and geometric modification of the site can improve the site level of service.

When Immigration signalized intersection was considered, the vehicular volume along the major approaches (Churchill-Bherawi) was significantly higher than that of the minor approach (Tikur Anbessa- Post office). This caused an inverse relation to the adjustment of the Cycle time in regard to the major and minor approaches. The provision of additional lane along the minor road can improve the intersection level of service.

The existing condition at Ethiopian hotel/Harambae signalized intersection is better than that of the above two. Yet this intersection is in a condition where major improvements regarding geometry were almost incapable of due to the location of the intersection. But with proposed engineering mitigations such as cycle time adjustment and delineation of movements in addition to changing the signal phase adjustments, level of service and delay could be improved.

Lastly, the Saris Adey Ababa site was completely different from the rest of the three intersections as the intersection has LRT that passes through it in the South – North direction. The arrival time of the trains has been significantly variable which necessitates designing and optimizing of signal controls on the intersection. Moreover, constructing Overpass Bridge over the intersection can improve the level of service and delay.

CONFLICT OF INTEREST

The authors declare that they have no conflict of interest.

ACKNOWLEDGEMENTS

The author acknowledges the Ethiopian Roads Administration and the Addis Ababa Traffic Management Agency for their support.

REFERENCES

[1] Ministry of Transport (2011). Transport Policy of Addis Ababa. Addis Ababa, Ethiopia.

[2] Akcelik & Associates Pty Ltd (2021). Sidra Intersection User Guide

[3] U.S. Department of Transportation, Federal Highway Administration (2013). Signalized Intersections Information Guide, Second Edition

[4] Highway Research Board (2010). Highway Capacity Manual, Washington DC: Transportation Research Board of the national Academies.

[5] National Academies of Sciences, Engineering, and Medicine (2015), Signal Timing Manual - Second Edition, Washington, DC: The National Academies Press.

[6] Mekonnen, F. (2015). Evaluation Of Traffic Congestion and Level of Service at Major Intersections in Adama City.

[7] Gashaw, T., “Evaluating the Performance of Signalized Intersection and the Associated Economic Impact of Congestion: (A Case Study on Ras Mekonnen Street of Addis Ababa, Ethiopia)”, Addis Ababa, 2018.

[8] Wondwossen Taddesse, "Assessing and Quantifying the Level of Traffic Congestion at Major Intersections in Addis Ababa," Addis Ababa University, Addis Ababa, 2011.

[9] Temesgen, A. “Capacity evaluation of roundabouts and signalized junctions in ddis Ababa, Addis Ababa”, 2015.

[10] Haque, M.R., Rahman, M.A., Hossain, M.B. and Roknuzzaman, M., “Capacity Evaluation of Roundabout Intersections in Khulna Metropolitan City by Using SIDRA”. Research Gate, 2017. International Conference on Planning, Architecture and Civil Engineering (ICPACE-2017), Rajshahi, Bangladesh, 2017.

[11] Das, D.K. and Keetse, M.S.M., “Assessment of traffic congestion in the central areas of Kimberley city”, Interim : Interdisciplinary Journal, vol. 14, no. 1, 2015, pp. 70-82.

https://journals.co.za/doi/epdf/10.10520/EJC188841

[12] Bichi, AISHA HALADU. "Evaluation of Traffic Flow at Signalized Intersections: A Case Study of Kano City, Nigeria." PhD diss., Doctoral dissertation, Near East University, 2018.